Università Campus Bio-Medico di Roma

Corso di dottorato di ricerca in
Scienze Biomediche Integrate e Bioetica
XXXV ciclo a.a. 2019-2020

Use of TMS-EEG to directly assess cerebral neurophysiology in healthy humans

Dott. Alessandro Di Santo

Coordinatore
Prof Vincenzo Di Lazzaro

Tutor
Dott. Lazzaro di Biase
Dott. Massimo Marano

22 Marzo 2023

SUMMARY

Abstract

Transcranial magnetic stimulation (TMS) coupled with electroencephalography (EEG) has shown promising results to study cortical neurophysiology in humans. TMS-EEG allows studying directly in real-time cortical activity through the intact scalp, which permits to record of cerebral responses like TMS-evoked potentials (TEPs) and cortical oscillation. This opens up new possibilities for exploring human cerebral networks, including recording activity of remote areas and real-time high-temporal resolution acquisition of cortical connectivity. However, some Authors pointed out that TMS-EEG outcomes could be influenced by several confounding factors, including acoustic and somatosensory inputs.

For this reason, the aim of the first experiment of this thesis is to measure separately the contribution of auditory and somatosensory stimulation caused by TMS and to assess their contribution to the TEP waveform, when stimulating the motor cortex. Seven different EEG recording blocks were performed. To assess auditory responses was used a standard TMS figure of eight coil, with and without noise masking. In subsequential blocks, a standard TMS coil placed on a pasteboard cylinder was used, with and without noise masking. Finally, a possible contribution of somatosensory activation was tested using electrical stimulation of the scalp. The results showed that auditory stimulation induced a known pattern of EEG responses that appropriate noise masking could suppress. Electrical stimulation of the scalp alone only induces similar and non-specific EEG responses. Real TMS, coupled with appropriate noise and sensory input masking, elicited specific and lateralized responses at the stimulation site. In conclusion, if carefully controlled, TMS over the motor cortex can generate genuine lateralized EEG activity, while auditory and somatosensory inputs can confound TEPs waveform if masking procedures are not properly used.

Furthermore, TMS-EEG allows to explore functional connections between the motor cortex and remote areas, including cerebellar-cerebral pathways. TMS-EEG, compared to classical neurophysiology outcomes, like cerebellar brain inhibition (CBI), records pure cerebral activity and permits to explore cerebellar connections to

motor and non-motor areas of the cortex. For this, in the second experiment, TMS-EEG was used to detect cerebral activity on the whole brain following TMS of the cerebellum. Also, was explored if these responses could be influenced by motor learning paradigms. To do that, different recording blocks were performed to collect EEG responses with a) real TMS cerebellar; b) combined auditory and somatosensory inputs. Furthermore, was tested if cerebellar responses could be behaviourally sensitive by assessing subjects before and after learning a visuomotor reach adaptation task. The results showed that after real cerebellar stimulation could be recorded a specific and lateralized neural activity that could not be recorded after mixed auditory-somatosensory stimulation, suggesting that this EEG waveform reflects pure cerebellar stimulation. These cerebellar TEPs are influenced by different stages of learning.

In conclusion, TMS-EEG is a novel and powerful technique which allows to explore genuine cortical responses, including those from remote areas. A standardization of TMS-EEG procedures is required to improve acquisition and analysis, the accuracy of collecting data, and to avoid of misinterpretation of the results due to confounding factors.

Concurrent EEG recording and TMS in healthy humans: a new tool to explore central nervous system physiology

Coupling transcranial magnetic stimulation (TMS) with electroencephalography (EEG) has recently emerged as a non-invasive tool to directly assess the function of human brain circuits since the first attempt in 1989 (Cracco et al., 1989). This powerful and innovative technique combines TMS of brain areas with EEG high temporal and spatial resolution, opening up new possibilities for exploring human cerebral networks. The TMS pulse induces a discharge in below cortical areas that result in synaptic potentials that can be recorded on the EEG as potentials composed of positive and negative deflections, called TMS-evoked potential (TEP) (Tremblay et al., 2019). Thanks to EEG's temporal resolution (in range of ms) we can have a direct insight into the TMS neuronal effect during and immediately after a single TMS pulse. Moreover, EEG recording allows the recording of both local and remote changes in brain activity induced by a TMS pulse. Combining TMS and EEG offers the possibility to study neuronal activity in real-time, in near and far cortical areas, bypassing spinal cord activation that could affect the classical TMS outcome measures (i.e. motor evoked potential - MEP, see below). Indeed, TMS-EEG provides insight into patterns of cortical excitability and connectivity, without depending on a peripheral response, as happens with conventional TMS coupled with electromyography recording (EMG) - (TMS-EMG) and allows a comprehensive examination of different cortical areas including motor and other cerebral pathways.

First, TMS technique will be described and then the physical principles of EEG will be briefly introduced. Finally, TMS-EEG concurrent recording will be introduced including equipment, signal analysis and applications.

Principles of TMS

TMS is a non-invasive, painless tool used to investigate the human cortex, first introduced by Baker and co-workers in 1985 (Barker et al., 1985). A single TMS pulse deliver over the primary motor cortex (M1) elicits a MEP in the corresponding contralateral hand muscle, which can be recorded with surface EMG. This non-invasive technique is widely used to assess the integrity of the corticospinal tract, to study intracortical, cortico-cortical, and cortico-subcortical interactions and as a research, tool to investigate brain excitability and plasticity (Hallett, 2007; Rothwell, 2004).

TMS follows the Faraday's law of electromagnetic induction to activate cortical neurons: an electrical current pulse sent through a wire generates a time-varying magnetic field that induces a secondary electrical field in the nearby structures. TMS device comprise the TMS coil (called magnetic coil) and the stimulator main unit (see below). The magnetic coil consists of one or more well-insulated coils of copper wire and usually is placed tangentially to the intact scalp. A high-voltage electric pulse passes through wire and generated a magnetic field, which typically lasts <1 ms and reaches up to about 2 Tesla with the lines of flux directed perpendicularly to the plane of the coil. The magnetic field penetrates the intact scalp and skull with minimal attenuation, without activating skin nociceptive receptors and induces secondary eddy currents in the conductive brain tissues (Groppa et al., 2012; Rothwell, 2004). The resulting electric field is parallel to the magnetic coil and stimulates the nearby neurons (Barker et al., 1985). The electric field intensity is correlated to magnetic field power and reaches up to 1-20 mA/cm^2 (a similar intensity required for electrical stimulation of the scalp). Moreover, the power of the magnetic field decreases exponentially as the distance from the coil increases, so the induced electric field in the brain rapidly decreases with the distance to the coil. Then, the strength of stimulation is maximum below the coil while decreasing with the distance.

The stimulator main unit consists of voltage source (V) (a charging system that can generate 8.000 mA within several 100 ms); one or more energy storage capacitor (C) (to generate, store and discharge multiple energy pulses in quick succession with rating of 7.5 kV); an energy recovery system, the internal resistor

(R) associated with the cables and thyristors that switching large currents over a short period of time (Farzan et al., 2016; Rotenberg et al., 2014) (Fig.1). Thyristors are the bridge between capacitor (C) and the coil, transferring 500 J in less than 100 ms.

***Figure 1**: **Simplified circuit diagram of a single-pulse magnetic stimulator** (V voltage*

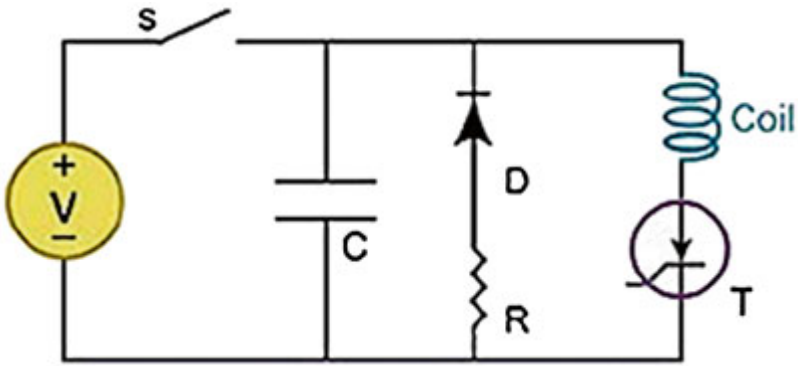

source, S switch, C capacitor, D diode, R resistor, T thyristor. (picture from (Wagner et al., 2007)

Also, the stimulator main unit has a pulse-shaping circuitry that controls the resonant frequency of this circuit and determines the pulse shape. A large majority of TMS devices generate two different TMS pulse shapes: monophasic and biphasic pulse (Groppa et al., 2012; Rotenberg et al., 2014) (Fig. 2). Monophasic pulse generates only unidirectional voltage and consists in a strong initial current flow that induces a magnetic field of 1-2.5 Tesla peaking approximately 50 μs after pulse onset. Biphasic pulse generates full positive/negative voltage oscillations and in contrast to monophasic pulse, each phase of the biphasic stimulus induces physiologically significant tissue current. The induced current can flow in the same or opposite direction as the initial rising phase of the biphasic pulse. Maintaining the same coil orientation, the two types of pulses excite different cortical neuronal populations. Also, the most relevant phase of the stimulus to excavate cortical axon are different between the two shapes: the initial phase is the most relevant for a monophasic pulse, whereas for biphasic pulses is the second part (the reversal) (Groppa et al., 2012). Interestingly, the direction of the magnetic field vector generated inside the coil is oriented to the coil handle whilst the vector of magnetic field inside the brain has opposite direction. In this way, to induce a posteroanterior stimulation (PA) in the brain the handle of the coil should be oriented posteriorly.

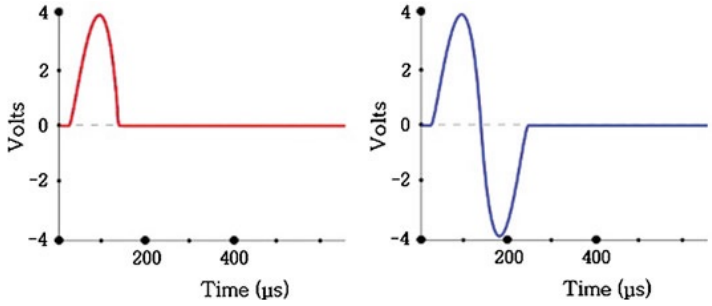

Figure 2: ***TMS pulse shapes***. *On the left, monophasic current induced by TMS coil. On the right, the biphasic pulse. Note that physiological effects are obtained by a positive slope in monophasic pulse, while biphasic pulse uses a negative slope (picture from* (Rotenberg et al., 2014)

Magnetic coils have different shapes and sizes, each one with unique characteristics. Several features determine different shapes, strengths and overall focality of the resultant induced electric field and consequent brain stimulation (Rosler et al., 1989). The circular coil (also called large round coil) has a diameter >10 cm and generates a spherical magnetic field perpendicular to the coil itself, is the most powerful coil and induces an electrical current in a large volume of brain tissue (non-focal stimulation). The induced current loops in the brain tissue are circular and have opposite directions compared to the electrical current in the coil. Hence, the strongest current will be below the annulus of the coil and the induced electrical field is attenuated towards the geometrical center of the coil (Groppa et al., 2012; Rotenberg et al., 2014) (Fig. 3) This coil is widely used for clinical application of TMS. Instead, figure-of-8-coil is formed by two single, circular coils placed side by side. The combined magnetic field is stronger under the contact point of the two coils and allows focal and deeper stimulation at low or moderate intensities of stimulation with respect to the circular coil. (Groppa et al., 2012; Rotenberg et al., 2014) (Fig. 3). This type of coil is preferred for neurophysiological research applications. Another type of coil is the H-coil which aims to stimulate deeper, non-superficial cortical layers. FDA recently approved this type of coil for the treatment of medication-resistant depression, instead for stimulate deeper areas (e.g., cerebellum) a double cone coil could be used.

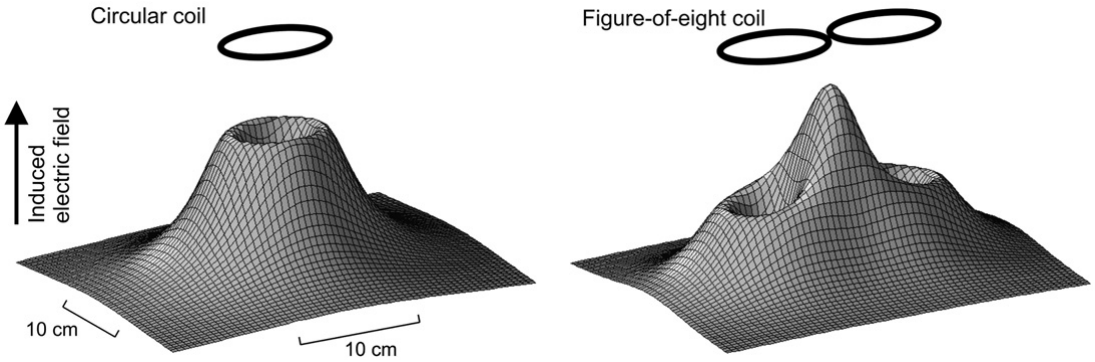

***Figure 3**: **Induced electric field obtained with different TMS coils**. On the left, circular coil induces an electric field with maximum intensities in the peripheric part and a null effect below the center of the coil. On the right, the induced electric field of figure-of-eight coil are maximum below the geometrical center of the coil. (picture from* (Ruohonen Jarmo; Ilmoniemi Risto, 2005)

Hints of TMS application: single pulse and paired-pulse paradigm to assess cortical excitability and connectivity

Single pulse TMS is widely used for analyzing the integrity of the corticospinal tract or to assess brain excitability. One of the commonest measures used is the corticomotor conduction time (CMCT) which represents the time that a single volley takes to travel along the corticospinal tract. CMCT is calculated by subtracting from single pulse TMS-cortical MEP latency the peripheral motor latency (PML) (i.e., the time that the descendent volley employs to descend from nerve root to peripheral muscle. PML can be measured as cervical or lumbar spinal MEP latency or can be calculated with a formula involving M-wave and F-wave latency: PML = (F-wave latency - M-wave latency – 1) *0.5. M-wave is the direct muscular response whilst F-wave is the muscular response induced by antidromic pulses and activation of alfa-motoneuron (Rossini et al., 1994) (Fig. 4)

Moreover, single-pulse TMS is able to test the resting motor threshold (RMT) which is defined as the lowest stimulation intensity able to evoke MEP at least 50 μV in relaxed muscles in 50% of 10 consecutive stimuli (Rossini et al., 2015). Instead, the active muscular threshold (AMT) requests a mild contraction of the target muscle (about 20% of maximal muscle strength) and is defined as the minimum stimulation intensities able to elicit MEP, at least 200 μV in amplitude in 50% of 10 consecutive stimuli. (Rossini et al., 2015).

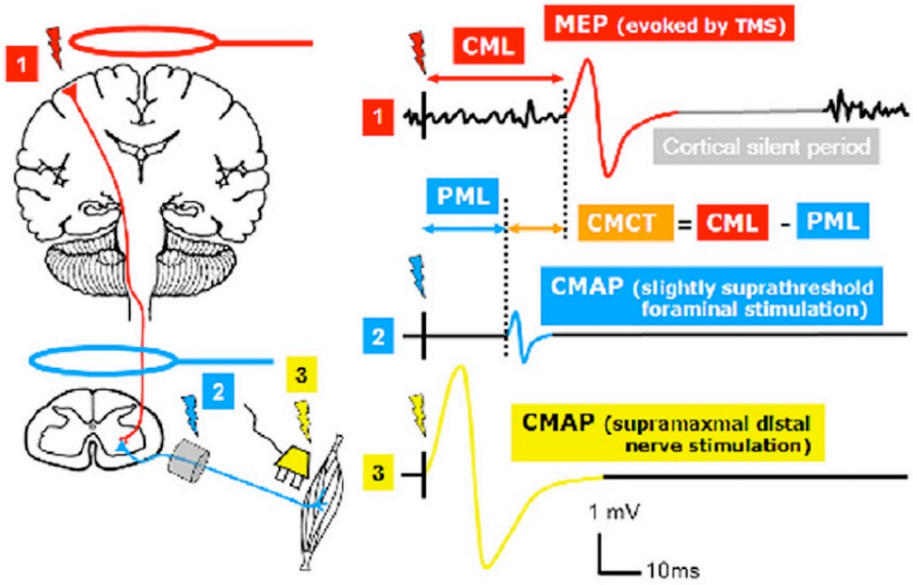

***Figure 4**: **Schematic representation of motor response elicited with TMS over M1**. See text for further details. (picture from* (Groppa et al., 2012)

Motor threshold, MEPs average (collected after a series of magnetic pulses at the same intensity), the area under the curve and the input/output curve (I/O curve) represent some parameters to assess cortical excitability and the integrity of the corticospinal tract (Currà et al., 2002). I/O curve is referred to progressive MEP amplitudes increase correlated to increase of TMS pulses intensities and seems origin from progressive recruitment of neuronal populations that are intrinsically less excitable or from neuronal populations more distant to center of stimulation (Hallett, 2007). Another important measure of cortical excitability is the cortical silent period (CSP) which is defined as inhibition of cortical activity after TMS cortical stimulation during a muscular contraction (Inghilleri et al., 1993).

Instead, paired-pulse TMS protocols give us a deeper insight into excitability and integrity of the cortical connection. In general, these protocols used two subsequential TMS pulses at different interstimulus interval (ISIs) to interfere with cerebral activity and test the intracortical connectivity in the same area or between two different and remote areas. There are several protocols used for this purpose, that involved the stimulation in the same area (single coil stimulation) or in motor cortex and a remote distal origin both peripherical or in another central area (respectively using an electrical peripherical stimulation or a double coil stimulation). Here will be mentioned only the most relevant paired-pulse paradigms.

The single coil stimulation paired-pulse protocol included excitatory and inhibitory responses. Short intracortical inhibition (SICI) is obtained with a subthreshold conditioning stimulus delivered 1-5 ms before a suprathreshold stimulus and this effect is observed as a reduction in amplitude of contralateral MEPs (Ziemann et al., 1996). SICI seems to involve the $GABA_A$ receptors pathways (V. Di Lazzaro et al., 2000). Instead, short intracortical facilitation (ICF) is obtained with a subthreshold conditioning stimulation of 8-30 ms delivered before suprathreshold pulse and it is observed as MEPs amplitudes increasing (Ziemann et al., 1996). Also, long interval intracortical inhibition (LICI) is an inhibitory response obtained with two suprathreshold TMS pulses given about 150 ms apart, that seem to reflect $GABA_B$ receptors activities (Di Lazzaro et al., 2002).

Besides, is possible to test motor cortex connection with distal areas coupling a stimulation of M1 with a peripherical or more remote central areas stimulation using a double site stimulation protocol. Interhemispheric inhibition (IHI) is achieved by stimulating the M1 of the contralateral muscles target and it seems to originate from cortical structures (Gerloff et al., 1998). Short latency afferent inhibition (SAI) is obtained with a peripheral stimulus (electrical stimulation to the median nerve) delivered 20-25 ms before a cortical TMS pulse that results in reduced MEPs amplitudes in contralateral muscle, mediated by muscarinic fibers (V Di Lazzaro et al., 2000; Tokimura et al., 2000). Finally, cerebellar inhibition (CBI), using a double cone coil ideally located just rostral to *foramen magnum* level, is used to test inhibition on MEPs elicited from contralateral M1 (Iwata and Ugawa, 2005; Ugawa et al., 1995). CBI seems to be involved in the activation of Purkinje cells which in turn suppress deep cerebellar nuclei excitatory connection to contralateral M1 (Iwata and Ugawa, 2005; Ugawa et al., 1995).

TMS neurophysiology

As briefly mentioned above, a single pulse TMS over M1 depolarizes neuronal cortical populations that activate descent volleys that run inside corticospinal nerve fibers that evoke a muscular twitch in the contralateral corresponding peripheral muscle, visible like a MEP recorded with surface EMG.

The MEP is a complex indirect measure of motor cortex output since it has been filtered by synaptic connections in the spinal cord. In humans, using a high cervical-cord epidural electrode is possible to record a high-frequency repetitive discharge of corticospinal neurons in response to a single TMS pulse, which represents a direct recording of activity evoked by corticospinal output neurons. These descent volleys result in a group of waves (Fig.5). The earliest wave is thought to originate from the direct activation of the axons of the fast-pyramidal tract neurons (PTNs) that was termed "D" wave (i.e. direct wave). (Di Lazzaro, 2013; Patton and Amassian, 1954). The latter waves seem to need integrity of cortical grey matter and were thought to originate from indirect, trans-synaptic activation of PTNs and were termed "I" waves (i.e. indirect waves) (Di Lazzaro, 2013; Patton and Amassian, 1954). These waves have a frequency discharge of 667 Hz (i.e. I-waves interpeak interval is 1.5 ms) (Di Lazzaro, 2013). Depending on coil position, a single TMS pulse can evocate direct and indirect descendent volleys (Di Lazzaro et al., 2008; Rothwell, 1997). Several models were proposed to explain how TMS induces its neurophysiological effects (Amassian et al., 1987; Day et al., 1987; Di Lazzaro, 2013; Di Lazzaro and Rothwell, 2014; Ziemann and Rothwell, 2000). Since the canonical cortical circuit was proposed by Douglas and co-workers in 1989 (Douglas et al., 1989), a lot of models have been proposed to explain how corticospinal volleys are generated by TMS and transcranial anodal electrical stimulation (TES) pulses, here will be discussed the model proposed by Di Lazzaro in 2003 (Di Lazzaro, 2013). This model can be extended to the entire cortex and seem involved different neuronal populations: superficial populations of excitatory pyramidal neurons of layers II and II (named P2 and P3 respectively), the axons of the PTNs of layer V (named P5), inhibitory GABA interneurons and the thalamocortical projections (Di Lazzaro, 2013) (Fig. 5). Thresholds for the activation of different components of descending volleys are substantially different (Di Lazzaro et al., 2008). At low intensities, using a focal figure-of-eight coil over M1 with monophasic pulse waveform and PA orientation is possible to evoke a single descending wave (called I1-wave) that originates from monosynaptic activation of P5 cells by axons of P2-P3 cells, that are the most excitable elements in cerebral cortex (Di Lazzaro, 2013). D-wave and I1-wave have a 1 ms difference in latencies, which is compatible with monosynaptic activation. As TMS pulses intensities increased, the I1-

wave increase in size and is followed by later volleys, called late I-waves (I2-I3 and I4-waves) that originate from a more complex circuit whose activation produces a repetitive discharge of PTNs. As mentioned before, the late I-waves interpeak interval is about 1.5 ms which indicates a discharge frequency of about 670 Hz. P5 cells have excitatory monosynaptic reciprocal connections with layer 2 and 3 pyramidal neurons and interneurons, thus these cells are activated after P5 discharge and they will in turn reactivate the P5 cells (Di Lazzaro, 2013) (Fig. 5).

Interestingly, late I-waves but not I1-wave are depressed with the SICI paradigm, which is thought to depend on $GABA_A$ pathways (Di Lazzaro et al., 1998; Weise et al., 2013). Moreover, was found that late I-waves were suppressed by SAI whereas I1-wave was not (Tokimura et al., 2000). Finally, was shown that LICI, which seems to reflect $GABA_B$ activities, suppressed late I-waves and not I1-wave (Di Lazzaro et al., 2002; Ni et al., 2011). Two hypotheses can explain how in paired-pulse paradigms conditioning inputs could reduce recruitment of late I-waves: 1) decreasing the excitability of the oscillating neurons which produce the late I-waves; 2) inducing a direct suppression of PTNs excitability (V. Di Lazzaro et al., 2000). The model proposed by Di Lazzaro and Rothwell suggests that the P2-P3 neurons could inhibit apical dendrites of P5, that have reciprocal connections with superficial layer 1 (P1) neurogliaform cells (Jiang et al., 2013). This superficial neuronal population might be activated by low-intensity magnetic stimulation in paired-pulse protocols (like SICI) and in turn suppress late I-wave onto pyramidal cell dendrites (Di Lazzaro and Rothwell, 2014) (Fig. 6).

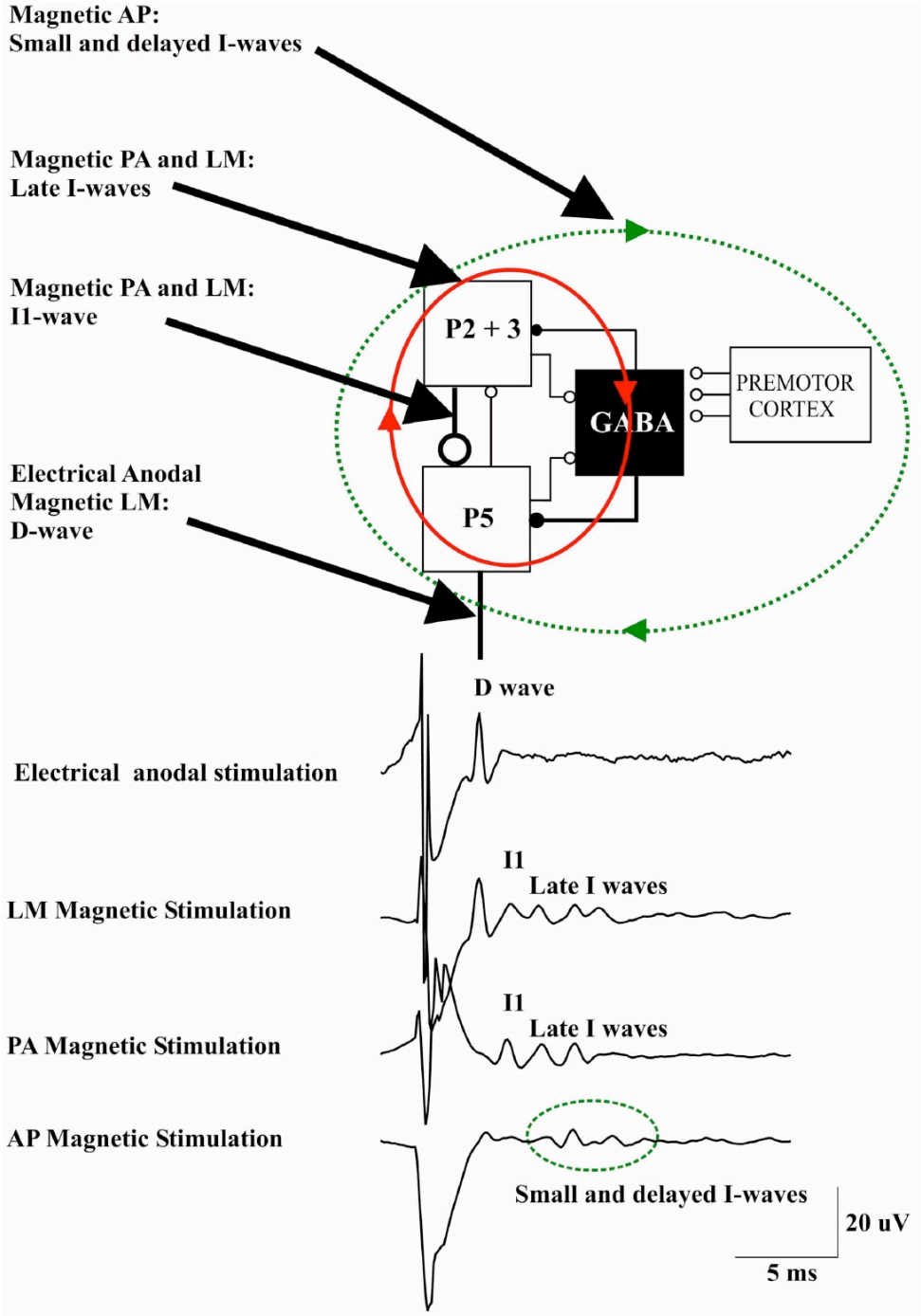

***Figure 5**: **Model of corticospinal volleys generations** based on canonical cortical circuits proposed by Douglas and coworkers in 1989 (picture from* (Di Lazzaro and Ziemann, 2013)

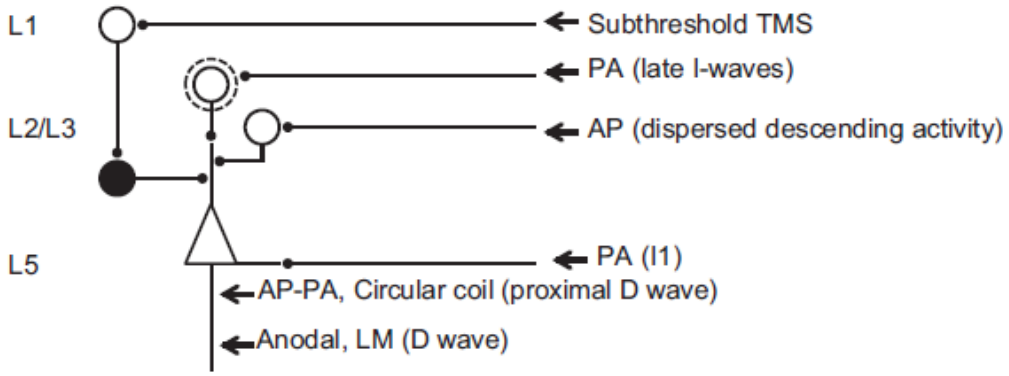

Figure 6**: **Possible preferential site of activation using different TMS techniques (Di Lazzaro and Rothwell, 2014)

Introduction to electroencephalography

Human EEG was first described in 1929 by Berger (Berger, 1929). This technique enables non-invasive assessment of neural activity resulting from local and long-range neural communication across different spatial scales at millisecond temporal resolution (Ingber and Nunez, 2011). Neural activity is conducted through brain volume to the scalp without any measurable time delay (an effect known as volume conduction). A pair of EEG electrodes on the scalp measures the potential differences between two regions because the brain activity recorded by one sensor is always compared to another value. EEG signal represents electrical activities generated through spatial and temporal summation of the excitatory and inhibitory postsynaptic potentials. EEG-recorded activities are oscillatory and are thought to originate from intrinsic properties of neurons, structural proprieties, functional proprieties of neurotransmitter systems and network interactions and feedback loops (Farzan et al., 2016). Importantly, the resultant spontaneous brain activities recorded with EEG are several orders of magnitude smaller (μV amplitude) than the electric field induced by TMS.

Two kinds of EEG recording are generally considered: continuous recording or even-related recordings. Conventional modern EEG systems include sensors (electrodes), amplifiers and analog-to-digital convertors for data digitalization.

TMS-EEG

Equipment

Compared to traditional EEG systems, TMS-compatible EEG systems need electrodes that avoid amplifier saturation and TMS-induced heating to minimize artifacts during data acquisition.

One of the biggest problems in early TMS-EEG attempts was that although TMS pulse lasted less than 1 ms many EEG amplifiers did not recover for up to several ms after the stimulus and that resulted in huge EEG artifacts. One of the first solutions was to use a sample-and-hold circuit with EEG electrodes. This was decoupled from the amplifier shortly before TMS pulses (-50μs to 2.5 ms post-TMS) allowing for EEG recordings as early as 2 ms following the pulse (Ilmoniemi et al., 1997). Recently, direct current (DC) amplifiers (that do not contain an initial capacitor to be saturated) and EEG amplifiers with high sampling rates (>5 kHz) were developed (Daskalakis et al., 2012). The combinations of these features enable the recording of wide voltage range sensitivity (μV to several mV) permitting the accurate acquisition of low amplitude brain signals shortly after capturing the true shape of the high voltage TMS artifact (Farzan et al., 2016).

Also, TMS magnetic field creates a secondary current in the nearby conductors, including EEG electrodes, and this may produce repulsive forces that can cause movement and heating of the ring-shaped EEG electrodes (Pascual-Leone et al., 1990). Besides, the temperature of EEG electrodes increased as a function of stimulation parameters (Roth et al., 1992). For that reason, was suggested that EEG TMS-compatible electrodes should have a small current loop area (Roth et al., 1992). Moreover, electrode conductivity mass can be reduced by using conductive plastic pellet electrodes coated with a thin layer of silver epoxy (Ives et al., 2006).

Current EEG TMS-compatible systems can have from 32 to 128 electrodes. Beyond classical passive electrodes, several qualities of electrodes were produced in the last years. In particular, active electrodes have a pre-amplification module, this allows the signal to be amplified before additional noise is added between the electrode and the system that capture, process or amplify the signal. Also, active electrodes

provide a less disconformable preparation for the subject and a better quality of the EEG signal. Furthermore, a direct comparison between passive and active electrodes showed that active and passive electrodes recorded similar EEG signals suggesting that active electrodes could be a reasonable and easier setting for acquiring TMS-EEG signal (Mancuso et al., 2021). However, no particular electrodes were recommended, thus the choice between different electrodes should be based on study goals or TMS-EEG availability.

TMS-EEG outcome measures

As previously described TMS pulse induces an electric field in nearby conductive brain tissue, including both grey and white matter. This electric field generates an action potential that spread from the stimulated area to interconnected brain regions through short- or long-range cortico-cortical, thalamocortical pathways. The recorded EEG signal origins from TMS-induced generation or modification of excitatory and inhibitory postsynaptic potentials whose spatial and temporal summation are recorded by EEG sensors. This response is called TMS-evoked potentials (TEPs), which are a series of positive and negative deflections on EEG signals lasting 200-300 ms and are an index of cortical reactivity (Tremblay et al., 2019) (Fig.7). Importantly, TMS-EEG recording require around 50-200 stimuli to obtain a stable and reproducible outcome.

Cortical activities induced by TMS can be recorded after few milliseconds after TMS stimulation and with TMS-EEG is possible to quantify and characterized this activity that spreads to cortical areas of the contralateral hemisphere around 20 ms after the stimulus (Ilmoniemi et al., 1997). Although the origin of TEPs remains to be determinate, a growing body of evidence suggests that involves spatial and temporal summation of excitatory and inhibitory post-synaptic potentials, that originate from cortical large pyramidal neurons and interneurons (Hill et al., 2016; Kirschstein and Köhling, 2009).

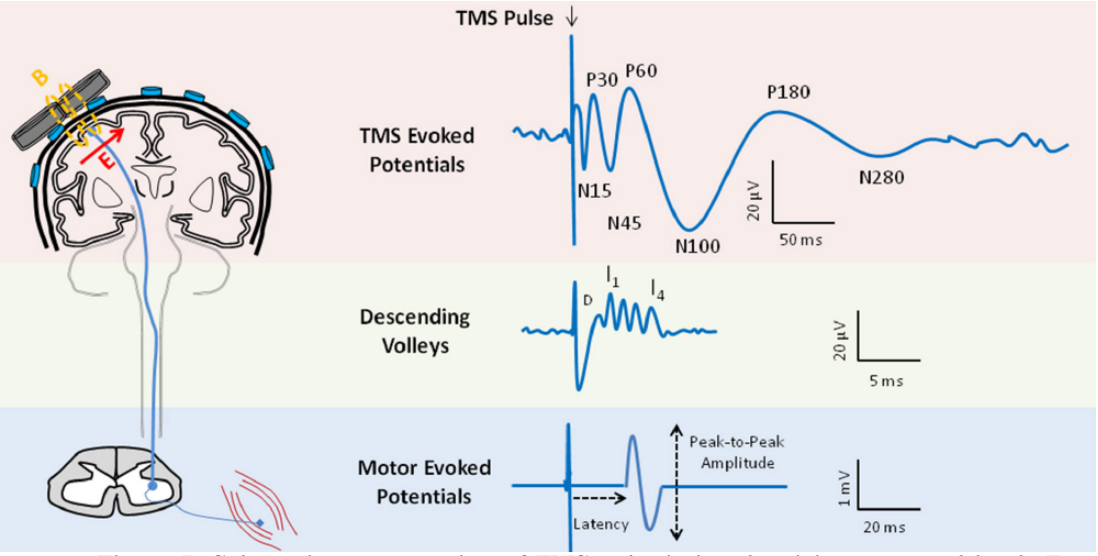

***Figure 7**: **Schematic representation of TMS pulse induced activity on several levels** First line: TMS-Evoked potentials, that are cortical response to TMS pulse. Second line: epidural recording of descending volleys induced by TMS stimulus. Third line: muscular activity recording induced by TMS (MEP). **B**: TMS-induced magnetic field; **E**: TMS-induced electric field (from* (Farzan et al., 2016)

TEP is a complex waveform time-locked to TMS pulse composed of a series of peaks, each one with specific latencies, globally lasting around 200-300 ms (Hill et al., 2016). As opposed to MEPs, TEPs are already measurable in M1 with subthreshold intensities (Komssi and Kähkönen, 2006). Shreds of evidence suggest that TEPs can be recorded only from intact and functional areas of the cortex (Gosseries et al., 2015). TEPs from M1 are the most studied: have an amplitude in order of µV and usually and are characterized by the following peaks: N15, P30, N45, P 60, N100, P180, N280 (Komssi and Kähkönen, 2006; Lioumis et al., 2009) (Fig. 7). Stimulating left M1 with focal TMS coil the earliest peak (N15) occurs in the electrodes below the stimulated area. Then, this impulse spreads near central sites (P30) and subsequently to the contralateral side (N45). Finally, late-peaks (N100 and P180) have a bilateral central and centrofrontal distribution (Bonato et al., 2006; Kicić et al., 2008). Some peaks (such as P30, N45 and N100) are more reliable compared to the others (Lioumis et al., 2009). Some evidence suggested that early peaks (N15-P30) reflect cortical excitatory activities, while later peaks (N45-N100) reflect cortical inhibition (Tremblay et al., 2019). TEPs from other cortical areas, e.g. from the dorsolateral prefrontal cortex – DLPFC, are smaller in amplitude compared to TEPs obtained from M1 (Lioumis et al., 2009). DLPFC TEPs have a high concordance and low measurement errors, and good within- and between-session reliability. Particularly, N100 and P180 showed the

greatest reliability (Lewis J Kerwin et al., 2018). TEPs from other non-motor areas are less well characterized, so further studies are necessary to determine TEPs morphology and physiology in different brain regions (Hill et al., 2016). To date, some open questions remain to be clarified about TEPs peaks' origin, the possible involvement of subcortical structures in TEP generation and the influence of possible confounding factors like indirect somatosensory and auditory responses (see further in "Artifacts on EEG signal").

Other measurements can be obtained from TMS-EEG recording. Briefly, TMS pulses induce modifications on ongoing spontaneous cortical oscillations (in particular evaluated in the frequency domain) and those modulations are important to study the functional specificity of brain rhythms, to evaluate the effects of plasticity- protocols, to assess the efficacy of pharmacological and non-pharmacological treatment and the pathophysiological role in several diseases (Assenza et al., 2017; Tremblay et al., 2019). Also, TMS-EEG allows studying cortical connectivity in terms of propagation in time and space of the signal induced by TMS pulses to other anatomically and functionally connected brain regions (Tremblay et al., 2019). These measurements will be not further discussed given the non-relevance with this thesis's aims.

Artifacts on EEG signal

Despite the introduction of several TMS-compatible EEG systems (briefly described before), several factors may contaminate the resulting EEG signal. Usually, this includes specific TMS-related artifacts and common EEG artifacts such as environmental noise (e.g. powerline noise and slow drifts in the position of the electrodes) and physiological noise (e.g. cardiac rhythm, eye blinks, head movements, muscular facial/scalp activity) (Farzan et al., 2016; Tremblay et al., 2019). These physiological EEG-induced artifacts have specific temporal, spatial and spectral characteristics and can be removed with post-processing analysis as independent component analysis (ICA) (Farzan et al., 2016).

TMS-related artifacts can depend on specific physical characteristics of the TMS coil or can be induced by magnetic and electric fields. TMS-induced electromagnetic pulse artifact occurs in the first 50 ms and is several orders of magnitude larger than electrophysiological activity (Ilmoniemi et al., 1997). However,

with the current TMS-compatible EEG technologies and post-analysis processing (further described below) TMS electromagnetic pulse artifacts can be characterized and removed offline during posthoc analysis (Daskalakis et al., 2012). As already briefly mentioned, several TMS-related physiological and instrumental noises could theoretically contaminate the resulting TMS-EEG signal. For example, TMS could induce time-locked activation of peripheral nerves and cranial muscles near the coil (Mäki and Ilmoniemi, 2011; Mutanen et al., 2013), which could be easily removed during off-line analysis. Further evidence highlighted the importance of "TMS induced-decay artifact" (a large positive shift in the signal that linearly recovers within up to 50 ms) which is due to several factors like electromagnetic forces and TMS coil vibration that induce electrodes movement at each TMS pulse or to TMS capacitator recharge or to electrodes-skin interface (Sekiguchi et al., 2011; Veniero et al., 2009). Besides, each TMS pulse produces a tapping sensation on the scalp and a loud clicking noise (around 100db, 0.5 rise time) (Starck et al., 1996). This auditory stimulation can evocate auditory evoked potentials (AEP) that could mask real TMS-induced potentials (Nikouline et al., 1999), while the TMS tapping sensation may activate peripheral sensory nerves which would produce somatosensory evoked potentials (SEP) (Cruccu et al., 2008; Rocchi et al., 2017)

Some strategies were suggested to avoid or attenuate TMS-related artifacts during the TMS-EEG session. First, to minimize the effect of electrodes' movement induced by TMS coil, reference and ground sensors should be placed far from TMS (Farzan et al., 2016). Also, to avoid the induction of eddy current in EEG electrode wires, these should be free of the loop, grouped together and placed as far away as possible from TMS coil (Veniero et al., 2009). Skin-sensors impedance should be kept under 5kΩ using a mini-puncturing technique applied to each skin-sensor contact through the sensor hole (Julkunen et al., 2008). Wearing sound protective headphones or playing loud (about 90dB) white noise in earphones are strategies used to maximal suppress auditory stimulation effects (ter Braack et al., 2015). Moreover, to attenuate TMS tapping sensation and the bone-conducted TMS click sound, a thin layer of foam can be inserted between TMS coil and the scalp (Massimini et al., 2005). Moreover, recent studies tried to quantify the amount of AEP and SEP influence on TEP waveform using concomitant somatosensory and auditory stimulation to obtain a so

called “realistic sham conditions” (Conde et al., 2019; Gordon et al., 2018) but the results were conflicting (see next chapter -experiment 1- for a more detailed discussion). Despite previous evidence on confounding factors control being encouraging, some Authors suggest using a sham stimulation condition as a control to limit sensory-related confounding factors. These sham conditions can be subtracted in offline analysis from real stimulation EEG signals to eliminate artefacts and obtained genuine cortical activation (Daskalakis et al., 2008).

Indeed, despite all the precautions described above, some artefactual activity could remain in raw EEG signal but can be removed with offline procedures. These analyses can be performed with different EEG analysis toolboxes of MATLAB as EEGLAB (Delorme and Makeig, 2004), Fieldtrip (Oostenveld et al., 2011) and TESA software (Rogasch et al., 2017).

The first approach is to early remove during analysis processing the contaminated data obtained from sensors, trials or from a specific time segment to preserve the subsequent analyses. Single contaminated sensors can be removed and replaced with spherical interpolations (Litvak et al., 2007), however, this approach could create regional bias since the electrodes closer to the stimulation site have a high probability to be contaminated. Removing contaminated trials can be performed to preserve the highest number of sensors (Reichenbach et al., 2011), or an alternative is possible to remove and interpolate selected electrodes to preserve the single trial. Still, this approach could be susceptible to bias because usually the trials near the stimulation site were predominantly deleted. Moreover is possible to selectively remove contaminated time segments and the removed data can be interpolated or set to zero (Huber et al., 2008; Reichenbach et al., 2011).

Another approach is selectively removing the TMS-related artifacts and that is possible with different offline techniques as template subtraction and recursive prediction-correction filters (Bayesian models). However, the most used tools are represented by the blind source separation techniques, which use mathematical procedures to separate EEG signals from noise and decompose EEG signals into independent components (e.g., independent component analysis – ICA) or orthogonal components (e.g., principal component analysis – PCA). These techniques should

remove components associated with noise and then the noise-free signals are mixed to reconstruct the dataset. ICA is based on assumption that EEG signal originates from temporally and spatially independent sources compared to the noise and that EEG signals can be modeled as a linear combination of cortical and non-cortical sources with independent time course (Onton et al., 2006). Thus, in the ICA approach noise components are identified based on spatial and temporal features. ICA algorithms include: FastICA (which maximize non-Gaussianity of source components), Run ICA (which minimizes mutual information between the sources) and temporal decorrelation source separation (which utilizes temporal information in the source signal) (Farzan et al., 2016).

One of the biggest problems in TMS-EEG studies is the lack of a gold standard approach for processing analysis and artifacts removal. This adds difference between TMS-EEG laboratories and contributes to increase heterogeneity outcomes of TMS-EEG studies.

TMS-EEG analysis

In this paragraph will briefly describe the main and common strategies to analyze TEPs. Despite several methods were suggested in the literature, to date does not exist standardized protocol to analyze TEPs. The choice between the different approaches depends on the goals of the single study.

The most common approach to evaluate TEPs is to measure the amplitude and latency of TEP peaks over a specific subset of electrodes (Hill et al., 2016; Rocchi et al., 2018a). This set of electrodes of interest could be estimated a priori based on scalp regions where responses are expected or could be identified after recording session using data-driving methods like cluster-based permutation statistics. The data typically are expressed in the form of a waveform, which includes all common peaks and represents the neural activity variation (express in terms of amplitudes - μV) in function of time, and in form of the topographic map representing the scalp voltage distribution for each peak to visualize and quantify spread activity across the cortex (Fig. 8).

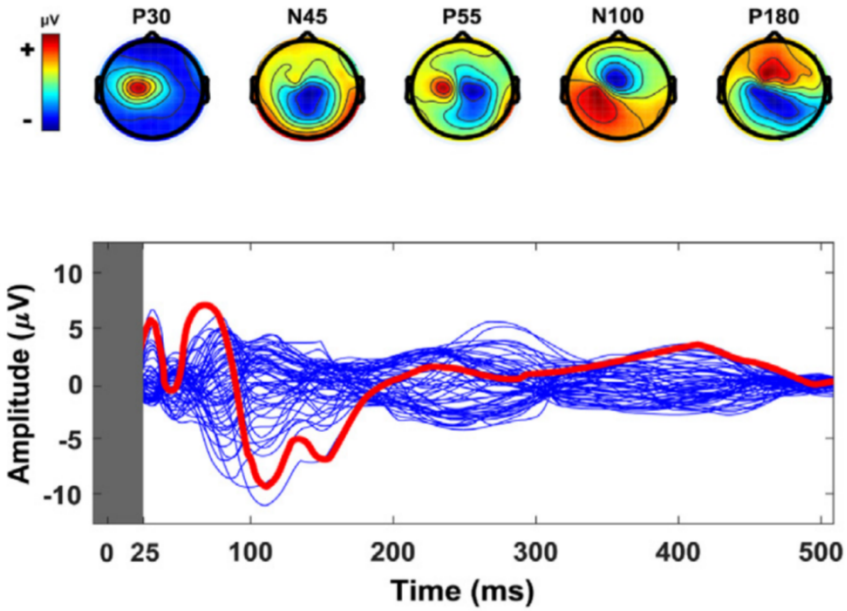

***Figure 8*: M1 TEP in a representative subject**. *Upper line: scalp maps voltage distribution. Bottom line: butterfly plots, red line represent mean from electrode of interest and grey box the interpolated data (picture from* (Tremblay et al., 2019)

Another possible way to measure TEP is using the local mean field power (LMFP) that corresponds to the area under the curve (i.e. the integral) of the rectified signal or standard deviation (root mean square) across specific electrodes of interest at a given time point (usually at TEP peaks) (Romero Lauro et al., 2014). LMFP doesn't need a clear peak, given that considers width and peaks of evoked activity regardless of polarity. However, the polarity of induced response is an important information on the nature of brain activation. A similar analysis approach is to use the global mean field power (GMFP) that measures the impact of TMS pulse over all electrodes. GMFP corresponds to the averaged signal of TMS activity over the entire surface of the head or to the standard deviation (root mean square) across all electrodes at a given time point (Lehmann and Skrandies, 1980a). As mentioned before, the choice between these methods depends on the study's goals. For example, using the electrodes of interest system is important when there is a supposed localization of brain responses, while LMFP is more relevant when are hypothesized changes in brain activities localized and not related to specific TEP peaks. GMFP is the method to prefer when the study goal is to explore global brain activity following TMS pulse.

Finally, an alternative method to analyze TEPs is to use non-parametric cluster-based permutation tests to compare all EEG data across space and time (Maris and

Oostenveld, 2007). This analysis takes into account any combination of space, time and frequency while controlling for the multiple comparison problems inherent in mass-univariate analyses (Maris and Oostenveld, 2007). This class of analysis is advantageous compared to others because is valid for both exploratory and hypothesis-driven TEPs comparison and does not require assumptions of data normality.

Neurophysiological and clinical application of TMS-EEG

Paired-pulse TMS-EEG

A lot of studies have investigated the paired-pulse paradigms with TMS-EEG recording. As mentioned before, paired-pulse protocols are expression of specific neurotransmitters' activity on cortical activity. These studies will be briefly reported here. LICI protocol ($GABA_B$ receptor-mediated) has been demonstrated that reduce induced cortical EEG activity in M1 and DLPFC (Daskalakis et al., 2008); in particular were described a suppression of P30, N45, N100 and P180 in M1 (Premoli et al., 2014) and a suppression of N40; P60 and N100 in DLPFC (Rogasch et al., 2015). SICI protocol (associated with $GABA_A$ receptor) and ICF paradigm ($GABA_A$ receptor and NMDAR associated) were shown to induce an increase of N100, while inducing a different modulation of P30 and P60 between the protocols: SICI induce a inhibition of these components while ICF enhance P30 and P60 (Ferreri et al., 2011). Moreover, a subsequent study demonstrated that SICI and ICF in older adults (>60 yrs) have less SICI N100 inhibition and less ICF N45 potentiation compared to younger subjects (Noda et al., 2017). Regarding SAI paradigm contrasting results were found: a reduction of N100 and P60 attenuation was demonstrated in one study (Ferreri et al., 2012); whilst another study demonstrated an increase of N100 (Noda et al., 2016).

Cerebellar TMS-EEG

As shown, TMS-EEG has arisen as a new tool that provides new insights into cortical excitatory and inhibitory connections within the motor cortex. For this reason, recently, a few studies have used TMS-EEG to investigate the connection between the cortical motor cortex and more remote areas, including the cerebellar-cortical pathway (Fernandez et al., 2021; Gassmann et al., 2022; Sasaki et al., 2022). However, one of

the biggest problems is the use of a double-cone coil over the cerebellum which inevitably leads to activation of cervical muscles, which could result in a significant artefact on EEG signal, that could confound the pure cerebral response. Some studies which investigated paired pulse cerebellar-cortical protocols using TMS-EEG, showed controversial results. Fernandez and colleagues compared TMS-EEG recording of cerebellar activity with a "realistic" control condition that theoretically simulate real cerebellar stimulation. They found that the signal from both conditions appears to have a common spatiotemporal distribution after 50 ms, also found that after the real stimulation, there is a very large artefact in the EEG signal (Fernandez et al., 2021). Nevertheless, the real and control condition have different components in the early interval especially in the parietal area, suggesting a genuine cortical activation. Indeed, Gassmnan and colleagues used a similar approach and they found that real cerebellar TMS stimulation has a peculiar response compared to a sham condition, further suggesting that is it possible to use TMS-EEG to test cerebellar-cortical pathway (Gassmann et al., 2022). Finally, a recent study investigate CBI with TMS-EEG using different coils to stimulate the cerebellar hemisphere (both double cone coil and figure eight coil) (Sasaki et al., 2022). They found that both coils were able to suppress M1 TEP, whereas sham stimulation did not. For this, the Authors suggest that TMS-EEG could be used as an index of CBI activity. However, despite the enormous potential of using TMS-EEG to test cerebellar activity, these controversial results require further studies.

TMS-EEG in neurological disease

Furthermore, TMS has been used for investigating neuro-physiopathology and finding a possible treatment approach (including the use of plasticity protocols) for several psychiatric and neurological diseases. A growing body of evidence suggests that TMS-EEG, due to its peculiar characteristics, could be a powerful tool to indagate abnormalities in cortical mechanisms that occur in neurological disease, to assess the efficacy of several drugs treatment and to design new neuromodulation protocols. For example, in Alzheimer's disease TMS-EEG was used for several purposes: to assess drugs treatment efficacy, as a marker of neuroplasticity changes and to develop an innovative treatment approach based on a neuromodulation protocol with the goal to

reactivate latent memories (Rose et al., 2016; Tremblay et al., 2019). Recent findings suggest that in stroke patients with aphasia, TMS-EEG outcomes could be biomarkers to assess the effects of the neuromodulation treatments (Cipollari et al., 2015). Furthermore, some authors suggest that in stroke patients TMS-EEG could be a valuable prognostic measure (Tremblay et al., 2019). Finally in Parkinson's disease (PD) patients, TMS-EEG was used to assess the impact and the cortical modulations of subthalamic deep brain stimulation (Elias Paolo Casula et al., 2017), but in the future could give further insight into PD pathophysiology mechanisms, could be used to assess responses to different PD pharmacological and non-pharmacological treatments and to find a possible cortical biomarker for the different disease stages.

The aim of this thesis is to explore the potential and innovative role of TMS-EEG to investigate cerebral neurophysiology in humans directly and in a non-invasive way. To this end, two different TMS-EEG experiments are presented. The first investigates whether the resulting EEG signal following a single TMS pulse can be influenced by peripheral sources such as auditory and somatosensory stimulation. A thorough and comprehensive disentanglement of the EEG responses will clarify whether TMS-EEG could be a good index of neuronal activation and whether peripheral influences can be reduced by masking strategies. These findings could help to define a systematic approach to reduce the influence of these factors and to standardize the TMS-EEG acquisition protocol.

In the second experiment, TMS-EEG will be used to test the cerebellar-cortical connection using CBI and EEG signals across the whole scalp. In addition, these cerebellar TEPs will be tested before and after performing a cerebellar-dependent motor learning paradigm. These findings could help to use TMS-EEG CBI as a reliable index of cerebellar-cortical connectivity activity regardless of motor learning state.

Experiment 1 - Peripheral signals influence on neural EEG recording after TMS

As seen in the previous chapter, TMS-evoked potentials (TEPs) can be used to assess neurophysiological mechanisms in healthy subjects and to investigate neurophysiological abnormalities in several neurological diseases. As mentioned earlier, it is still not clear how TMS-artifacts affect TEP signal. In particular, the specific contribution of somatosensory evoked potential (SEP) and auditory evoked potential (AEP) to the resulting TEPs, remain to be clarify. For these reasons, some Authors have suggested to use a sham condition as a control to obtain genuine brain activation. However, it is still debate whether a sham condition is really necessary and which type of sham stimulation should be used. As seen before, at each TMS discharge, magnetic coil produce a loud "click" sound and a tapping sensation on the scalp that may evoked AEP and SEP, respectively (Nikouline et al., 1999; Rocchi et al., 2017). Several strategies can be employed to reduce the auditory and somatosensory contributions to the TEP waveform with the application respectively of noise masking and placing a thin layer of foam between the coil and the cap. Nevertheless, these strategies are imperfect, and disentangling the contributions of AEPs and SEPs to TEPs from the signal reflecting cortical processes would strengthen the conclusions that can be drawn from TMS-EEG studies.

As already briefly mentioned before, previous studies have attempted to determinate the genuine cortical origin of the TEP waveform but have produced conflicting results. Gordon and colleagues (Gordon et al., 2018) compared TEPs evoked by TMS over M1 at two different intensities (90% and 110% RMT) with a sham stimulation condition. The study aimed to address the potential confounding factors discussed above by opting for a simultaneous somatosensory and-auditory sham condition, thereby producing auditory and somatosensory stimuli, without TMS inducing an electrical current in the brain. This was done by holding a sham coil 5 cm far from M1 and pairing the sound of the real TMS stimulation with electrical stimulation of the scalp. The results from this study showed significant differences between real and sham stimulation conditions in the amplitude and spatial distributions

of the N45, P70, and P180 components of the TEP. In contrast, a recent work by Conde and co-workers (Conde et al., 2019) used a similar study design but did not find significant differences in TEP components between sham and real stimulation conditions. In addition to using a somatosensory-auditory sham condition similar to that described above, this work aimed to minimize muscle contraction and reduce afferent contributions to the TEP by stimulating two non-motor areas (prefrontal and parietal cortex) with two different coil orientations. Based on the similar TEP waveforms observed between sham and real stimulation conditions in this study, the Authors suggest that the TEP results largely result from the auditory and somatosensory stimulation that is incidental in TMS. Based on this result, the Authors emphasize the importance of using a multisensory sham control condition in TMS-EEG experiments. As suggested by Belardinelli and colleagues (Belardinelli et al., 2019) different methodological approaches may partly contribute to these conflicting results, e.g. these studies used different electrical stimulation intensities, offline analysis procedures, coil size, localization and orientation, stimulation intensity in both TMS and sham conditions. Since these studies found contrasting results, is still unsolved the question whether TEPs could reflect at least in part direct cortical activation. In addition, both studies used multimodal sham stimulation that combined simultaneous somatosensory and auditory inputs, which is important because it should mimic the combinations of sensations that TMS produces, while it is also important to apply these stimulations separately to quantify their respective impact on the resulting EEG potentials. Considering that investigating the origins of TEPs is fundamental to understanding how optimally use this technique to understand cortical physiology and pathophysiology of neurological disease, addressing these questions is crucial to understanding how to control sensory stimulation in TMS-EEG. Furthermore, the results of such an investigation will inform details of future experimental design, with specific focus on the utility and usefulness of including a sham condition in TMS-EEG studies.

The aim of this experiment is to understand the mechanism of TEP origins by investigating the contributions of possible confounding factors to the TEP waveform evoked from subthreshold stimulation over the M1. Specifically, instead of using sham stimulation which includes both auditory and realistic somatosensory stimulation, this

experiment compares a range of conditions with varying levels of isolated somatosensory and auditory contributions: TEPs obtained with real TMS stimulation with and without noise masking, pure auditory stimulation with and without noise masking, scalp electrical stimulation and sham coil stimulation. Furthermore, to better assess possible residual AEP during TMS due to incomplete suppression of the so-called "TMS-click", the responses obtained from pure AEP and masked TMS will be compared, as done previously (Conde et al., 2019).

With this approach, we sought to separate the contribution of SEP and AEP to the TEP waveform and understand to what extent noise masking and foam layer can minimized AEP and SEP. Generally, we hypothesized that while auditory and somatosensory stimuli would partially contribute to the TEP response, there would also be TEP components that are reflective of pure neuronal cortical activation that could be obtained and could be recognize from human M1 without need to use sham condition. The results of this experiment suggest that, at least for subthreshold stimulation of the M1 hand area, it is possible to obtain genuine brain responses by using appropriate masking of the “TMS click”; in this location, the somatosensory stimulation by the TMS pulse contributes only marginally to the TEP.

Materials and methods

Participants

Nineteen healthy right-handed individuals (Oldfield, 1971) (10 female, age: 29.7±4.2) were enrolled in the study. Participants had no history of neurological or psychiatric diseases and were not taking drugs active at the central nervous system level at the time of the experiment. All procedures were performed in accordance with the Declaration of Helsinki. Participants gave written informed consent prior to the experimental session.

Experimental design

Participants were sitting in a comfortable chair, in a quiet room, with forearms resting on a pillow placed on their lap. They were asked to fixate a white cross (6x6

cm) in the middle of a blank screen, to avoid eye movements during the EEG recordings. Participants wore earphones which, in some recording blocks (named "masked"), continuously played a masking noise, composed of white noise mixed with specific time-varying frequencies of the TMS click, to minimize the AEP (Massimini et al., 2005). Unlike most TMS-EEG studies, subjects also wore ear defenders (SNR=30) on top of the earphones, to further improve masking of the TMS click. The intensity of the masking noise was adjusted for each participant by increasing the volume (always below 90 dB) until the participant was sure that s/he could no longer hear the "TMS click" (Paus et al., 2001).

The experiment consisted of a single session in which participants underwent a total of 7 blocks of TMS-EEG recording, each consisting of 120 trials, organized as follows (Fig. 9): 1) stimulation with a standard TMS coil on a 5 cm thick pasteboard cylinder placed on the scalp without noise masking (TMS-AEP NOT MASKED; see below: responses in this block were similar to block 2, so it has not been used for statistical comparison); 2) stimulation with a sham coil on the pasteboard cylinder placed on the scalp without noise masking (AEP NOT MASKED); 3) stimulation with a sham coil on the pasteboard cylinder placed on the scalp with noise masking (AEP MASKED); 4) stimulation with a sham coil placed directly on the EEG cap with noise masking (SHAM); 5) stimulation with a standard coil directly on the EEG cap ad using noise masking (TEP MASKED); 6) stimulation with a standard coil placed on the cap without noise masking (TEP NOT MASKED) and 7) electrical stimulation of the scalp (ES). Standard procedures for collecting TEP involve responses generated from cortical stimulation, as well as from auditory and somatosensory components arising from the nature of TMS application. As a result, the conditions in this study were designed to inform about the contribution of auditory, somatosensory, and direct cortical activation to the TEP waveform by altering the somatosensory and auditory stimulation in the various blocks. The comparison between conditions where only auditory stimuli were provided, with or without noise masking, allowed the characterization of AEP and the extent to which AEP could be cancelled by nosie masking. Placing the sham col on the head ensured current was not induced, while investigating the potential influence of vibration arising when the TMS coil is placed directly on the head. Comparing standard TMS blocks with and without noise masking

allowed for the assessment of the contribution of AEP to the TEP and, importantly, allowed to investigate specifically which TEP components were influenced by AEP. Finally, the ES block was designed to investigate somatosensory responses to scalp stimulation.

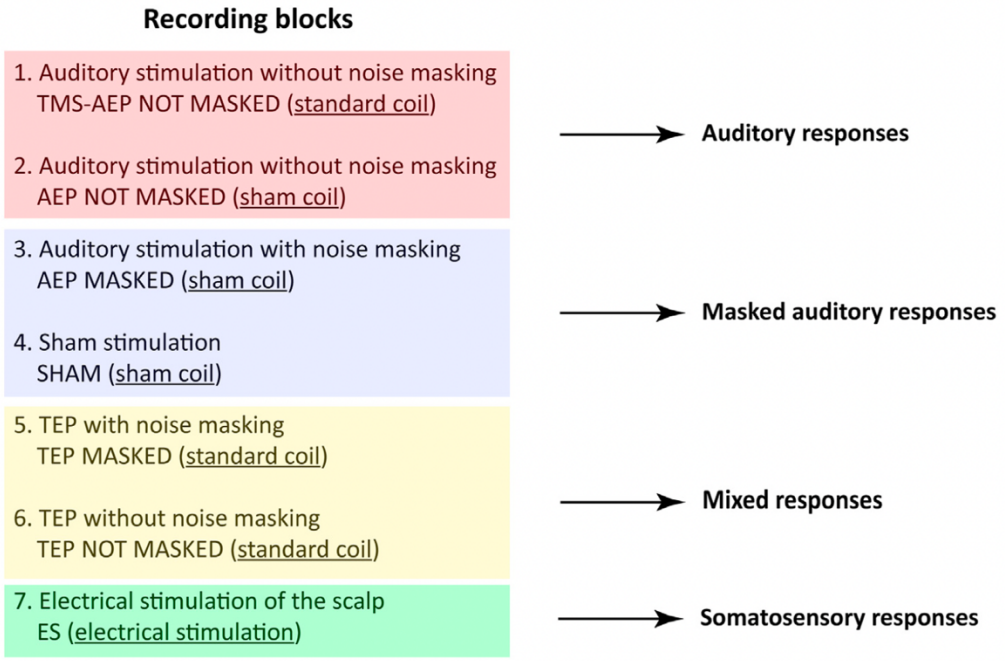

***Figure 9**: Diagrammatic representation of protocol's blocks*
See text for further details.

TMS-EMG

Single-pulse, monophasic TMS was delivered using a Magstim 200[2] device connected to a 70-mm figure-of-eight coil held with the handle backwards at 45° to the midline, inducing current in the posterior-anterior direction (Magstim Company Limited, Whitland, UK). Sham stimulation was delivered with a specialized sham coil (70 mm alpha sham coil, Magstim UK), which uses unique coil winding to impart a very small, shallow magnetic field and diverts part of the current to an inner device to produce the auditory click. Importantly, when placed on the EEG cap, the sham coil does not induce current in the brain, but retains the auditory component associated with standard coil. TMS was delivered over the cortical hotspot, defined as the site within M1 where TMS elicited the largest motor evoked potential (MEP) in the contralateral first dorsal interosseous (FDI) muscle. This location was sampled in MNI space, and the coil was maintained in the correct position throughout the stimulation

by using a Brainsight neuronavigation system (Rogue Research Inc, Montreal, Canada) coupled with a Polaris Spectra optical measurement system (Northern Digital inc, Waterloo, Canada). An estimated individualized MRI scan in the MNI space was used for all the participants. Resting motor threshold (RMT) was calculated as the lowest intensity of stimulator output that produced a MEP of at least 50μV in 5 out of 10 consecutive trials in the relaxed contralateral FDI (Rocchi et al., 2017; Rossini et al., 1994). When using the standard coil, the stimulation intensity was set at 90% RMT. In the recording blocks where the sham coil was used, the stimulation intensity was increased to match the sound generated by the standard coil. Surface EMG was recorded through a pair of Ag/AgCl 10 mm cup electrodes placed over the right FDI muscle in a belly-tendon montage using a Digitimer D360 (Digitimer Ltd. Welwyn Garden City, UK). Raw EMG signal was sampled at 5000 Hz, amplified (gain: 1000x), and bandpass filtered between 5 and 2000 Hz before being then digitally converted with a CED 1401 analog-to-digital laboratory interface (Cambridge Electronic Design). Loudness of the TMS click was assessed by each participant by means of a visual analogue scale (VAS) ranging from 0 (no perception) to 10 (maximal perception) in the recording blocks where auditory masking was used (AEP MASKED, SHAM, TEP MASKED), and a possible correlation between VAS scores and RMT was investigated by means of the Spearman's correlation coefficient. AVAS assessment was also done to assess discomfort due to stimulation, and all blocks were considered. A Friedman's ANOVA was performed to investigate possible difference in the two variables across different blocks.

Electrical stimulation of the scalp

Electrical stimulation of the scalp was performed using 10 mm Ag/AgCl cup electrodes. The electrode placement was chosen to approximate the location of the coil (hot spot position) and the direction of the current. In order to localize the position of the electrodes, the EEG cap was placed on the head, and measurements were made from Cz to the midpoint between electrodes C1, C3, CP1, and CP3 (anode) and Cz, FCz, C1, and FC1 (cathode). Stimulating electrodes were placed directly on the scalp and underneath the EEG cap at each of these locations. Care was taken to keep the recording electrodes in the middle of the described electrode clusters, to minimize

stimulation artefact. Electrical stimulation intensity was set to be similar to the intensity of somatosensory stimulation evoked by a single TMS pulse. In order to determine this intensity, first was found the electrical stimulation threshold (eST), defined as the lowest electrical stimulation intensity at which the participant could consistently perceive the electrical pulse (square-wave, 200 μs, Digitimer DS7A, Digitimer Ltd. Welwyn Garden City, UK). Next, TMS somatosensory threshold (tST), defined as the smallest TMS intensity at which the subject could consistently perceive the pulse, was measured. This was done with noise masking to ensure individuals were only focusing on the somatosensory feedback. Then, as TEP were evoked with a stimulation intensity of 90% RMT, we determined the ratio between the tST and 90% RMT, and this ratio was applied to the electrical stimulation. Therefore, the electrical stimulation intensity (eSI) was derived with the following formula: eSI = eST*[RMT*90/100)/tST]. The equation relies on the assumption that somatosensory perception scales linearly with changes in both TMS and electrical stimulation intensity, at least in the range of 90-100% RMT. Compared to other methods used in previous papers (Gordon et al., 2018; Conde et al., 2019), the present one has the advantage of calculating an individualized intensity for electrical stimulation which is not reliant on subjective matching of perceived somatosensory input from electrical and magnetic stimulation. At the end of the recording, participants were asked whether they could perceive any difference in the location or the subjective perception of stimulation intensity between the TMS blocks where the standard coil was used and the electrical stimulation.

EEG Recording and analysis

EEG was recorded using a DC-coupled, TMS-compatible amplifier (Actichamp, Brain Products, GmbH). Signal was recorded from 63 active electrodes mounted on a cap (actiCAP), in accordance with the international 10-10 system, including: Fp1, Fz, F3, F7, FT9, FC5, FC1, C3, T7, TP9, CP5, CP1, Pz, P3, P7, O1, FCz, O2, P4, P8, TP10, CP6, CP2, Cz, C4, T8, FT10, FC6, FC2, F4, F8, Fp2, AF7, AF3, AFz, F1, F5, FT7, FC3, C1, C5, TP7, CP3, P1, P5, PO7, PO3, POz, PO4, PO8, P6, P2, CPz, CP4, TP8, C6, C2, FC4, FT8, F6, AF8, AF4, F2. Recordings were online referenced to Oz and the ground electrode was placed on Fpz. In the offline analysis,

an average reference was used. Skin impedances were kept below 5 kΩ and the sampling frequency during recording was 5000 Hz. When required, in order to mask the TMS-induced noise and avoid possible AEPs, participants wore in-ear headphones continuously playing white noise mixed with specific time-varying frequencies of the TMS click (E P Casula et al., 2018; Rocchi et al., 2018a). Additionally, when the coil was in direct contact with the EEG cap, a 0.5 cm foam layer was placed underneath the coil to minimize bone conduction of the TMS click and scalp sensation caused by coil vibration. Offline EEG pre-processing was performed with EEGLAB 14.1.1 (Delorme and Makeig, 2004) with the addition of some functions included in the TMS-EEG signal analyzer (TESA) toolbox (Rogasch et al., 2017) and in Fieldtrip open source MATLAB toolbox (Oostenveld et al., 2011), all running in MATLAB environment (Version 2016b, MathWorks Inc., Natick, USA). EEG signal recorded during TMS was epoched (-1.3 to 1.3 s) and demeaned using a baseline from -1000 to -10 ms. The epochs were visually inspected and those with excessively noisy EEG were excluded (remaining epochs were on average 116.4 ± 2.37, ranging from 113 to 120). A Friedman's ANOVA was performed to verify that there were no significant differences in the number of residual epochs in different blocks. The TMS artefact was removed from -5 to 10 ms around the trigger and interpolated by means of a cubic function. At this point, a first independent component analysis (ICA) was run, using a fastICA algorithm. Only the 15 components explaining the largest variance were plotted, in a time window ranging from -200 to 500 ms, and those reflecting residual scalp muscle or decay were eliminated after visual inspection, based on time, frequency, scalp distribution and amplitude criteria (Elias P Casula et al., 2017; Rogasch et al., 2014, 2013). Albeit the use of ICA to remove these short-latency artefacts may lead to decrease of some of the TEP components, this effect has been demonstrated to be small (Elias P. Casula et al., 2017) and, despite this limitation, ICA is widely used for the removal of early TMS-EEG artefacts (Rogasch et al., 2014, 2013). ICA has also been used to remove artefacts caused by electrical stimulation of the scalp in an experimental setting similar to the present one (Gordon et al., 2018). After this, a band-pass (1-100 Hz) and a band-stop (48-52 Hz) fourth order Butterworth filter were applied. The signal was further epoched (-1 to 1 s) to reduce possible edge artefacts and a second round of fastICA was performed to remove residual artefacts

(e.g. eye blinks, continuous muscle activity, etc.). Lastly, EEG signals were referenced to the common average reference.

The TEP was first averaged in a cluster of electrodes surrounding the area of the stimulation (C1, C3, CP1, CP3) (Rocchi et al., 2018a). This allowed us to recognize the most common peaks described in the literature (N15, P30, N45, P60, N100, P200) (Hill et al., 2016) and to give a qualitative description of the signals at the stimulation site. We then calculated the global mean field power (GMFP), averaged across subjects, based on the following formula:

$$GMFP = \sqrt{\frac{[\sum_i^k (V_i(t) - V_{mean}(t))^2)]}{K}}$$

where t is time, K the number of channels, V_i the voltage in channel i and V_{mean} is the mean of the voltage in all channels (Lehmann and Skrandies, 1980a). To this purpose we used the recording obtained from block 6 (TEP NOT MASKED) since we anticipated that it would contain a larger signal compared to the other blocks, resulting from the sum of TEP, AEP and potentially SEP. Based on the GMFP waveform (Fig. 10), we selected three time regions of interest (ToI) for the following analysis (early: 15-65 ms; middle: 65-120 ms; late: 120-270 ms) as previously done (Conde et al., 2019). In each ToI we calculated map-based statistics using the whole set of electrodes. This approach was chosen to reduce bias due to the fact which TEP components can vary in terms of scalp distribution, the latter not necessarily corresponding to the stimulation site (Hill et al., 2016). We used a permutation statistic as implemented in Fieldtrip open source MATLAB toolbox (Oostenveld et al., 2011); correction for multiple comparisons was performed using a cluster-based algorithm (Maris and Oostenveld, 2007). We used t-tests for cluster-based statistics. To rank the found clusters, the sum of t values of all points in a cluster were computed. A p value of 0.05 was used to find clusters and the minimal number of channels per cluster was 1. The permutation was performed in the channel x time domains for the entire set of channels recorded and for the time intervals of interest. Corrected p values < 0.05 (two-tailed) were considered significant. By using the described procedure, in most of our analyses, we performed pairwise comparisons between the same ToIs of different conditions. In a further analysis, aimed to define the duration of significant activity in the TEP

MASKED condition, pairwise comparisons were performed between each ToI and a baseline of the same condition, of the same duration of the ToI compared and ending 5 ms before the TMS pulse.

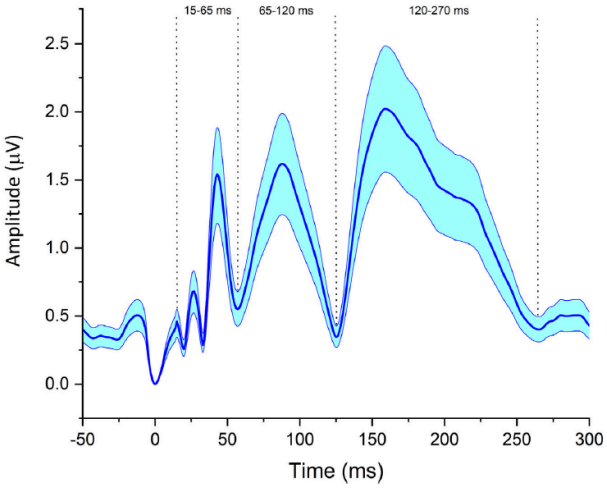

***Figure 10**: **GMFP across subjects in block 6 (TEP NOT MASKED)**. Dotted lines represent boundaries of chosen ToI(15-65 ms; 65-120 ms; 120-270 ms). Shadowing represents the standard error of the mean*

Two different correlation analyses were also performed, as described in a previous study (Conde et al., 2019). In the first, designed to assess similarity between conditions at the scalp map level, correlation coefficients were calculated for each electrode and were averaged in the same ToI described before (early: 15-65 ms; middle: 65-120 ms; late: 120-270 ms), plus for the global time window (15-270 ms). In the second analysis, designed to give a more accurate assessment of correlation in time, correlation coefficients were calculated in each time point and averaged across channels. In both analyses, the coefficients' z-transform (Fisher's z-transform) were averaged and subsequently inverse z-transformed. To assess statistical significance, correlation coefficients were compared with those calculated in a baseline ranging from -400 to -100 ms by means of paired t-tests with false discovery rate correction for multiple comparisons. The analyses were performed with two different metrics: the Spearman's correlation coefficient, and the concordance correlation coefficient (CCC). The former is the nonparametric version of the Pearson's correlation coefficient and essentially quantifies association between distributions, based on covariance (Bonita et al., 2014). The CCC is a form of intraclass correlation coefficient

optimally tuned to assess agreement between distributions and is calculated with the following formula:

$$CCC = \frac{2\sigma_{12}}{\sigma_1^2 + \sigma_2^2 + (\mu_1 - \mu_2)^2}$$

where σ_{12} is the covariance between two distributions, σ_x^2 is the variance of distribution x, and μ_x is the average of distribution x (Lin, 1989; King et al., 2007; Lewis J. Kerwin et al., 2018). By using this procedure, we computed correlation and concordance in three pairs of conditions: 1) TMS-AEP NOT MASKED vs AEP NOT MASKED, to investigate the similarity between the AEP generated by the standard and the sham coil; 2) AEP NOT MASKED vs AEP MASKED, to assess the effectiveness of AEP suppression by noise masking; 3) TEP MASKED vs AEP NOT MASKED, to check a possible relation between potentials putatively generated only by direct cortical activation and pure auditory responses.

Results

The test sessions were well-tolerated, no participants reported any side effects. Thresholds and stimulation intensities in the various blocks are summarized in Table 1.

	tST (% MSO)	TMS RMT (% MSO)	SHAM RMT (% MSO)	TMS/SHAM RMT	eST (mA)	eSI (mA)
AV	26.05	48.79	78.21	1.63	3.17	5.78
SD	4.18	9.66	12.32	0.03	1.09	2.20
SE	0.96	2.22	2.83	0.01	0.25	0.51

Table 1: Summary of stimulation parameters*. eST: electrical stimulation threshold; tST: TMS somatosensory threshold; eSI: electrical stimulation intensity, given by the formula eSI=eST*(RMT*90/100)/tST). AV = average; SD: standard deviation; SE: standard error.*

Real TMS pulses induced a known pattern of negative and positive deflections (E P Casula et al., 2018; Hill et al., 2016). Butterfly plots of time-domain signals and voltage scalp distributions maps for each block are reported in figure 11.

Overall, evoked activity in the middle and late ToI was observed when auditory stimulation only was delivered (blocks 1 and 2, rows A and B respectively). These

potentials were much smaller when the TMS click was masked (blocks 3 and 4, rows C and D respectively) and when only eletrical stimulation of the scalp was delivered (block 7, row G). A different pattern resulted when the standard coil was used, i.e., TEP in the early ToI were observed, with vertex potentials in late ToI being present only when noise masking was not used (blocks 5 and 6, rows E and F respectively). Subjects judged the location of TMS and electrical stimulation of the scalp to be roughly the same. Importantly, 10 subjects out of 19 reported that electrical stimulation resulted in stronger scalp sensation compared to TMS delivered with the standard coil, whereas the remaining 9 reported the opposite. Since there were no statistically significant differences between TMS-AEP NOT MASKED and AEP MASKED conditions, and the two showed very high correlation and concordance, only the latter (block 2) was used for further comparisons.

The Friedman's ANOVA performed on the number of residual epochs did not show significant effects ($\chi2(6) = 1.821$, $p = 0.935$). The VAS scores for the perceived click intensity were 0.42 ± 0.69 (range 0-2) for the AEP MASKED condition, 0.42 ± 0.61 for the SHAM condition (range 0-2), and 0.37 ± 0.68 for the TEP MASKED condition (range 0-2), with the Friedman's ANOVA again not showing a significant effect ($\chi2(2) = 0.286$, $p = 0.867$). There was a significant positive correlation, investigated with the Spearman's correlation coefficient, between the VAS score and RMT, in the three conditions where VAS for perceived click intensity was administered (AEP MASKED: $r = 0.563$, $p = 0.012$; SHAM: $r = 0.795$, $p < 0.001$; TEP MASKED: $r = 0.666$, p ¼ 0.002). Since the VAS scores for discomfort were 0 for all subjects in all blocks, no statistical analysis was performed.

Results of map comparisons and cluster statistics are reported in Table 2 and briefly described here. In some cases where a highly significant cluster was found in the location of interest (either the stimulation site or the vertex), a further significant cluster in the same ToI was noted in the surrounding electrodes; the latter reflects an opposite dipole due to the use of an average reference. For the sake of clarity in the presentation of the results and given that these additional clusters surrounding the ones over the area of interest did not add any meaningful information, so was not graphically represented it in Figure 12, which summarizes the findings.

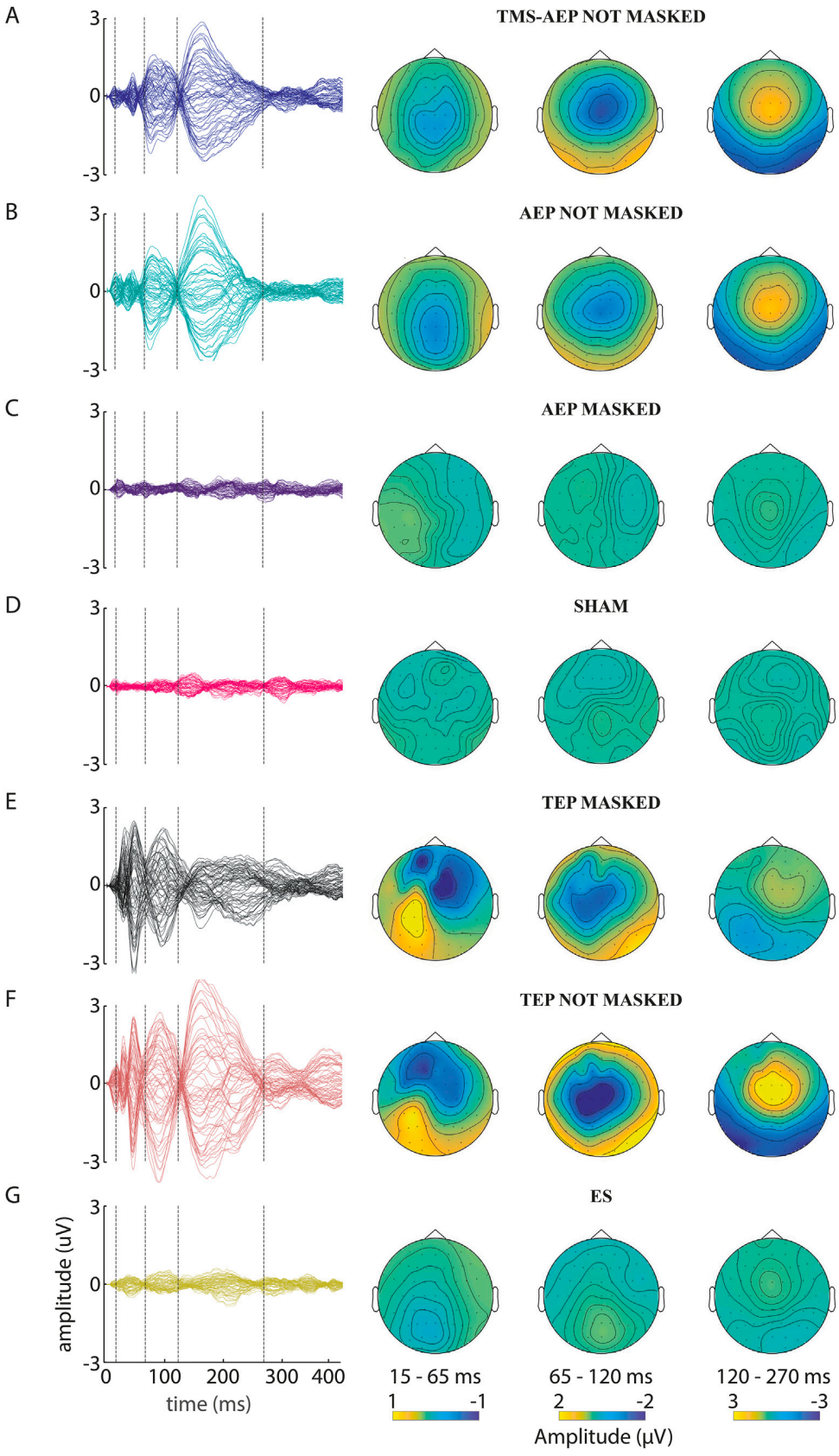

***Figure 11**: **descriptive summary of results**. First column represents butterfly plot of all subjects' averaged trial. Second to fourth columns represents voltage maps distribution in different ToI. Each of*

the seven rows correspond to a different recording block: (A: block 1, auditory stimulation, standard coil, no noise masking (TMS-AEP NOT MASKED); B: block 2, auditory stimulation, sham coil, no noise masking (AEP NOT MASKED); C: block 3, auditory stimulation, sham coil, noise masking (AEP MASKED); D: block 4, sham stimulation (SHAM); E: block 5, TMS, standard coil, noise masking (TEP MASKED); F: block 6, TMS, standard coil, no noise masking (TEP NOT MASKED); G: block 7, electrical stimulation, noise masking (ES).

Conditions compared	**Blocks compared**	**Cluster direction**	**Early ToI (ms, p value)**	**Middle ToI (ms, p value)**	**Late ToI (ms, p value)**
AEP NOT MASKED vs AEP MASKED	2 vs 3	Positive	-	65-120 ms p = 0.001	121-270 ms p = 0.001
		Negative	-	65-114 ms p = 0.001	121-264 ms p = 0.001
SHAM vs AEP MASKED	4 vs 3	Positive	-	-	-
		Negative	-	-	-
TEP MASKED vs AEP NOT MASKED	5 vs 2	Positive	16-57 ms p = 0.001	-	121-203 ms p = 0.001
		Negative	15-54 ms p = 0.001	-	121-203 ms p = 0.002
TEP MASKED vs TEP NOT MASKED	5 vs 6	Positive	-	65-106 ms p = 0.004	124-242 ms p = 0.001
		Negative	-	-	125-249 ms p = 0.001
TEP MASKED vs ES	5 vs 7	Positive	18-55 ms p = 0.001	67-120 ms p = 0.002	-
		Negative	18-59 ms p = 0.001	76-119 ms p = 0.009	-
SHAM vs ES	4 vs 7	Positive	22-54 ms p = 0.022	-	126-225 ms p = 0.005
		Negative	-	-	-
TEP MASKED vs BASELINE	5	Positive	17-65 ms p= 0.001	65-120 ms p=0.004	147-270 ms p=0.001
		Negative	17-54 ms p=0.001	72-108 ms p=0.004	191-264 ms p=0.015

Table 2: *summary of comparison results*

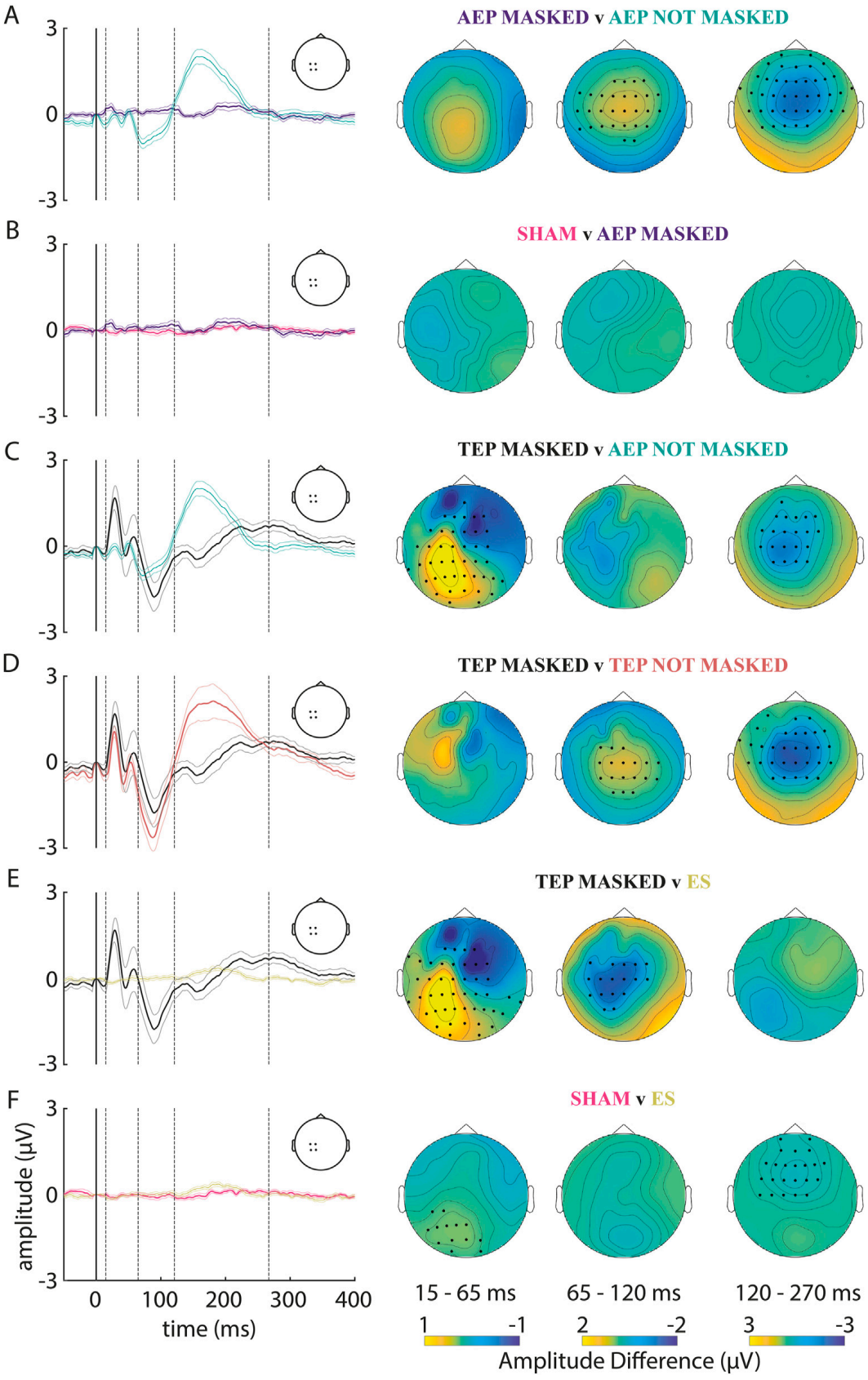

***Figure 12*: Comparisons of several stimulation blocks.** *The first column represents time-domain signals averaged across four channels corresponding to the stimulation site (C1, C3, CP1,*

CP3). Shadowing indicates standard error of the mean. Vertical dashed lines indicate separation of the three ToI (early: 15-65 ms; middle: 65-120 ms; late: 120-270 ms). Columns 2 to 4 illustrate comparisons between two blocks at a scalp map level, averaged across the three ToI. Black dots represent significant clusters, either positive or negative. Note that, for graphical reasons, only one cluster for each map is shown, i.e. the one corresponding to the area of interest. ***Row A****: comparison between AEP NOT MASKED (block 2, green line) and AEP MASKED (block 3, purple line) conditions. A significant positive cluster in the middle ToI (65-120 ms, p = 0.001) and a significant negative cluster in the late ToI (121-270 ms, p = 0.001) were found in the electrodes surrounding the vertex.* ***Row B****: comparison between SHAM (block 4, pink line) and AEP MASKED (block 3, purple line) conditions. No significant clusters were found.* ***Row C****: comparison between TEP MASKED (block 5, black line) and AEP NOT MASKED (block 2, green line) conditions. A significant positive cluster at the stimulation site in the early ToI (16-57 ms, p = 0.001) and a significant negative cluster around the vertex in the late ToI (121-203 ms, p = 0.001) were found.* ***Row D****: comparison between TEP MASKED (block 5, black line) and TEP NOT MASKED (red line, block 6) conditions. A significant positive cluster at vertex in the middle (65-106 ms, p=0.004) and late ToI (124 – 242 ms p= 0.001) and a significant negative cluster at vertex in late ToI (125-249 ms, p= 0.001) were found.* ***Row E****: comparison between TEP MASKED (block 5, black line) and ES (block 7, gold line) conditions. A significant positive cluster at the stimulation site in early ToI (18-55 ms, p=0.001) and middle ToI (67-120 ms, p=0.002) and a significant negative cluster at stimulation site in early ToI (18-59 ms, p = 0.001) and middle ToI (76-119, p=0.009) were found.* ***Row F****: comparison between SHAM (block 4, pink line) and ES (block 7, gold line). A significant positive cluster around vertex in early ToI (22-54 ms, p=0.022) and late ToI (126-225 ms, p=0.005) were found.*

AEP NOT MASKED vs AEP MASKED

When comparing AEP NOT MASKED and AEP MASKED conditions (blocks 2 and 3; figure 12, row A), no significant clusters were found in the early ToI, despite some very low amplitude responses in the central-posterior electrodes observed when noise masking was not used. In the middle ToI, a significant positive cluster was found in the central electrodes (65-120 ms, p = 0.001), with a negative one in the surrounding peripheral electrodes. In the late ToI, an inverse pattern was observed: a negative cluster in the central area and a positive one in the peripheral electrodes (121-270 ms, p = 0.001). This result indicates that a clear scalp potential due to TMS click is observed, including a negative peak around 100 ms and a positive peak around 200 ms, both distributed around the vertex. Importantly, these potentials could be effectively suppressed with noise masking.

SHAM vs AEP MASKED

In the comparison between SHAM and AEP MASKED conditions (blocks 4 and 3; figure 12, row B) no significant clusters were found. This means that in both conditions it was possible to effectively mask AEP by using white noise, and that the position of the coil (directly over the cap or separated by with by means of a pasteboard cylinder) did not lead to differences in recorded potentials.

TEP MASKED vs AEP NOT MASKED

TEP MASKED condition induced a different scalp response than AEP NOT MASKED (blocks 5 and 2; figure 12, row C). There was a significant positive cluster in the early ToI around the left central area, corresponding to the site of the stimulation (16-57 ms, $p = 0.001$), with a significant negative cluster in the surrounding electrodes, especially in the right frontal region. This corresponds to an early cortical activation at the TMS site, which was not present with auditory stimulation in the middle ToI, indicating a negative response around 100 ms due to TMS stimulation, this did not reach statistical significance. In the late ToI there was a large significant negative cluster at the vertex (121-203 ms, $p = 0.001$) and a large positive one in the peripheral electrodes, indicating a strong positive component at the vertex evoked by auditory stimulation. Overall, these findings indicate that standard TMS elicit early TEP components larger than auditory stimulation, whereas the late central positive component induced by the latter is not present when TEP are obtained during noise masking.

TEP MASKED vs TEP NOT MASKED

When comparing TEP MASKED and TEP NOT MASKED conditions (blocks 5 and 5; figure 12, row D), there were no significant clusters in the early ToI, meaning that early TEP components were not significantly affected by the TMS click. The middle ToI showed a significant positive cluster around the vertex (65-106 ms, $p = 0.004$), indicating a larger negativity when noise masking was not applied. In the late ToI there was a large significant negative cluster at the vertex (125-249 ms, $p = 0.001$) and a large positive one in the peripheral electrodes, indicating a strong positive component at the vertex evoked by auditory stimulation.

TEP MASKED vs ES

The comparison between TEP MASKED and ES conditions (block 5 and 7; figure 12, row E) resulted in a clear significant positive cluster in the early ToI around the left central area, at the site of the stimulation (18-55 ms, p = 0.001), with a negative cluster in the surrounding electrodes, especially in the right frontal region. In the middle ToI there was a large, significant negative cluster close to the stimulation site (76-119 ms, p = 0.009), surrounded by a significant positive cluster at the posterior periphery of the right hemisphere. This indicates that TMS, differently from electrical stimulation, was able to activate the cortex at the site of stimulation not just early after the stimulus but also around 100 ms. Notably, the latter activation is different from the negative peak around the same latency induced at the vertex by auditory stimulation. There were no significant clusters in the late ToI, again indicating that noise masking effectively suppressed the positive peak at the vertex around 200 ms.

SHAM vs ES

In the early ToI, the last contrast between SHAM and EP conditions (blocks 4 and 7; figure 12, row F) showed a weakly significant positive cluster in the posterior midline-left electrodes (22-54 ms, p = 0.022), reflecting a negative posterior activation present in the ES condition. There were no significant differences in the middle ToI, whereas in the late ToI we found a weakly significant negative cluster at the vertex (126-255 ms, p = 0.005), indicating a small positive component evoked by the scalp ES. It should be noted that the statistical significance of these clusters was weaker than those listed in the other comparisons and would not hold if a Bonferroni correction for multiple comparisons was applied to control for inflation of type I error.

TEP MASKED vs BASELINE

When comparing activity in each ToI with baseline in the TEP MASKED condition (Fig. 13), a significant positive cluster in the left central area, at the site of the stimulation was found, with a negative cluster in the right frontal region. The same analysis on the middle ToI showed a significant negative cluster close at the posterior periphery of the right hemisphere. In the late ToI, we observed a significant negative cluster in the left central-posterior electrodes and a significant positive one in the

central-anterior electrodes of the right hemisphere. Statistics are summarized in Table 2. Overall, significant and lateralized activity was observed in all the ToI, suggesting that direct brain activation due to TMS lasts for the whole-time window considered.

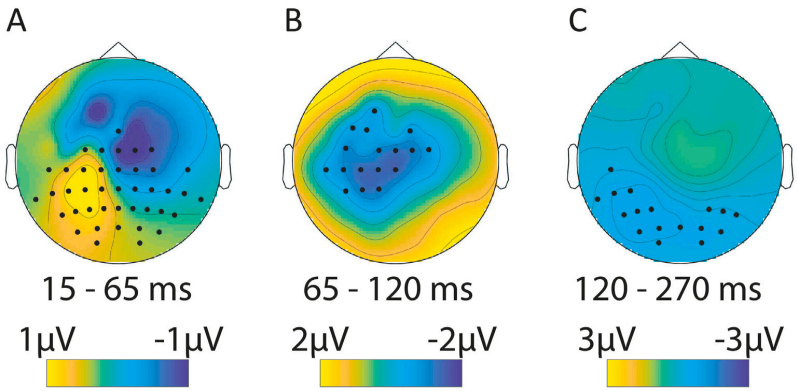

Figure 13*: Comparisons of activity in each ToI in the TEP MASKED condition with a baseline of the same condition**, *of the same duration of each ToI compared and ending 5 ms before the TMS pulse. Note that, for graphical reasons, only one cluster for each map is shown, i.e., the one corresponding to the area of interest.* ***Panel A*: early ToI. A significant positive cluster (17-65 ms, p = 0.001, plotted) and a significant negative cluster (17-54 ms, p = 0.001, plotted) were found.* ***Panel B****: middle ToI. A significant positive cluster (65-120 ms, p = 0.004) and a significant negative cluster (72-108 ms, p = 0.004, plotted) were found.* ***Panel C****: late ToI. A significant positive cluster (147-270 ms, p = 0.001) and a significant negative cluster (191 -264 ms, p = 0.015, plotted) were found.*

Correlation analysis

AEP obtained with the standard and sham coil (TMS-AEP NOT MASKED and AEP NOT MASKED conditions, blocks 1 and 2) showed statistically significant correlation (Fig. 14) and concordance (Fig. 15). In analysis 1, the correlation was clear in all three ToI, and particularly in the middle and late ones, where higher correlation and concordance values were found in electrodes around the vertex, corresponding to the main potentials following auditory stimulation (N100/P200). In analysis 2, significant correlation and concordance were obtained for time points ranging between 15 and approximately 250 ms, with islands of significance up to 400 ms. By contrast, AEP NOT MASKED, and AEP MASKED conditions (blocks 2 and 3) showed no correlation (Fig. 16) or concordance (Fig. 17); this suggests that auditory responses were effectively suppressed by noise masking and confirms the results obtained in the comparison between the two conditions. Similarity, there was no correlation (Fig.18) or concordance (Fig. 19) between conditions TEP MASKED, and AEP NOT

MASKED (blocks 5 and 2), indicating that potentials in the two blocks have independent sources; this further support the conclusion that AEPs were effectively suppressed by noise masking.

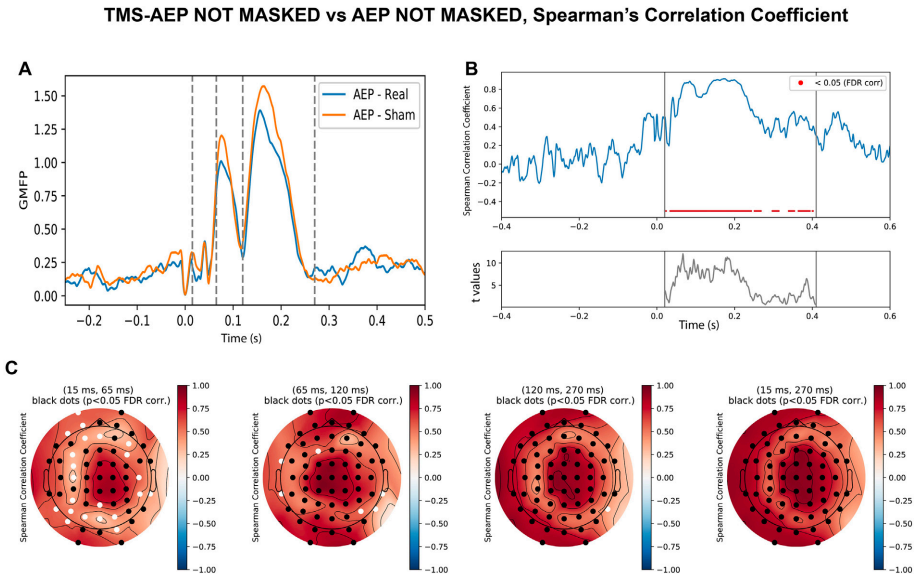

<u>Figure 14</u>: Similarity between conditions TMS-AEP NOT MASKED and AEP NOT MASKED, investigated with the Spearman's correlation coefficient. Panel A*: global mean field power of the two conditions (AEP - Real = TMS-AEP NOT MASKED; AEP - Sham = AEP NOT MASKED).* ***Panel B****: <u>upper chart</u>: correlation coefficient, averaged across all channels and calculated in each time point; the red bar shows statistically significant correlation between the two conditions, in the range of 15e400 ms. <u>Lower chart:</u> t statics.* ***Panel C****: correlation investigated in all electrodes, in four different ToI, one in each column (early: 15-65 ms; middle: 65-120 ms; late: 120-270 ms; global: 15.270 ms). Electrodes with statistically significant correlations are plotted in black, while those not showing statistically significant correlations are plotted in white.*

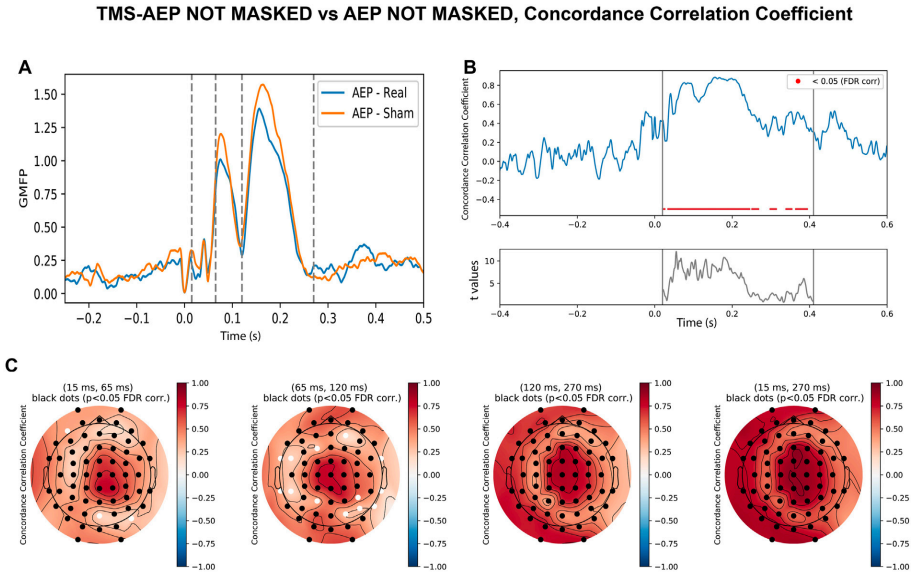

***Figure 15*: Similarity between TMS-AEP NOT MASKED, and AEP NOT MASKED, investigated with the concordance correlation coefficient (CCC). Panel A**: *global mean field power of the two conditions (AEP - Real = TMS-AEP NOT MASKED; AEP - Sham = AEP NOT MASKED).* ***Panel B**: upper chart: correlation coefficient, averaged across all channels and calculated in each time point; the red bar shows statistically significant correlation between the two conditions, in the range of 15-400 ms. Lower chart: t statics (see text for details).* ***Panel C**:correlation investigated in all electrodes, in four different ToI, one in each column (early: 15-65 ms; middle: 65-120 ms; late: 120-270 ms; global: 15.270 ms). Electrodes with statistically significant correlations are plotted in black, while those not showing statistically significant correlations are plotted in white.*

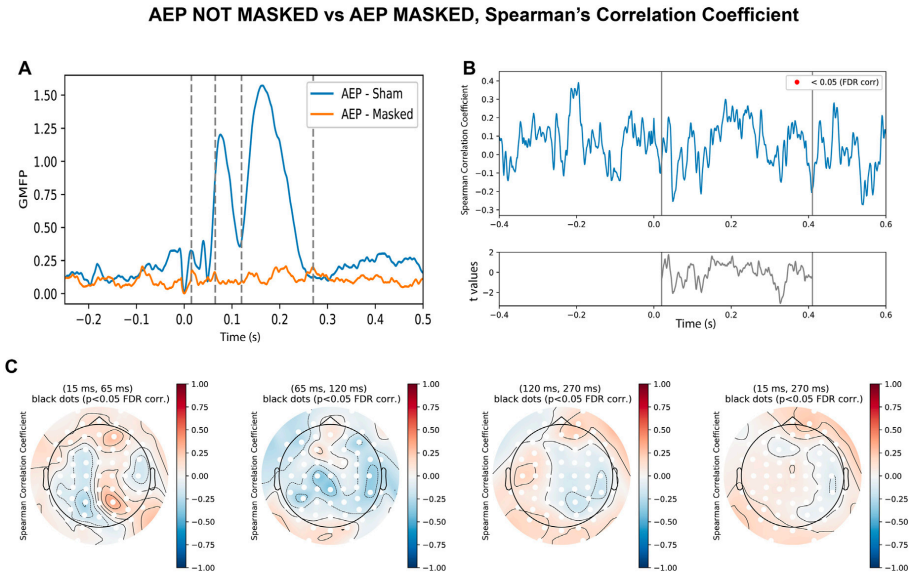

***Figure 16*: Similarity between conditions AEP NOT MASKED and AEP MASKED, investigated with the Spearman's correlation coefficient (CCC)t. Panel A**: *global mean field power of the two conditions*

(AEP - Sham = AEP NOT MASKED; AEP - Masked: AEP MASKED). ***Panel B:*** *upper chart: correlation coefficient, averaged across all channels and calculated in each time point; no statistically significant correlation was found. Lower chart: t statics.* ***Panel C****: correlation investigated in all electrodes, in four different ToI, one in each column (early: 15-65 ms; middle: 65-120 ms; late: 120- 270 ms; global: 15.270 ms). Electrodes with statistically significant correlations are plotted in black, while those not showing statistically significant correlations are plotted in white.*

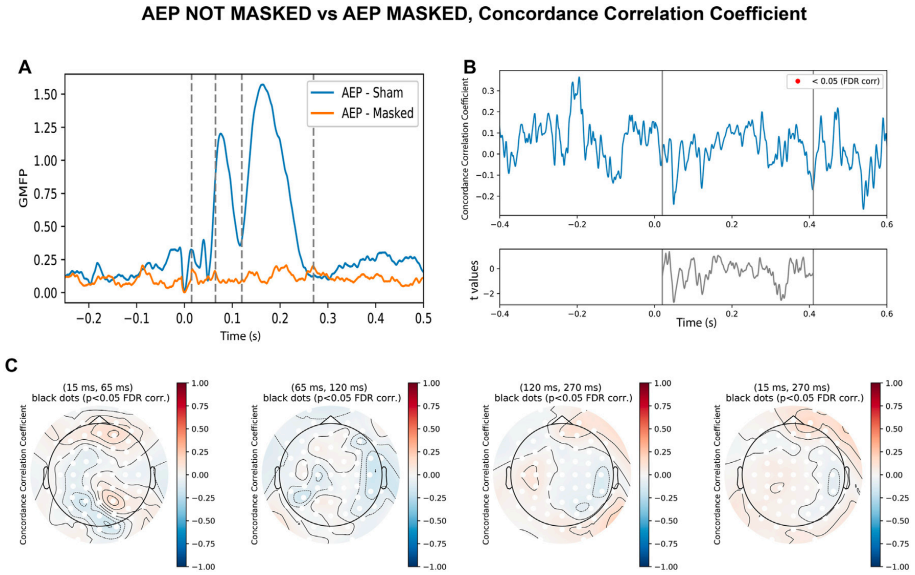

Figure 17*: Similarity between conditions AEP NOT MASKED and AEP MASKED, investigated with the concordance correlation coefficient.* ***Panel A****: global mean field power of the two conditions (AEP - Sham = AEP NOT MASKED; AEP – Masked = AEP MASKED).* ***Panel B****: upper chart: correlation coefficient, averaged across all channels and calculated in each time point; no statistically significant correlation was found. Lower chart: t statics.* ***Panel C****: correlation investigated in all electrodes, in four different ToI, one in each column (early: 15-65 ms; middle: 65-120 ms; late: 120-270 ms; global: 15.270 ms). Electrodes with statistically significant correlations are plotted in black, while those not showing statistically significant correlations are plotted in white.*

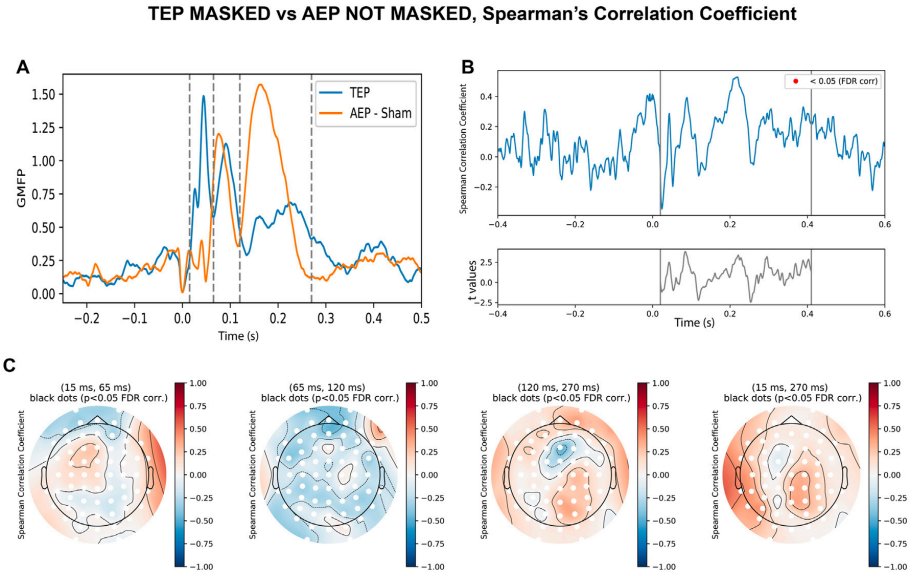

Figure 18*: Similarity between conditions TEP MASKED and AEP NOT MASKED, investigated with the Spearman's correlation coefficient. Panel A**: *global mean field power of the two conditions (TEP = TEP MASKED; AEP e Sham = AEP NOT MASKED).* ***Panel B: *upper chart: correlation coefficient, averaged across all channels and calculated in each time point; no statistically significant correlation was found. Lower chart: t statics.* ***Panel C***: *correlation investigated in all electrodes, in four different ToI, one in each column (early: 15-65 ms; middle: 65-120 ms; late: 120-270 ms; global: 15.270 ms). Electrodes with statistically significant correlations are plotted in black, while those not showing statistically significant correlations are plotted in white.*

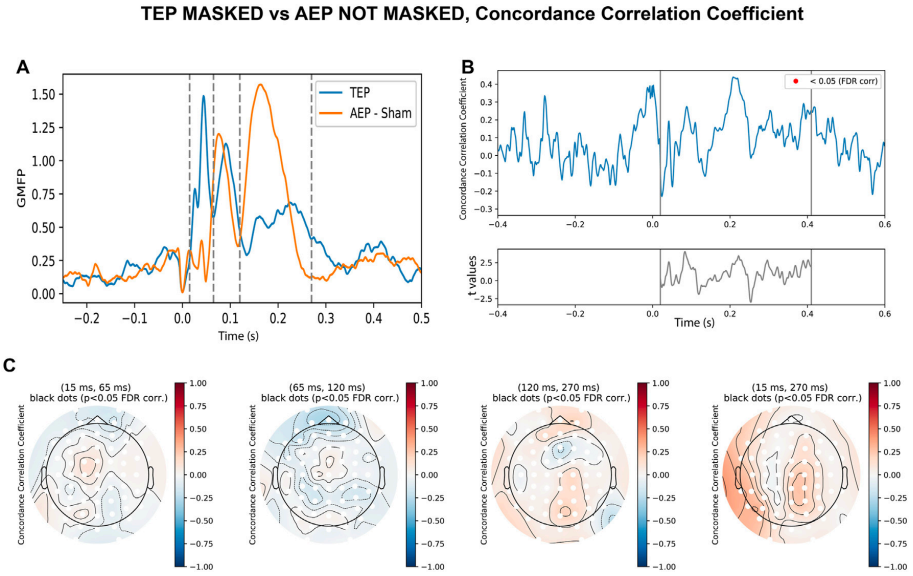

Figure 19*: Similarity between conditions TEP MASKED and AEP NOT MASKED, investigated with the concordance correlation coefficient (CCC). Panel A:** *global mean field power of the two conditions (TEP = TEP MASKED; AEP e Sham = AEP NOT MASKED).* ***Panel B: *upper chart: correlation*

coefficient, averaged across all channels and calculated in each time point; no Statistically significant correlation was found. Lower chart: t statics (see text for details). Panel C: correlation investigated in all electrodes, in four different ToI, one in each column (early: 15-65 ms; middle: 65-120 ms; late: 120-270 ms; global: 15.270 ms). Electrodes with statistically significant correlations are plotted in black, while those not showing statistically significant correlations are plotted in white.

Discussion

The aim of this experiment is to separately assess EEG responses due to auditory and somatosensory stimulation produced by TMS, and therefore to measure their impact on the TEP. Overall, we found that standard TMS evoked a clear and pronounced early cortical activity at the stimulation site, which was not contaminated by AEP, provided that appropriate masking of the TMS click is performed. A negative peak around 100 ms was observed close to the stimulation site, which was not suppressed by noise masking and likely represents another direct cortical response. Auditory stimulation alone induced potentials between 100 and 200 ms; however, it was possible to suppress these components by appropriate noise masking. Electrical stimulation of the scalp alone did not induce SEP, as one would have expected if there had been substantial activation of the somatosensory pathways. Overall, our data suggest that, by careful control of confounding sources, it is possible to obtain a good estimate (over the first 300ms or so) of the "true" genuine brain responses produced by TMS on M1. These responses show a high degree of lateralization, whereas responses distributed around the vertex mostly derive from indirect brain activation caused by auditory and somatosensory input.

Contribution of auditory stimulation to the TEP

The first interesting finding of this study is the clear definition of scalp responses generated by the "TMS-click". AEP are generally described in terms of early, middle, and late, based on their latency. The early ones reflect brainstem activation; they last for a few ms after the stimulation (Picton et al., 1974) and are not considered here, since pre-processing of TMS-EEG data usually implies removal of such an early time window (Farzan et al., 2016; Rogasch et al., 2014). Using both a standard and sham coil, we reproduced a known pattern of middle- (N15, P30, N40, P50) and late-latency auditory responses (N100, P200) (ter Braack et al., 2015;

Nikouline et al., 1999). Since the two sets of responses showed no significant differences and exhibited very high and significant correlation and concordance values, we propose that, at least in this context, psychophysically matched sound intensity is the most important factor in the generation of AEP, regardless of the coil used. Interestingly, with noise masking, middle- and late-latency AEP were suppressed. This demonstrates that, when using an intensity of 90% RMT over M1, with an accurate noise masking, it is possible to obtain TEPs which are not contaminated by AEP. Additionally, the same result was obtained in the sham condition, where the coil was laying directly over the EEG cap. This means that bone conduction of sound was effectively suppressed using the foam layer, as demonstrated in a previous report (ter Braack et al., 2015). Moreover, recent evidence suggests that each sound peak corresponds to mechanical vibrations of the TMS coil, which in standard TMS coils are known to be driven by the Lorentz forces which are proportional to the squared TMS coil current, and hence have their spectral power peak at double the coil's current frequency (Koponen et al., 2020, 2021). Theoretically, but this was not proven before, it is possible that these coil vibrations could induce an evoked potential on EEG signal. However, in our SHAM condition, we did not evoke a clear EEG potential, suggesting that these coil vibrations were effectively suppressed by our masking procedures.

The contribution of the AEP on the TEP was clarified by two other observations. The first comes from the comparison between TEP obtained by using a standard coil with noise masking and pure auditory stimulation without noise masking. In this case, it was clear that standard TMS elicited larger early responses, especially the P30 peak; while the pure auditory stimulation induced a very small amplitude early responses, but substantial N100 and P200 components around the vertex. This is confirmed by the comparison between the TEP obtained using the standard coil, with and without noise masking. Here, there was no difference in the components earlier than 60 ms, and again this makes it unlikely that they received a significant contribution from the AEP. The N100 was larger and located in the midline central electrodes when no noise masking was used; by contrast, the N100 present in the block with noise masking is smaller and lateralized in correspondence of the stimulation site (as can be further noticed in the comparison between TEP with noise masking and

electrical stimulation of the scalp). Finally, the central P200 is present only when no noise masking was used. Overall, the present data demonstrate the presence of two distinct negative peaks, around 100 ms, that likely involve different mechanisms. The first is localized close to the stimulation site and likely reflects direct cortical activation by TMS; the second, by contrast, has a wider distribution around the vertex and is followed by a P200 with the same distribution. This conclusion is based on several independent arguments: a) the auditory N100 is suppressed by noise masking, as indicated by the significant difference (Fig. 12, row A) and by the absence of correlation or concordance (Figs. 16 and 17) between AEP MASKED and AEP NOT MASKED conditions. By contrast, the TMS N100 is not suppressed by noise masking, as it is present in a condition where masking noise is used (TEP MASKED); b) the auditory N100 is always followed by a vertex P200 (Fig. 3, rows A and B), whereas the TMS N100 is not (see TEP MASKED condition); c) the latency of the TMS N100 is significantly longer than that of the auditory N100; d) there is no correlation or concordance between conditions TEP MASKED and AEP NOT MASKED (Figs. 18 and 19). This finding suggests that the N100 observed in the TEP MASKED condition was not significantly contaminated by the AEP. In conclusion, considering previous literature, it is likely that the N100 found at the stimulation site reflects direct cortical activation by TMS (Hill et al., 2016), whereas the central N100 and P200 represent saliency-related multimodal responses (SRMR), which are non-specific responses, possibly linked to arousal and/or attentional reorientation following an external stimulus, regardless of its modality (Mouraux and Iannetti, 2009).

Our set of results appears different from those obtained by Conde and co-workers (Conde et al., 2019) who found a substantial correlation between cortical responses obtained by using a standard coil and those following a “realistic sham” stimulation, similar to the one used here. A possible reason for this is that masking of the TMS click was more effective in the present study: indeed, in the paper by Conde and coworkers, VAS scores for residual TMS click were much higher than in the present study (respectively up to 3.82 on average, with values of 8 in some subjects, against an average of 0.42, with maximal individual values of 2). At least part of this difference might be due to the use, in our study, of ear defenders on top of the earphones playing the masking noise, which probably helped in suppressing the AEP.

Contribution of electrical stimulation of the scalp to the TEP

It has previously been suggested that somatosensory activation due to TMS could contribute to the TEP waveform. However, previous reports (Gordon et al., 2018; Conde et al., 2019) were focused on the impact of simultaneous somatosensory and auditory stimulation on TEP, and did not assessing the possible effects of electrical stimulation alone, the latter represent a novel contribution of this experiment. To the best of our knowledge, only one study previously described responses induced by scalp electrical stimulation. However, only one subject was tested, and details of the stimulation, such as intensity and location, were not mentioned (Paus et al., 2001); thus, a comparison with the present findings is difficult. An advantage of our protocol is that we measured individual thresholds for electrical stimulation and scaled the stimulation intensity according to the ratio between somatosensory and motor thresholds to TMS, in an attempt to give an electrical pulse which, in terms of intensity, closely resembled the intensity perceived with TMS. The attempt was successful and confirmed by the fact that participants were evenly split over whether they perceived the electrical stimulus to be stronger or weaker than the TMS. Electrical stimulation of the scalp alone elicited a very small response compared to other blocks where standard TMS was used (Fig.11 and 12). When compared to sham stimulation, there was significantly weak activation in the posterior electrodes in the early ToI, around 40 ms. This probably represents a resetting of the resting alpha rhythm, as observed with stimuli of other sensory modalities (Brandt, 1997). The second weak potential was found in comparison to sham, represented by a positivity around 200ms in the central electrodes. Again, this is interpretable as SRMR (Mouraux and Iannetti, 2009), although its amplitude was considerably less than from auditory stimulation. We can conclude that a positive wave recorded around 180-200 ms and distributed around the vertex represents a SRMR due to peripheral input (Mouraux and Iannetti, 2009); thus, it is shared by several of the experimental conditions in our work (Fig. 11). This finding is also in line with a previous report, where a similar vertex activation was found with electrical stimulation in the shoulder region (Biabani et al., 2019). It is very important to note that EEG responses following electrical stimulation of the scalp were not observed at the site of stimulation. This was expected since the intensity necessary to obtain direct cortical responses with electrical stimulation is much higher than that

used here (Day et al., 1989). We also did not obtain SEP, making it unlikely that the potentials observed were due to activity in the somatosensory cortex. This is not surprising considering that EEG signals following stimulation in the cranio-facial region are difficult to obtain. Clear SEP has been observed only by stimulating branches of the trigeminal nerve with needle electrodes (Leandri et al., 1985; Zhu et al., 2017), different from TMS, where stimuli are not applied on a nerve trunk. Secondly, the somatosensory threshold at the scalp level is much higher compared to other body areas, due to the low density of cutaneous receptors (Mehrabyan et al., 2011). For these reasons, we believe that our electrical stimulation was not sufficient to elicit a synchronous afferent volley large enough to elicit a SEP.

Limitations

It is important to note that the present results have been obtained using a 90% RMT stimulation intensity. The use of a higher intensity might lead to changes in the TEP waveform due to incomplete suppression of AEP by noise masking and the introduction of reafference potentials that accompany peripheral EMG activity; thus, caution should be used in extending the present results to different experimental conditions, such as stimulation of different scalp sites and the use of larger currents. Additionally, stimulation of peripheral nerves supplying the scalp by the sham coil used in the present paper is not comparable to that induced by the standard coil; hence, the need to control for somatosensory activation by using electrical stimulation of the scalp in several recording blocks. Finally, the present work relies on the assumption that ICA can be used to remove artefacts associated to TMS stimulation, with reasonable preservation of the underlying EEG signal. While this approach has theoretical limitations, its applicability has been empirically demonstrated (Rogasch et al., 2014, 2013). It should also be noted that TMS applied over M1, as in the present work, results in a substantial artefact due to scalp muscle activation, which needs to be removed to properly assess the TEP. ICA has proven to be efficient to achieve this and, importantly, other methods have not been shown to be definitely superior (Rogasch et al., 2014; Biabani et al., 2019). As a consensus on the matter has yet to be reached (Tremblay et al., 2019), further studies comparing and validating different approaches to TMS-EEG artefacts removal are certainly warranted.

Conclusion

In conclusion, the data from this experiment suggest that, when TMS is applied over M1 with an intensity slightly lower than motor threshold, it is possible to obtain genuine cortical EEG responses which are lateralized, specific for the stimulation site and last about 300 ms, provided that procedures to minimize indirect cortical activation (noise masking and foam layer) are properly adopted. These responses include a positive peak around 30 ms, a negative one around 100 ms, and a shallower negativity peaking around 250 ms, whereas other TEP components appear less reliable. This topography is replaced by non-specific central components (in particular, a prominent positivity around 200 ms) in conditions where the brain is only indirectly activated by peripheral stimulation (AEP NOT MASKED, TMS-AEP NOT MASKED, ES and control experiments listed in the Supplementary Material). The same pattern becomes prominent when TMS is performed with a standard coil, without noise masking (TEP NOT MASKED condition). Thus, sensory evoked components, if present, are associated with a late, negative-positivewaves with symmetrical central distribution, compatible with a SRMR (Mouraux and Iannetti, 2009). Importantly, these components, particularly the auditory N100, can contaminate signals generated by direct brain activation, if masking procedures of sensory stimulation are not carefully applied.

Experiment 2 - TMS-EEG using to directly test cerebellum-cerebral connectivity: the cerebellar TMS-evoked potentials

TMS-EEG could be a fundamental tool to thoroughly explore connections between remote cortical areas (e.g. cerebellum-cortical pathway) and provide new insights into the functional relationship among motor and non-motor pathways. In addition, cerebellar control are involved in preparation of movement and non-motor behaviours, including cognition and emotion (Strick et al., 2009; Strata, 2015; Benagiano et al., 2018). Therefore, as explained in Chapter 1, CBI, which is an inhibitory index of M1 suppression following contralateral cerebellar TMS stimulation, is restricted to the cerebellum-M1 connection and did not give us insight into connectivity to other cortical non-motor areas. For this reason, in the last years cerebellar TMS-EEG arise as a powerful tool to assess cerebellar-cerebral connectivity, although as discussed in Chapter 1, further studies are needed to standardize and better qualify these responses.

In recent decades a variety of human neuroimaging techniques (e.g., structural and functional magnetic resonance imaging (MRI); magnetoencephalography (MEG); EEG and other neurophysiological tools have been used to investigate interactions between the cerebellum and cortical areas (Allen et al., 2005; Hallett et al., 2017; Du et al., 2018; Fernandez et al., 2021; Sasaki et al., 2022). However, each method has its limitations. For instance, brain imaging techniques are associated with high costs and low temporal resolution and cannot directly infer the directionality of changes in cerebellar activity. Scalp-recorded EEG and EMG have poor resolution electrical activity of the cerebellum because it is located far from the scalp surface. On the other hand, as briefly explained in the Chapter 1, paired-pulse TMS can test the cerebellocortical pathways at ms resolution using CBI (see Chapter 1) (Ugawa et al., 1995; Spampinato et al., 2021). These studies have examined changes in cerebellar-M1 connectivity during movement as well as before and after cerebellar-dependent motor learning. However, CBI is limited to cerebellum-M1 connectivity and alternative approaches are needed to probe connectivity to other non-motor areas of the brain. Indeed, as discussed in detail in Chapter 1, MEP is used to quantify

excitability of M1 which reflecting the activity of corticospinal tract and may not represented a comprehensive measure of cerebral responsiveness to cerebellar stimulation. Instead, coupling TMS with EEG recordings may be a better tool to quantify global responses to cerebellar stimulation and connectivity to motor and non-motor areas. As mentioned in the previous chapters, TMS-EEG combines high temporal resolution (ms) of cortical excitability with a high spatial resolution and allows to record TEP.As already mentioned in Chapter 1, a few studies have provided preliminary evidences for integrating cerebellar TMS and EEG concurrent registration (Fernandez et al., 2021; Gassmann et al., 2022; Sasaki et al., 2022). These studies have shown promising results that suggest it is feasible to record TEPs and oscillatory activity following cerebellar stimulation, albeit with some differing results due to the selection of control conditions and stimulation parameters. One of the major issues across these studies is the lack of evidence showing whether signals recorded from TMS-EEG are sensitive to behaviors that involve cerebellar-cortical interactions. Thus, the aim of the present experiment it to further characterize EEG responses produced by cerebellar TMS and test whether any components of the response are changed by a visuomotor adaptation task known to depend on cerebellar function (Koch et al., 2020; Spampinato and Celnik, 2021; Tzvi et al., 2022). The hypothesis is that since this type of task changes CBI, it would also affect the cortical response to cerebellar stimulation and aid to separate the activity evoked by cerebellar outflow activation from the artefactual activity produced by sensory input associated with the discharge of the TMS coil. Given that double-cone (DC) coil is the only type that produce reliable CBI in healthy subject, DC coil was used in this experiment to stimulate cerebellum. The data of this experiment showed that the main signature of cerebellar TEPs (cbTEPs) is a positive component peaking around 80ms in the prefrontal area contralateral to the stimulated cerebellar hemisphere. This wave was side-specific, was not elicited by sensory stimulation alone and was modulated by the visuomotor adaptation task. Overall, this evidence suggests that it may be possible to probe cerebellar-cortical connections with TMS-EEG.

Materials and Methods

Participants

Thirty-two right-handed (Oldfield, 1971) (26.5 ± 7.6 years old, 15 male and 17 female) individuals without any history of neurological or psychiatric diseases, and who were not taking drugs active at the central nervous system, participated in the study after providing written informed consent. All experimental procedures were in accordance with the Declaration of Helsinki and followed international safety guidelines for non-invasive brain stimulation.

Experimental design

As described in the previous experiment, during the experimental sessions recorded at rest, participants were seated in a comfortable chair in a quiet room, with their forearms resting on a pillow placed on their lap. For the experimental sessions that involved the motor task, subjects sat on a comfortable chair of suitable height and controlled a robot arm with their right arm. During TMS-EEG recordings, participants were instructed to fixate on a white cross displayed on a computer screen to prevent excessive eye movements. To mask the TMS-induced noise and minimize possible AEPs, participants wore earphones (MDR-EX110LP, Deep Bass Earphones, Sony, Japan) that continuously played a masking noise composed of white noise mixed with specific time-varying frequencies of the TMS click (ter Braack et al., 2015) (Biabani et al., 2019; E. P. Casula et al., 2018; Fernandez et al., 2021; Massimini et al., 2005; Rocchi et al., 2018b). The volume of the masking noise was adjusted for each participant by increasing the intensity until the TMS click could not be heard or to the maximum tolerated level (always below 90 dB) (E. P. Casula et al., 2018; Massimini et al., 2005; Rocchi et al., 2018b).

Four different experiments were performed. Experiments 1, 2, and 3 involved resting state recordings of cbTEPs. These were designed to investigate the effects of cerebellar stimulation on EEG signals recorded from the whole scalp and to isolate the contribution of direct cerebellar stimulation from that of pure sensory input e.g. air-

and bone-conducted auditory stimulation (ABCAS), scalp skin sensation and somatosensory input mimicked by electrical stimulation (ES) generated in the context of a cerebellar TMS pulse. Experiment 4 assessed changes in cbTEPs prior to and following different stages of a visuomotor learning task known to depend on cerebellar function (Spampinato and Celnik, 2021).

Twenty-five subjects (27.4 ± 6.5 years old, 12 female), were enrolled in Experiment 1, designed to assess EEG responses over the whole scalp after TMS pulse either to the left or right cerebellar hemisphere (respectively LCS and RCS), in two separate recording blocks. In each block, CBI was also measured from the first dorsal interosseous muscle (FDI) to calibrate the TMS intensity to effectively activate cerebello-cortical projections. To minimize subjects' discomfort and coil overheating, each block was separated into three parts, as previously done by Sasaki and colleagues (Sasaki et al., 2022)

In Experiment 2, ABCAS was tested in 14 subjects (27.7 ± 7.7 years old, 9 female) by holding the DC coil over a 5 cm rigid pasteboard cylinder which allow to avoid directly stimulating the scalp (as performed in previous experiment, see previous chapter). Twenty subjects (28.1 ± 6.7 years old, 9 female) were enrolled in Experiment 3, designed to mimic the broad muscle contraction induced by right cerebellar TMS; this was done by administering electrical stimulation (ES) simultaneously over the right masseter and trapezius muscles with two sets of electrical stimulators, as described by Gassmann and co-worker (Gassmann et al., 2022)

Finally, a total of 14 subjects (25.6 ± 8.7 years old, 8 female) were tested in Experiment 4. First, a stimulation intensity to elicit reliable CBI was found. Then, RCS cbTEPs was delivered at 3 different stages of a visuomotor learning task: prior to baseline training (PreBase), after baseline training (PostBase) and after adaptation (PostAd) (Fig.20). In all the experiments above, each condition consisted of 100 TMS pulses, delivered at an ITI of 5 s ± 10%.

After each session, were asked to quantify loudness of the TMS click after RCS and ABCAS, intensity of muscle twitch after RCS and ES, and discomfort by RCS (Experiment 1 and 4) by means of a visual analog scale (VAS) with values ranging from 0 to 10 (absent to maximal perception).

Cerebellar transcranial magnetic stimulation and auditory stimulation

Cerebellar stimulation was performed with a 110 mm DC coil (Rocchi et al., 2019; Ugawa et al., 1995) (Magstim, Whitland, Dyfed, UK), located 3 cm lateral to the inion (Di Biasio et al., 2015; Monaco et al., 2018; Werhahn et al., 1996), such that current was induced upwards in the neural tissue to provide reliable and reproducible CBI(Fernandez et al., 2018; Hardwick et al., 2014; Spampinato et al., 2020). Stimulation intensity was based on brainstem active motor threshold (AMT_{BS}) (Ugawa et al., 1995), defined as the minimum intensity able to elicit a MEP of at least 50 μV amplitude in the right preactivated the FDI muscle (i.e., during 10% of maximal voluntary contraction), with pulses given over the inion (Galea et al., 2009; Spampinato et al., 2020). The intensity used for cerebellar stimulation was AMT_{BS} minus 5% of the maximal stimulator output (MSO) (AMT_{BS}-5%) (Schlerf et al., 2015; Ugawa et al., 1995). Twelve participants had measurable AMT_{BS} (37.5% of all participants, averaged AMT_{BS}: 66.7 ± 6.5% MSO); in those in which AMT_{BS} could not be obtained, we used the maximum tolerable intensity for cerebellar TMS – 5% MSO (maximum 80%).

ABCAS was performed by using the same DC coil used for cerebellar stimulation, with the same cerebellar intensity in experiment 1. A 5 x 5 x 15cm wooden rigid cuboid was placed between the DC coil and scalp to create 5cm gap.

Electrical stimulation

To mimic the contraction and somatosensory input of neck and jaw muscles induced by DC coil RCS, ES was simultaneously applied over the right masseter and trapezius muscles. For each muscle, stimulation was delivered over the middle of the muscle belly in a bipolar fashion using Ag/AgCL cup electrodes. Electrodes were connected to a constant-current stimulator (DS7A, Digitimer Ltd, Welwyn Garden City, UK); monophasic square wave pulses of 200 μs duration were used. Stimulation intensities were set to produce a muscle twitch which participants subjectively judged to be matched to that generated by RCS, as in previous work (Conde et al., 2019).

Behavioural task

The behavioural task was performed on a three-degree of freedom manipulandum (3DOM) robotic interface (Klein et al., 2014). Participants sat on a chair with their forehead supported on a headrest. Their semi-pronated right hand gripped a manipulandum located underneath a horizontally suspended mirror. The mirror prevented direct vision of the hand but showed a reflection of a computer monitor mounted above that appeared to be in the same plane as the hand. Visual display of the hand was translated as an on-screen white circle cursor (0.5 cm in diameter) representing the hand, as well as a small white square target (0.7cm x 0.7cm) and a white home square (1.0cm x 1.0cm). In each trial, participants were instructed to control the cursor to make a fast-shooting movement through the presented target, thus preventing any online corrections. When the cursor passed through the invisible boundary circle (invisible circle centered on the starting position with an 8 cm radius), the cursor was hidden, and participants were instructed to move back to the home square. Both the hit angle and target angle were recorded in each trial, and the angular error was calculated by the hit angle subtracting the target angle. Targets were displayed pseudo-randomly in one of eight positions located at 25, 65, 115, 155, 205, 245, 295 and 335 degrees around the white home square.

The task was delivered during Experiment 4 and consisted of 5 blocks of 96 trials each. In the first two blocks (baseline training), participants were provided with online visual and end-point error feedback relative to the target position. In the following two blocks, a 30-degree anticlockwise rotation was imposed on the visual cursor that required participants to adapt their movements to hit the target accurately (adaptation). In the fifth block, the visual manipulation and visual cursor were removed to determine if individuals had learned the rotation (no vision) (Fig. 20).

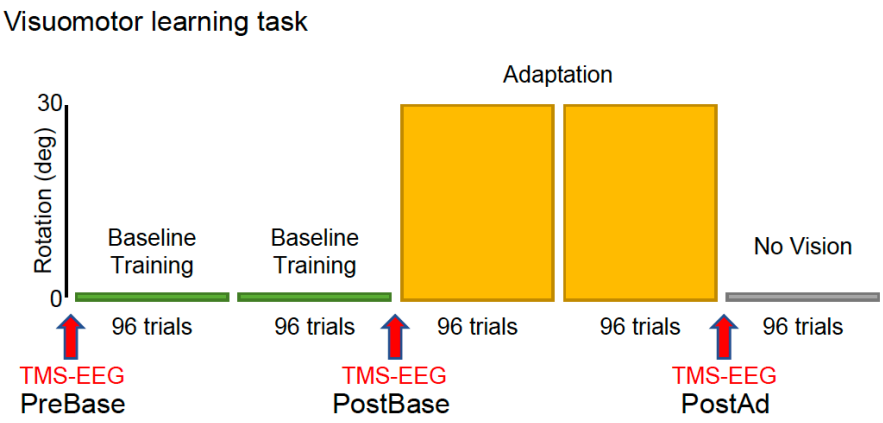

***Figure 20*: Protocol of cerebellar visuomotor adaptation.** *Sequence of behavioural task and the timing of cerebellar TMS (red arrow) in experiment 4. See text for details.*

Electroencephalography recording and pre-processing

Similar to the previous experiment (see previous chapter), EEG was recorded with a set of 63 low-profile active electrodes (ActiCap Slim, Easycap GmbH, Wörthsee, Germany) linked to a DC-coupled TMS compatible amplifier (Actichamp, Brain Products GmbH, Gilching, Germany); this technical solution has been shown to allow the recording of reliable TMS-EEG signals (Mancuso et al., 2021; Rawji et al., 2021). The scalp of each subject was prepared for EEG recording using an abrasive/conductive gel (V17 Abralyt 2000, Easycap, Herrsching, Germany). Electrode locations were based on the 10-10 international EEG system and included Fp1, Fz, F3, F7, FT9, FC5, FC1, C3, T7, TP9, CP5, CP1, Pz, P3, P7, O1, FCz, O2, P4, P8, TP10, CP6, CP2, Cz, C4, T8, FT10, FC6, FC2, F4, F8, Fp2, AF7, AF3, AFz, F1, F5, FT7, FC3, C1, C5, TP7, CP3, P1, P5, PO7, PO3, POz, PO4, PO8, P6, P2, CPz, CP4, TP8, C6, C2, FC4, FT8, F6, AF8, AF4, F2. The ground electrode was located at Fpz and the online reference was at FCz. Impedances were kept lower than 5KΩ during the whole experiment, and the sampling rate was 5000 Hz. As explained in the previous chapter, a masking noise was played during all blocks (ter Braack et al., 2015). The EEG offline preprocessing was performed in a similar way as described before, using analysis procedures from several open-source programs, such as EEGLab version 14.1 (Delorme and Makeig, 2004) and TMS-EEG signal analyser (TESA) toolbox (Rogasch et al., 2017), all running in MATLAB environment (Version 2015b, MathWorks, Inc., Natick, MA, United States). The raw EEG signal

was first epoched from -1.3 to +1.3 seconds with respect to the TMS pulse, using a baseline correction from -1000 to -10 ms. The TMS artefact was removed from -5 ms to +12 ms around the TMS trigger. An independent component analysis (ICA) was then performed using a fastICA algorithm. Only the 15 components explaining the largest variance were inspected in a time window ranging from -200 to 500 ms. According to parameters such as amplitude, frequency content and scalp distribution (Rogasch et al., 2014, 2013), we removed the components which reflected EMG activity from cranial muscle and possible voltage decay. Later, the previously removed data points around the TMS artefact were interpolated with a cubic function, and the signal was downsampled (1000 Hz) and filtered with a band-pass (1-100 Hz) and band-stop (48-52 Hz) zero-phase, fourth order Butterworth filters. Epochs were restricted (from -1 to +1 s) to reduce possible edge artefacts caused by filtering, and a second round of fastICA was applied, this time focusing on residual, non-TMS-locked artefacts (e.g., continuous muscle activity, eyeblinks, lateral eye movements). At this stage, there was usually a dominant vertex N100/P200 complex, reflecting insufficient masking of auditory input, as evidenced from experiment in the previous chapter. This was retained in one set of pre-processed data (i.e. RCS_AEP and LCS_AEP) and removed it in a second set (i.e. RCS and LCS) (see details in EEG data below). As a last step before the analysis, TMS-EEG signals were re-referenced to the common average reference.

Data processing and statistics

For all of the non-EEG data in this experiment, normality of distribution was checked by Kolmogorov-Smirnov test, and the assumption of sphericity in analysis of variance (ANOVA) was checked by Mauchly`s test. Bonferroni's method was used to correct for multiple comparisons in post-hoc tests. In case of non-normal distributions, Wilcoxon signed-rank tests were used. All analyses for non-EEG data were done with SPSS version 22 (IBM, USA). P values < 0.05 were considered significant.

Analysis of VAS scores related to loudness of the TMS click, intensity of muscle twitch and discomfort

The average and standard deviation of VAS was calculated. A violin plot of VAS in each condition was computed and graphed by a custom script in MATLAB environment (Version 2015b, MathWorks, Inc., Natick, MA, United States). Two paired tests were arranged to compare the loudness score between RCS and ABCAS in 14 subjects and the muscle twitching between RCS and ES in 20 subjects.

Calculation of CBI

Peak-to-peak MEP amplitudes were measured offline. Trials containing background EMG activity > 100 μV in the 100 ms preceding the TMS pulse were excluded (0.6% of all trials). CBI was calculated as the ratio of conditioned to test MEP amplitudes.

EEG analysis

Calculation of global mean field potential (GMFP) and determination of Time windows of Interest (ToI)

After EEG pre-processing, global mean field potential (GMFP) was calculated from 13 to 250 ms after the TMS pulse and averaged across subjects, according to the formula:

$$GMFP(t) = \sqrt{\frac{[\sum_i^k (V_i(t) - V_{mean}(t))^2]}{K}}$$

where t is time (ms), K indicates the number of channels, V_i is the voltage in channel i, and V_{mean} is the averaged voltage from all channels (E. P. Casula et al., 2018; Lehmann and Skrandies, 1980a, 1980b). Time regions of interest (ToIs) for following statistical analyses were determined from the peaks in GMFP waveforms, separately for each comparison), as outlined in Fig. 21 and Table 3.

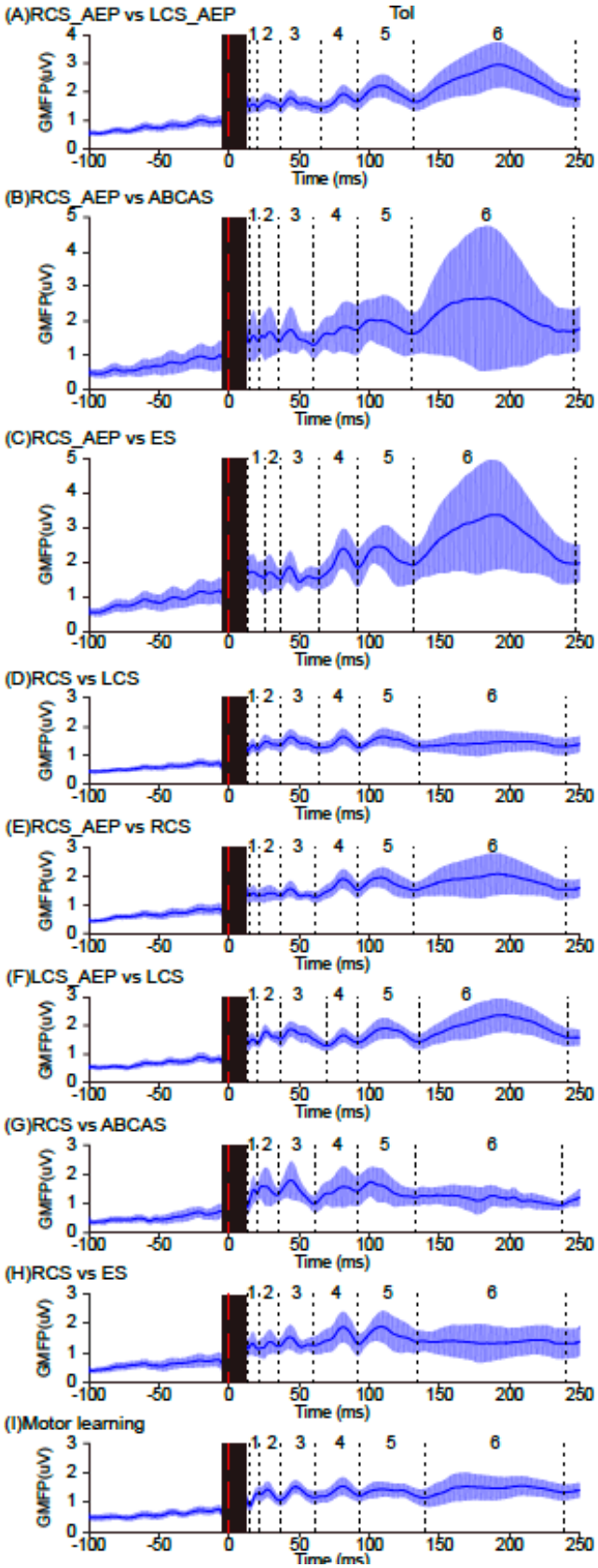

***Figure 21*: GMFP**. *GMFPs for each analysis are plotted. ToIs boundaries are indicated with black dotted lines. The red dashed line is the time point of TMS pulse. The black panel around the TMS pulse*

is the time window which was cut to remove the TMS pulse artefact where the TMS pulse artefact (-5 to 12 ms). The blue areas are the 95% confidence interval of each GMFP curve. ***Panel A****: average GMFP of RCS_AEP and LCS_AEP conditions.* ***Panel B****: average GMFP of RCS_AEP and ABCAS conditions.* ***Panel C****: average GMFP of RCS_AEP and ES conditions.* ***Panel D****: average GMFP of RCS and LCS conditions.* ***Panel E****: average GMFP of RCS_AEP and RCS conditions.* ***Panel F****: average GMFP of LCS_AEP and LCS conditions.* ***Panel G****: average GMFP of RCS and ABCAS conditions.* ***Panel H****: average GMFP of RCS and ES conditions.* ***Panel I****: average GMFP of the three recording blocks of experiment 4.*

	ToI 1	**ToI 2**	**ToI 3**	**ToI 4**	**ToI 5**	**ToI 6**
Fig.21-A	14-20 ms	20-37 ms	37-66 ms	66-91 ms	91-132 ms	132-247 ms
Fig.21-B	14-21 ms	21-35 ms	35-60 ms	60-91 ms	91-130 ms	130-246 ms
Fig.21-C	13-25 ms	25-36 ms	36-64 ms	64-92 ms	92-131 ms	131-247 ms
Fig.21-D	13-20 ms	20-36 ms	36-64 ms	64-93 ms	93-135 ms	135-240 ms
Fig.21-E	15-21 ms	21-37 ms	37-61 ms	61-92 ms	92-132 ms	132-250 ms
Fig.21-F	13-20 ms	20-36 ms	36-69 ms	69-91 ms	91-135 ms	135-242 ms
Fig.21-G	13-21 ms	21-35 ms	35-61 ms	61-91 ms	91-133 ms	133-237 ms
Fig.21-H	13-21 ms	21-35 ms	35-60 ms	60-92 ms	92-133 ms	133-240 ms
Fig.21-I	15-22 ms	22-36 ms	36-61 ms	61-93 ms	93-140 ms	140-239 ms

Table 3. TOIs for each comparison

Cerebellar TMS evoked Potentials (cbTEPs) at rest

To characterise EEG responses evoked by cerebellar TMS, several paired comparisons were performed: 1) RCS_AEP vs. LCS_AEP, to investigate possible lateralized cortical activation after cerebellar TMS; 2) RCS_AEP vs. ABCAS and 3) RCS_AEP vs. ES, to disentangle cbTEPs of cerebellar origin from sensory responses.

Unlike previous experiment, in the present experimental setting suppression of the AEPs induced by TMS DC loud click was difficult to obtain (e.g. ear defenders could not be used along with DC). However, previous work has demonstrated the feasibility of offline removal of AEPs using ICA. Independent components reflecting AEPs were identified based on time (N100/P200 peaks) and scalp distribution (symmetrical, vertex-centered) (Elias P Casula et al., 2017; Rogasch et al., 2014, 2013; Ross et al., 2022); these were highly similar to signals obtained in the ABCAS

condition (Ross et al., 2022). After the removal of auditory-related components from RCS_AEP and LCS_AEP (which were then named RCS and LCS, respectively), the second set of analyses was performed, as follows: 1) RCS_AEP vs. RCS and 2) LCS_AEP vs. LCS, to check the effect of removing the AEP; 3) RCS vs. LCS, similar to the analysis performed previously to explore possible lateralized cortical activation, but this time without the confounding presence of AEPs; 4) RCS vs. ABCAS and 5) RCS vs. ES, as previously, to disentangle possible cbTEPs of cerebellar origin from sensory responses, without the confounding presence of the AEP.

cbTEPs in visuomotor learning

Instead, analysis of cbTEPs in motor learning consisted of three pairwise comparisons: 1) PreBase vs. PostBase, to test possible changes on cbTEPs due to motor practice, without changes in task parameters; 2) PostBase vs. PostAd, to investigate the effects of visuomotor adaptation on cbTEPs; 3) PreBase vs. PostAad, to test net cbTEP changes after the entire learning process.

Statistics for cbTEPs and sensory input conditions

The pairwise comparisons indicated above were performed at the scalp level by the built-in "Study" function in EEGlab (Delorme and Makeig, 2004). Monte Carlo permutation statistics were applied and the empirical distributions for each comparison were built by permuting conditions with 1000 iterations (Maris and Oostenveld, 2007). The permutations were performed in the spatio-temporal domain, including all electrodes and time points in each ToI (Rogasch et al., 2014, Opie et al., 2017). Cluster correction as implemented in Fieldtrip toolbox was used to control for type I errors (Oostenveld et al., 2011). The minimal number of neighboring electrodes was two. For significant clusters (p-value < 0.05), related t statistics and exact corrected p values (two tailed) at the electrode level were extracted.

N110 in cbTEP and N100 in ABCAS

A lateralized, negative peak around 110 ms (N110) was identified in the RCS and LCS conditions (see Results section). Despite topographical differences, the comparison between RCS and ABCAS using the ToI approach did not result in

statistically significant differences (see Results), since a vertex negativity around 100 ms was recorded in the ABCAS condition as well (N100). This result seems at odds with the removal of components related to the AEPs performed to obtain RCS and might indicate that the ICA failed to remove the AEP effectively or the nature of the two waves was different. For the former, the effectivity of removing AEP in ICA would be examined by RCS_AEP vs RCS and LCS_AEP vs LCS. For the latter, we applied one paired comparison to test the latencies of the peak in each condition, and another procedure used previously to investigate similarity between signals of interest, with the assumption that physiologically distinct components would not show any intra subject agreement. First, in the test for latencies, to further investigate differences between the two negative components peaking around 100 ms, we extracted the latency from the electrode having the maximal negative amplitude in each condition in ToI5. Thus, the electrodes chosen were F1 in RCS and FCz in ABCAS. A paired comparison was performed to compare their latency. Second, we calculated the concordance correlation coefficient (CCC) to investigate possible similarities between the N110 of RCS and N100 of ABCAS (Mancuso et al., 2021) it is a form of intraclass correlation coefficient optimized to examine agreement between the distribution of two variables. It was calculated by the formula below:

$$CCC = \frac{2\sigma_{12}}{\sigma_1^2 + \sigma_2^2 + (\mu_1 - \mu_2)^2}$$

Here σ_{12} indicates the covariance between two distributions, σ_x^2 is the variance of distribution x, and μ_x is the average of distribution x (King et al., 2007; Lin, 1989). First, we calculated the z value of each signal (ABCAS and RCS) in ToI5 (91-133 ms) and in a baseline window (-950 to -100 ms before TMS) separately. Next, in each electrode and in each subject, CCC was calculated between baseline and ToI5 from the two sessions, resulting in CCC between baseline ($CCC_{baseline}$) from ABCAS and RCS and CCC between ToI5 (CCC_{ToI5}) from ABCAS and RCS. Finally, CCC_{ToI5} was compared to $CCC_{baseline}$ with dependent samples t-test. Correction for multiple comparisons was performed by false discovery rate (FDR) (Benjamini and Hochberg, 1995). The critical value (p-value) of 0.05 or less was considered as significant in all the above statistical analyses.

Behavioural task

Angular error was the primary outcome measure and was calculated by measuring the angular difference between the center of the target and the line connecting the starting position to the endpoint hand position. Epochs of angular error were created by binning 8 consecutive trials. For each block, the initial mean error ($error_{int}$) was determined by averaging over the second to sixth consecutive epochs, as in previous papers, in order to sample the fast-learning phase observed during adaptation (Galea et al., 2011; Krakauer et al., 2005). Large angular errors (over 60 degress) were considered outliers and rejected (1.6% of all trial) (Galea et al., 2015; Schlerf et al., 2015). To assess motor learning, a one-way repeated measure ANOVA (RM-ANOVA) was arranged to compare $error_{int}$ across baseline training ($error_{baseline\ training}$), adaptation ($error_{adaptation}$), and no vision ($error_{no\ vision}$).

Spearman`s correlation coefficient was employed to measure the relationship between the change in cbTEP amplitudes and the change in learning (de Winter et al., 2016). To calculate the change in cbTEPs relative to different stages of the task, we measured the amplitude changes of each channel between PostBase and PreBase (i.e., $cbTEP_{Postbase\text{-}Prebase}$), and between PostAd and PostBase (i.e., $cbTEP_{Postad\text{-}Postbase}$). To quantify the amount of fast phase learning and initial retention relative to baseline, we calculated the change of error between baseline training and adaptation (i.e., $error_{change1}$) and between baseline training and no vision (i.e., $error_{change2}$), respectively [28]. The time windows for the above correlations were the ToIs with isolated cbTEPs in experiment 4. In each pair, the rho value of Spearman`s correlation in each channel at every ms in the ToIs were calculated by using the Fieldtrip toolbox in MATLAB. Monte Carlo permutation statistics was applied for these the spatio-temporal distribution of rho values during each ToI (channel x time) for spatial clusters and time clusters. The minimal number of neighboring electrodes for cluster-based multiple comparison was one. Other details in permutation statistics are the same as the method of statistics for cbTEPs and sensory input conditions.

Results

All participant tolerated the experiments, no dropout and no adverse events were reported.

Analysis of VAS

The VAS scores for all participants are plotted in Fig. 22. The two right-hand panels show that there was no significant difference in the perception of loudness between real RCS and the auditory control condition, ABCAS (14 subjects: t=1.963, df=13, p=0.071) nor between RCS and the somatosensory (muscle twitch) control condition, ES (20 subjects: t=1.648, df=19, p=0.116).

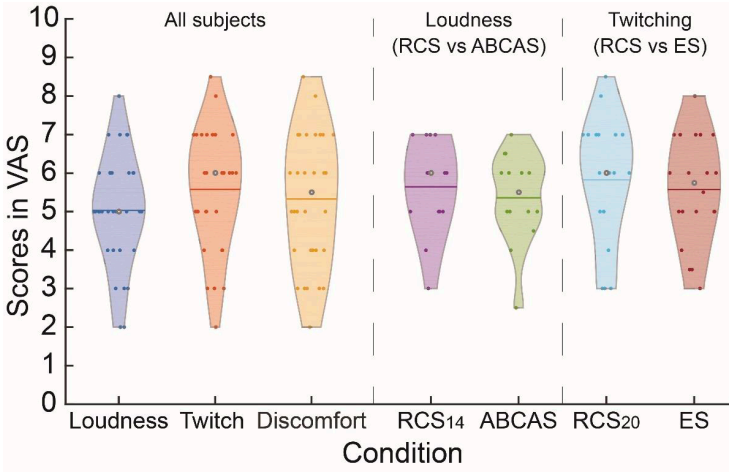

***Figure 22*: Distribution of VAS in each condition.** *VAS scores for each condition. The left panel with three violin plots represents the VAS scores for loudness (blue), twitch intensity (orange) and discomfort (yellow) by real cerebellar TMS from all 32 participants in experiment 1 and 4. In the middle panel with two violine plots, RCS_{14} indicates the VAS of 14 subjects` loudness scores in RCS in experiment 1 (purple). ABCAS indicates is the loudness scores in ABCAS of experiment 2 (green). There is no difference on VAS scores of loudness between RCS and ABCAS. In the right panel with two plots, $RCS_{20}$ indicates 20 subjects` muscle twitching scores in RCS in experiment 1 (cyan). ES refers to the scores of muscle twitching in ES of experiment 3 (carmine). There is no difference on muscle twitching between RCS and ES. Small dots indicate the individual`s score. The horizontal line in each plot means the mean of the score in each condition. The grey dot is the median of the score in each condition.*

Data processing and measurement of CBI

Details of the number of removed trials, channels and components during EEG preprocessing are listed in table 4.

Conditions	Trials	Electrodes	ICA1	ICA2
		Experiments 1-3		
RCS	12.6 ± 9.1	0.5 ± 0.7	7.0 ± 2.8	35.6 ± 5.6
LCS	10.6 ± 10.8	0.6 ± 0.8	7.8 ± 2.4	34.5 ± 5.1
ABCAS	4.2 ± 5.3	0.1 ± 0.3	2.7 ± 1.3	30.8 ± 6.0
ES	7.2 ± 9.8	0.1 ± 0.3	4.3 ± 2.3	37.1 ± 5.2
		Experiment 4		
PreBase	10.4 ± 9.9	0.4 ± 0.7	8.1 ± 2.1	30.9 ± 7.1
PostBase	3.4 ± 3.4	0.1 ± 0.3	6.9 ± 3.4	34.6 ± 7.2
PostAd	6.3 ± 5.9	0.4 ± 0.5	8.0 ± 3.0	29.8 ± 6.6

Table 4. *For each recording condition, the table lists the number of trials removed ("Trials"), the number of electrodes interpolated ("Electrodes") and the number of independent components removed in each round of ICA ("ICA1" and "ICA2" for the first and second round, respectively. Values are expressed as mean ± standard deviation.*

Characterization of cbTEPs evoked by single-pulse cerebellar stimulation

Fig. 21 illustrates the ToIs used in each set of experiments. These were estimated from the GMFP averages, which are also summarized in table 3. The intensities for each experiment are listed in Table 5. Moreover, Table 6 summarizes all statistical values obtained in cbTEP pairwise comparisons.

Stimulation	Average intensity	Standard deviation
Experiment 1		
RCS, LCS	66.0% MSO	7.8% MSO
Experiment 2		
ABCAS	66.0% MSO	7.8% MSO
Experiment 3		
ES: right masseter muscle	15.1 mA	5.7 mA
ES: right trapezius muscle	18.8 mA	11.9 mA
Experiment 4		
RCS	63.6% MSO	7.4% MSO

Table 5*. For each recording condition, stimulation intensities for TMS and ES are provided. Values are expressed as MSO and mA for TMS and ES, respectively.*

Comparisons	Cluster	TOI1	TOI4	TOI5	TOI6
Rest state (Experiment 1-3)					
RCS_AEP vs LCS_AEP	Positive	p=0.018	p=0.023	p=0.026	-
	Negative	p=0.005	-	p=0.022	-
RCS_AEP vs ABCAS	Positive	-	p<0.001	-	-
	Negative	-	p<0.001	-	-
RCS_AEP vs ES	Positive	p=0.006	p<0.001	-	-
	Negative	p=0.004	p<0.001	p=0.024	-
RCS_AEP vs RCS	Positive	-	-	-	p=0.002
	Negative	-	-	p=0.003	p=0.025
LCS_AEP vs LCS	Positive	-	-	-	p=0.013
	Negative	-	-	p=0.030	p=0.004
RCS vs LCS	Positive	p=0.008	p=0.022	p=0.013	-
	Negative	p=0.027	p=0.005	p=0.030	-
RCS vs ABCAS	Positive	-	p<0.001	-	p=0.015
	Negative	-	p<0.001	-	p=0.002
RCS vs ES	Positive	p=0.026	p<0.001	-	-
	Negative	p=0.035	p<0.001	p=0.042	-
Visuomotor adaptation (Experiment 4)					
PreBase vs PostBase	Positive	-	p<0.001	p=0.014	-
	Negative	-	-	p=0.003	-
PostBase vs PostAd	Positive	-	-	-	-
	Negative	-	p=0.004	-	-
PreBase vs PostAd	Positive	-	-	p=0.004	-
	Negative	-	-	p=0.002	-
Spearman`s correlation	Positive		p=0.037 (66-93ms)	-	
	Negative		p=0.030 (62-80ms)	-	

Table 6. Summary of statistically significant differences obtained in pairwise comparisons of TEPs

Resting TMS-EEG responses without removal of AEP components

Because of the strong auditory and somatosensory input produced by cerebellar stimulation, signals generated in RCS_AEP, LCS_AEP and ABCAS conditions share obvious similarities in ToIs 5 and 6, where their topography is dominated by a vertex N100 and P200 (Fig. 23A-C). Similar potentials around the vertex are also presented in the ES condition, albeit with a smaller amplitude (Fig. 23D). However, there appear to be differences in earlier ToIs, as confirmed by pairwise comparisons. Both RCS_AEP and LCS-AEP elicited two contralateral frontal waves, one positive (P80) in ToI4 and one negative (N110) in ToI5; due to this lateralization, pairwise comparisons led to statistically significant differences between them (Fig. 23G). The differences were bilateral over ToI5, as expected from a symmetrical mirrored N110. However, statistical differences only occurred in the left hemisphere in ToI4, suggesting that the P80 might have been smaller after LCS. This will be discussed

further in later sections. Cerebellar stimulation also elicited an earlier ipsilateral parietal negative wave in ToI1, again leading to a statistically significant bilateral difference between RCS_AEP and LCS_AEP (Fig. 23G).

The P80 in ToI4 in RCS_AEP was absent in both the ABCAS and ES conditions, replaced by central negativity (Figs. 23H-K). Additional differences between RCS_AEP and ES were present in ToI1 due to the ipsilateral parietal negative component induced by RCS_AEP and in ToI5, where the lateralized RCS_AEP N110 and the ES vertex N100 appeared (Fig. 23K).

In sum, these data suggest that, although much of the evoked EEG activity produced by TMS over the lateral cerebellum is due to sensory input, a significant frontal positive/negative potential in ToI4/ToI5 may result from activity in cerebello-cortical projections (cbTEP). In the second part of this experiment, this hypothesis will be probed by investigating if the amplitude of the cbTEP would be sensitive to state-dependent changes in cerebellar activation that occur during visuomotor adaptation in an arm-reaching task. The analysis of EEG signals is confined to ICA-processed data to remove the AEP.

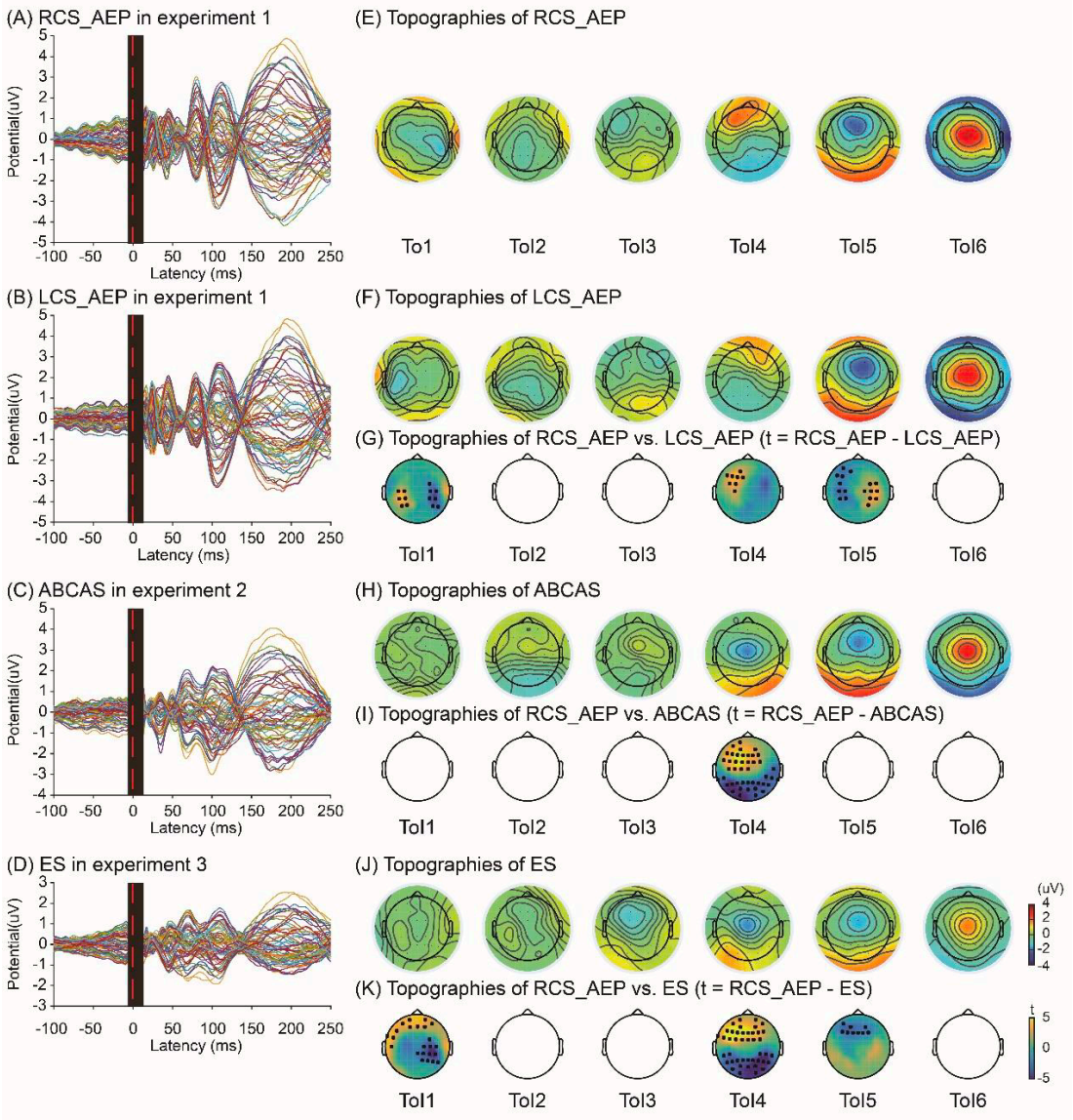

***Figure 23*: Descriptive summary and statistics of cbTEPs keeping AEP and sham controls from resting state experiments.** *Left panels illustrates the grand average butterfly plots of 25 subjects` RCS_AEP (A), 25 subjects` LCS_AEP (B), 14 subjects` ABCAS (C) and 20 subjects` ES (D) conditions. The red dashed line is the time point of TMS pulse. The black panel around the TMS pulse is the time window which was cut to remove the TMS pulse artefact where the TMS pulse artefact (-5 to 12 ms). The right panels show scalp topographies and t value maps for each paired comparison, referring to the same conditions of left panel ` RCS_AEP topographies (E) ` LCS_AEP topographies (F), t values map of RCS_AEP vs. LCS_AEP (G),` topographies of brain response to ABCAS (H), t values map of RCS_AEP vs. ABCAS (I),` topographies of brain activity evoked by ES (J), and t values map of RCS_AEP vs. ES (K). In the t value maps, black dots indicate significant electrodes by cluster-based permutation test.*

Resting TMS-EEG responses after removal of AEP components by means of ICA

After the removal of components related to AEPs, RCS_AEP and LCS_AEP conditions lost their prominent central N100/P200 waves in ToI5 and ToI6, respectively (Figs. 24A-D); this was clear in the pairwise comparisons between these conditions and their counterparts without AEP components (Figs. 24E-H).

Pairwise comparisons between stimulation conditions yielded results similar to those obtained prior to the removal of AEP components, but with some small differences. While the differences remained at ToI1 and ToI5 in the comparison of RCS and LCS, removal of the AEP now showed that the comparison of P80 in ToI4 was significant bilaterally, rather than solely on the left (Fig. 24J). The comparison between RCS and ABCAS confirmed the difference in ToI4, but there was also a significant negative cluster at the vertex site in ToI6, due to the removal of AEP components (Fig. 24L). The differences between RCS and ES observed in ToIs1, 4 and 5 were maintained (Fig. 24N).

The lateralization of the N110 after cerebellar stimulation is consistent with a cerebellar origin, so it was surprising that there was no statistical difference in ToI5 between RCS (or RCS_AEP) and ABCAS. We suspected this was due to the close spatial overlap of a cerebellar N110 and a sensory N100. Indeed, there was a significant difference in latency of the N110 after RCS and the N100 after ABCAS (108.2 ± 6.9 ms vs 91.9 ± 10.4 ms, z=-3.173, p=0.002). The CCC analysis performed to investigate possible similarities between RCS N110 and ABCAS N100 did not yield significant results, consistent with, although not proof of the idea that they may represent different cortical evoked potentials.

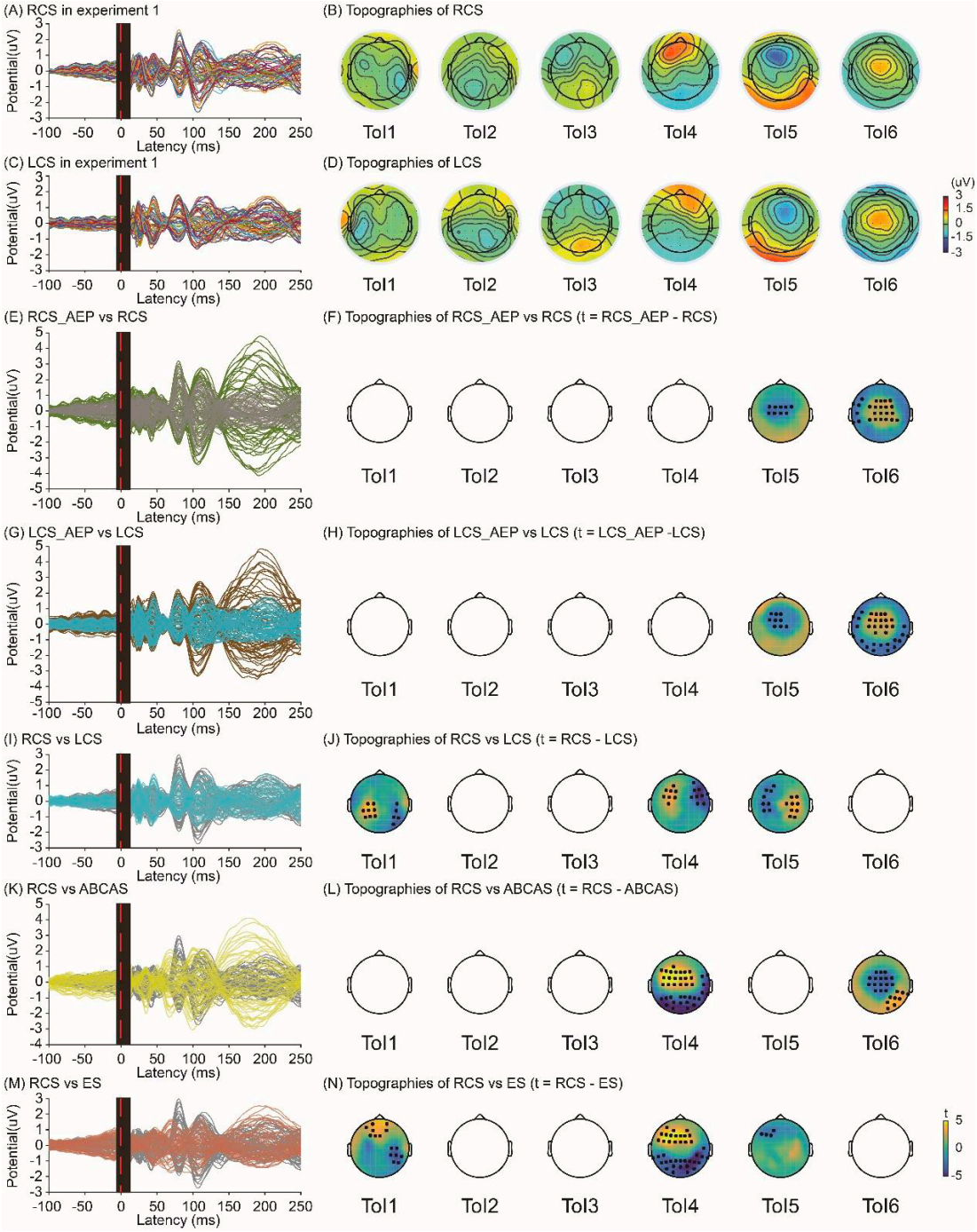

***Figure 24*: Descriptive summary and statistics of cbTEPs from resting state experiments**. *Grand average butterfly plot (A) and topographies (B) of 25 subjects` RCS. Grand average butterfly plot (C) and topographies (D) of 25 subjects` LCS. From third row below, left panels show the overlapped butterfly plots for each comparison, and the right panels indicate the t value maps for each comparison. In the left panels, the grey butterfly plot is always RCS, and the blue one is always LCS. When comparing RCS_AEP vs. RCS, a clear vertex N100 and P200 peaks are present in the green butterfly plot of RCS_AEP (E) and in the t value maps of ToI5 and ToI6 (F). LCS_AEP vs. LCS comparison showed similar results (G, H). The comparison between RCS and LCS conditions (I) showed significant clusters*

in ToI1, ToI4 and ToI5, consistent with contralateral cortical activation following cerebellar stimulation (J). In the RCS vs. ABCAS comparison (K, L), the larger vertex P200 of the latter resulted in a central significant negative cluster in ToI6, while a lateralized frontal P80 in the RCS condition resulted in a significant positive cluster in ToI4, but a peak of RCS in middle latency has higher amplitude than ABCAS (K). In the last row, RCS vs. ES comparison (M, N) demonstrates a very early peak in ToI1, another high peak in ToI4 and the other clear negative peak in ToI5 in butterfly plot of RCS (M), referring to the significance in t value maps (N). The red dashed line is the time point of TMS pulse. The black panel around the TMS pulse is the time window which was cut to remove the TMS pulse artefact where the TMS pulse artefact (-5 to 12 ms). In the t value maps, black dots indicate significant electrodes by cluster-based permutation test.

Analysis of angular error during visuomotor adaptation

In the baseline training, the mean angular error was -1.9 ± 1.55°. Following introduction of the visual rotation, the mean angular error increased to -9.6 ± 2.9°. After removing both visual rotation and the visual cursor, participants had a clockwise mean angular error of 13.6 ± 2.9°(Fig. 25). There was a significant difference in learning over the three blocks ($F_{2,26}$=224.143, p<0.001). Post hoc significant comparisons were: $error_{baseline\ training}$ vs $error_{adaptation}$ (p<0.001); $error_{adaptation}$ vs $error_{no\ vision}$ (p<0.001); $error_{baseline\ training}$ vs $error_{no\ vision}$ (p<0.001).

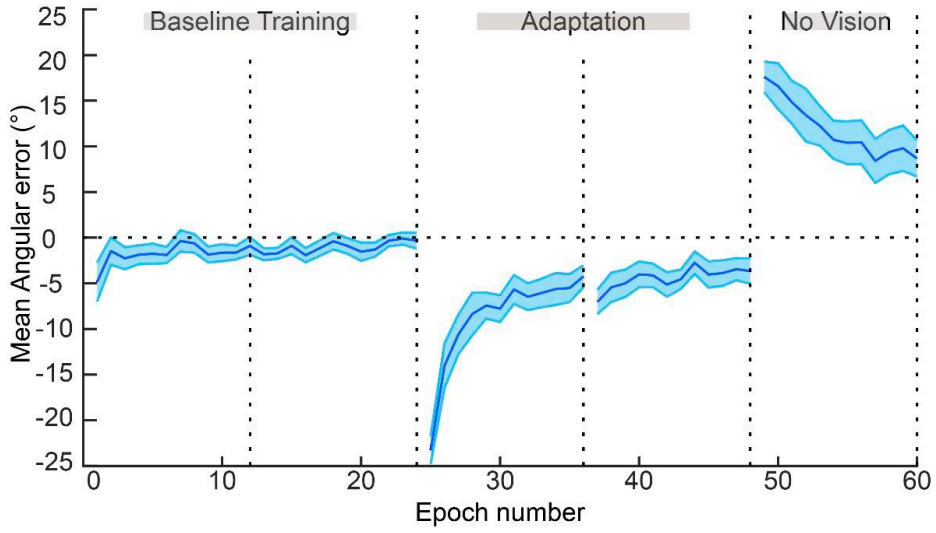

***Figure 25*: The learning curve of behaviour tasks**. *The learning curve of experiment 4 is represented. Blue shaded area indicates the 95% confidence interval of angular error.*

Cerebellar TMS-EEG responses during visuomotor adaptation

The averaged topographies of PreBase cbTEPs in experiment 4 were similar to those following RCS in experiment 1 (Fig. 26A and 26D). The comparison between PreBase and PostBase cbTEPs revealed that, after baseline training, the left frontal positive peak at ToI4 (P80) was significantly suppressed (Fig. 26G, note that positive t value is PreBase - PostBase); the amplitude of this positive cluster was restored to baseline levels after the adaptation block (Fig 26H and 26I). Changes in the negative deflection (N110) in ToI5 had a different time course: while it was suppressed at PostBase (Fig. 26G), it remained suppressed for the whole duration of the task (Fig. 26H and 26I).

We also explored potential relationships between motor learning and changes in amplitude of cbTEPs. There was a significant positive correlation (Spearman non-parametric) between the amount of retention ($error_{change2}$) and $cbTEP_{Postad\text{-}Postbase}$ of a large frontal-parietal network at P80 (Fig. 26J): the greater the retention, the more significant the change in amplitude of the P80. But there was no correlation between N110 and $error_{change1}$ or $error_{change2}$.

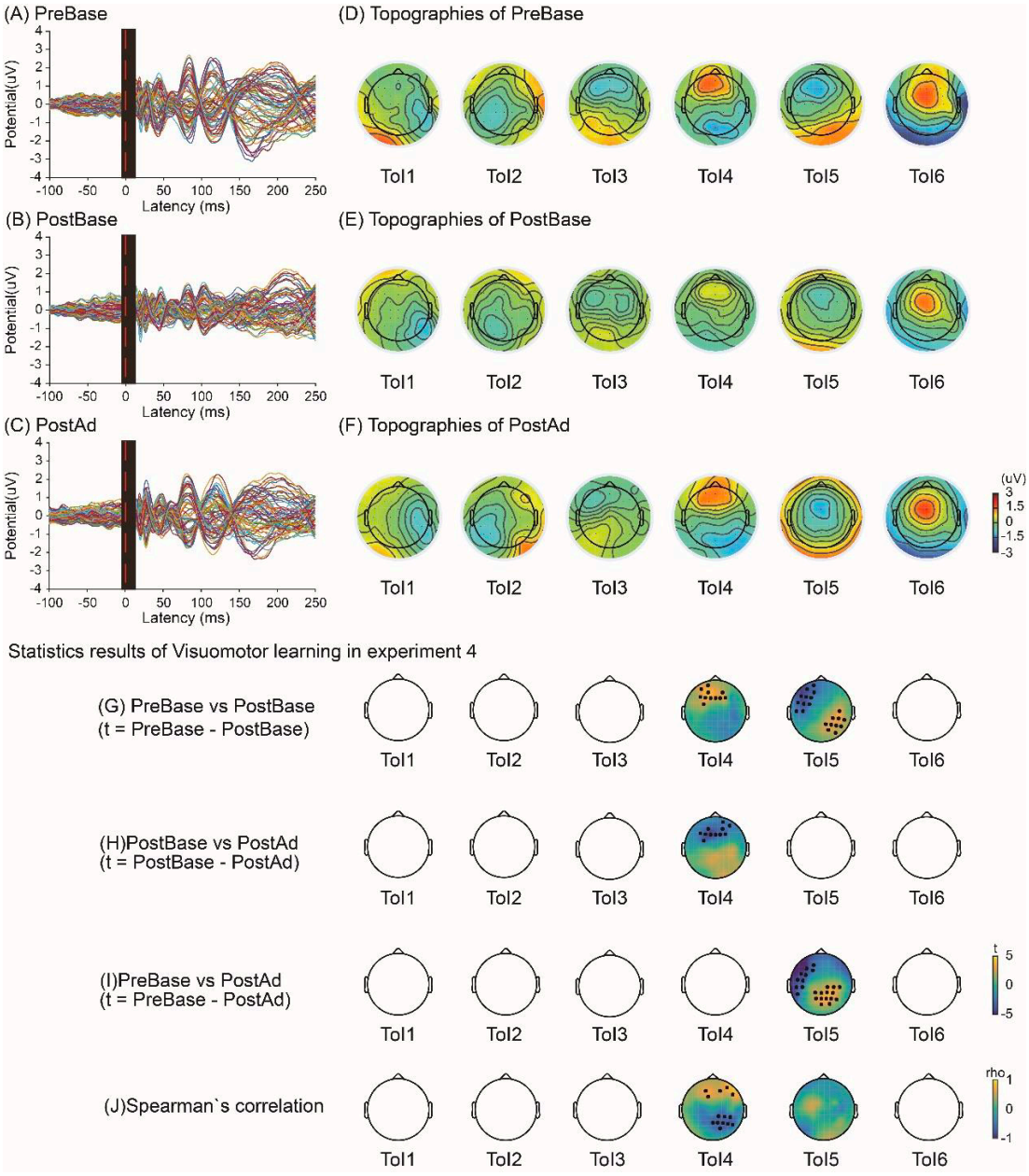

***Figure 26*: Summary of statistics from experiment 4.** *Upper left panels show butterfly plots of RCS cbTEP in PreBase (A), PostBase (B), and PostAd (C) recording blocks. The P80 and N110 amplitudes are clearly reduced in PostBase (B) and restored in PostAd (C). Upper right panels show topographies correlating to the left side: PreBase (D), PostBase (E), and PostAd (F). Again, the changes in P80 (ToI4) and N110 (ToI5) on topographies (D, E, F) are the same as the butterfly plots, whereas there are no obvious changes in other ToIs. The bottom panels plot the t value maps of paired comparison in upper three rows, including PreBase vs PostBase (G), PostBase vs PostAd (H), and PreBase vs PostAd (I). In ToI4, the P80 at PreBase is significantly higher than PostBase (G), and the P80 at PostBase is significantly lower than PostAd (H). In ToI5, N110 at PreBase has more negative amplitude than PostBase and PostAd (G, I). The bottom row depicts the rho value topographies of Spearman's correlation (J). The P80 correlates to the learning performance ($error_{change2}$). The red dashed line is the*

time point of TMS pulse. The black panel around the TMS pulse is the time window which was cut to remove the TMS pulse artefact where the TMS pulse artefact (-5 to 12 ms). In the t and rho value maps, black dots indicate significant electrodes by cluster-based permutation test.

Discussion

These results demonstrate that interactions between the cerebellum and cortex can be evaluated using TMS-EEG and that these change during motor learning. We argue that these results provide a neurophysiological read-out of cerebellar inputs that are processed by the cortex and are related to visuomotor learning.

Cerebellar TMS evoked potential (cbTEP) can be recorded with TMS-EEG

The goal of experiments 1-3, performed in resting state, was to determine whether it was possible to identify a cortical EEG response that was due to activity in cerebellar-cortical connections and that was separate from potentials evoked by auditory and somatosensory stimulation caused by discharge of the TMS coil. Separate control conditions were used to identify activity produced by auditory and somatosensory input since previous experiment (see experiment of previous chapter) has shown that the EEG produced by each summates linearly and therefore, it is not necessary to devise a single control condition that combines both sensations. We argue that comparing across all conditions (RCS_AEP, LCS_AEP, ABCAS, and ES, Fig. 23) provides sufficient evidence to disentangle sensory "EEG activity" from responses due to input from the cerebellum. Of note, all conditions have large potentials in ToI5 and ToI6 (see butterfly plots, approximately around 90-130 ms and 130-250 ms) that correspond to sensory-induced vertex N100 and P200 peaks (see topographic plots), a result that has been previously described in TMS-EEG studies (Gordon et al., 2021). The ABCAS and ES conditions, which activate auditory and somatosensory pathways, additionally showed a negative vertex potential at ToI4 (around 60-90 ms) similar to that described by others using a multisensory control condition (Fernandez et al., 2021; Sasaki et al., 2022), which was not seen when stimulation was given to the cerebellum.

In ToI4, RCS_AEP and LCS_AEP conditions were characterized by a contralateral positive peak (P80) over frontal cortex consistent with activation of cerebellar-cortical connections (Middleton and Strick, 2001; Strick et al., 2009;

Watson et al., 2014), together with an occipital negativity. Lateralized activity is also seen at ToI1 and ToI5 (Fig. 23E, F, G). While speculative, the differences at ToI1 (around 13-20 ms) are likely due to initial artefacts caused by the TMS coil activation (Fig. 23I) ipsilateral to the side of stimulation. It is more challenging to make a definite conclusion about the cause of the lateralized N110 produced by RCS_AEP at ToI5 since it overlaps with the auditory vertex negativity that occurs at a similar timing (see comparison of RCS_AEP with ABCAS in Fig. 23 H, I).

Similar conclusions were confirmed by analyzing signals after ICA removal of auditory artefacts (Fig. 24B, D, J). There was a clear contralateral frontal positivity at ToI4 and a contralateral negativity at ToI5. However, even though ICA removal of the AEP decreased amplitude of N100 and P200 components (RCS_AEP vs RCS and LCS_AEP vs LCS, Fig. 24H, J), the spatiotemporal distribution of the lateralized N110 could not be separated from the AEP in ABCAS (Fig 24L). However, the peak latency of the auditory potential evoked by ABCAS was earlier (N100) than the peak produced by cerebellar stimulation (N110), suggesting that although the two potentials share considerable similarities, there may be additional, lateralized differences between them. Consistent with this, the CCC analysis, which probes temporal similarities between potentials was not significant. On the basis of this analysis, we propose that the N110 may contain lateralized activity caused by input from cerebellum.

cbTEPs are modulated by visuomotor learning

As visuomotor learning is well-known to engage cerebellar interactions with both motor and cognitive cortical areas (Galea et al., 2015, 2011; Halsband and Lange, 2006; Spampinato and Celnik, 2021; Taylor and Ivry, 2014), we expected changes in the cbTEP to appear throughout frontal-motor areas following learning. We did not expect changes surrounding the occipital lobe, as previous work has shown that this area does not involve this area during cerebellar visuomotor adaptation (Boukrina and Chen, 2021; Haar et al., 2015; Striemer et al., 2019). Our data demonstrated that the frontal P80 was sensitive to different stages of training (Fig. 25). A decrease in this peak was found following task familiarization, which subsequently increased following adaptation. Interestingly, we found that changes in the P80 peak correlated to the amount of motor retention, indicating that this peak is an important marker for

learning. While we additionally found that the N110 peak was modulated following baseline performance, we found no behavioural correlations associated with this peak, hinting that P80 and N110 provide information about different processes that may be more or less directly related to motor learning and retention (Fig. 25J)

The fact that cbTEP changes were concentrated over frontal areas might not be surprising as the most likely cerebellar zones stimulated with TMS are ones associated with cognition (i.e., lobules IV to Crus I/II) (Bernard and Seidler, 2013; Krienen and Buckner, 2009; Strick et al., 2009). Additionally, adaptation to visuomotor rotations requires different forms of learning that are associated with distinct neural substrates, such as learning via sensory prediction errors that are calculated by the cerebellum and cognitive strategies (i.e., aiming) that involve frontal areas (Taylor and Ivry, 2014; Tzvi et al., 2020). As the P80 changes were concentrated in frontal areas following cerebellar stimulation, it is unclear whether these results are specifically due to changes in cerebellar excitability or in frontal areas receiving inputs from the cerebellum. Rather, it is likely that the P80 changes following adaptation are related to increased activity across the cerebellar-prefrontal network (Shadmehr and Holcomb, 1997), as collectively they play an important role in learning and consolidating new sensorimotor transformations (Caligiore et al., 2019; Tzvi et al., 2020). This is supported by evidence that the strength of connectivity in the cerebellar-cortical network updates dynamically after learning is completed, during consolidation and automatization (Doyon et al., 2009) and also during processes involving motor memory formation (Bédard and Sanes, 2011). In line with this, the P80 may reflect the overall state of the cerebellar-prefrontal pathway at different stages of visuomotor adaptation rather than a cerebellar state or prefrontal state alone.

Previous MRI studies have pointed out that the cerebellum and prefrontal cortex are engaged throughout visuomotor adaptation learning. Activation of both areas are seen at the initial stages of adaptation (Shadmehr and Holcomb, 1997; Tzvi et al., 2020), while the right anterior cerebellar and left premotor activity persist for several hours after individuals have adapted their movements during a consolidation period . This may explain why the change in P80 outlasts the period of learning and is related to a specific aspect of visuomotor learning. Indeed, the modulation of the P80 peak following adaptation was strongly correlated with the amount of

displacement observed in no vision trials. These trials, where no rotation or vision of the cursor was administered, were used to assess how much of the new reaching pattern has been stored following adaptation. Here, individuals who displayed more errors (an indicator of more retention) during these trials also had significantly larger changes in P80 peaks with respect to baseline (Fig 25J).

One question here is, why do the amplitudes of P80 and N110 fluctuate after baseline training as well as adaptation? We speculate that these data might reflect some aspects of initial learning that are driven by cognitive processes, such as aiming and tool learning (Nezafat et al., 2001). Indeed, participants initially showed a bias in their goal-directed reaches, which were found to reduce with repetitive training as they learned to use the manipulandum. Future work may consider probing changes in the cbTEP before and after simple reaching movement alone (i.e., without manipulandum), which avoids any learning effects.

Comparison with previous studies of cbTEPs

As stated before, results are not consistent across previous studies that investigate cerebellar-cortical connection and there are substantial differences in the methodology used (e.g., TMS coil type, laterality, and intensity). However, it is interesting to note that the study by Sasaki and coworkers (Sasaki et al., 2022), which used a DC coil as in the present experiment, yielded a contralateral frontal positivity at 80ms similar to that described here. However, they did not do a paired comparison with sham control, so the conclusion is based only on an inspection of their data.

In contrast, two studies which used the figure of eight coil do not comment on any activity specific to cerebellar stimulation around 80ms (Fernandez et al., 2021; Gassmann et al., 2022). Gassmann et al, using a 50mm F8 coil, report a diffuse negative contralateral potential at around 45ms, which is similar to the left frontal negative response at 48ms by Fernandez et al using 70mm F8 coil (Fernandez et al., 2021). It is important to note that the latter was not significantly different to their multiple sensory control. We conclude that in the future, a consistent method for stimulating cerebellum should be adopted, and that putative cerebellar evoked potentials are shown to be behaviourally sensitive.

EEG recording reveals more details of the neurophysiology of single-pulse subthreshold cerebellum TMS with a DC coil

Cerebellar Purkinje cells are thought to be activated by TMS, which inhibits the dentate nucleus neurons that project to the cortex via the thalamus (Battaglia et al., 2006; Reis et al., 2008). Given the large and non-focal stimulation applied with the DC coil, it is likely that cerebellar projections to the motor and cognitive areas are activated. Interestingly, the area of the cerebellar cortex closest to the scalp is the Crus I/II (~ 13-15 mm) (Benjamini and Hochberg, 1995; Galea et al., 2011), which connects to prefrontal cerebral areas (Benagiano et al., 2018; Middleton and Strick, 2001; Strick et al., 2009; Watson et al., 2014). In other words, the bulk of cerebellar stimulation likely activates Crus I/II, which would lead to more pronounced activation of projections to prefrontal areas (Fig. 23G, 23I, 23K, 24J, 24L, 24N). According to the model of cerebellar visuomotor learning, the prefrontal lobe performs sensorimotor adaptation and updates working memory (Galea et al., 2015; Halsband and Lange, 2006; Taylor and Ivry, 2014). This also supports why we see the changes in frontal activities after motor adaptation according to the model of cerebellar visuomotor adaptation (Figs. 25G-J).

Limitations

The high intensity and DC coil used to evoke cerebellar output present a challenge, as this may lead to large evoked auditory evoked potentials. In addition, slightly varying coil position, different coil types and stimulation intensities we might be able to stimulate different projections and hence get different cbTEPs. Thus, depending on how well this aspect is controlled for, these potentials could potentially drive variable results among future cerebellar TMS-EEG studies. Furthermore, the stimulus produces a large artifact in early EEG components that cannot be filtered. Thus, it is difficult to see the earliest response known to influence M1 activity, as demonstrated in CBI studies using EMG. Finally, we used a novel pre-processing system to analyze EEG signals using the removal of auditory evoked responses by ICA. Despite recent evidence suggesting that this system could provide consistent data, its validity has not been fully proven in previous literature. This approach is based

on AEPs non-automated identification based on component properties such as time course, topography, and spectral profile, which could be susceptible to human bias. However, in this experiment, our results seem similar regardless of auditory response removal by ICA, suggesting that this approach did not influence the main results.

Conclusions

Using the DC coil and enough stimulus intensity, together with careful EEG preprocessing, the results demonstrate that a cortical response to cerebellar TMS (i.e., cbTEP) can be isolated and is reproducible across different groups of subjects. Visuomotor learning influenced the amplitude of cbTEP consistent with its origin in the cerebellum.

Conclusions

In this thesis, the potential key role of TMS-EEG to assess in vivo and directly was discussed. In the last years, some Authors questioned the possible influence of confounding factors on the resulting TEPs waveform previously described and highlighted the need to include a sham stimulation condition as a control condition in TMS-EEG studies.

The first experiment of this thesis demonstrated that standard TMS induced clear and different responses compared to auditory and somatosensory stimulations. In particular, the early responses (before 50 ms, specifically the P30 peak) are present only following standard TMS stimulation and are not influenced by auditory stimulation. Moreover, standard TMS can evoke clear negative middle-latency responses (around 100 ms) with a different intensity and different topographic distribution compared to responses obtained with auditory stimulation. The noise masking and the thin layer foam can supper artefactual auditory and somatosensory inputs. So, these findings suggest that when stimulating M1 with an intensity slightly lower than the motor threshold it is possible to obtain genuine cortical EEG responses, provided that the confounding factors (TMS coil click and tap sensation) are properly masked. It follows that, according to our result, is not necessary to include a sham condition in TMS-EEG studies to obtain a pure and genuine cortical response. Moreover, TMS-EEG could be effectively used to test the pure neuronal connection between motor and non-motor remote areas. A growing number of evidence suggested that TMS-EEG could provide a pure neuronal index of functional cerebellar connection with M1 and other non-motor areas. However, to date data seem conflictual and reflect possible contamination from residual artefactual activity.

The result from experiment 2 of this thesis, highlighted that interactions between the cerebellum and cortex can be successfully evaluated using TMS-EEG and that these responses are influenced by motor learning processes. In particular, is possible to record EEG signals reflecting pure cerebellar activation that can be distinguished from sensory and auditory confounding potentials. The data from experiment 2 highlighted that is possible to record an EEG potential characterized by

positive and negative peaks (P80 and N110) which reflect cerebellar activation. This potential seems to change amplitude in response to different stages of motor learning.

All these shreds of evidence highlighted that TMS-EEG can be used to explore a pure and genuine neural response from near and remote areas when procedures to minimize indirect cortical activation (e.g. noise masking and foam layer) are properly adopted. Due to these peculiar characteristics, TMS-EEG could be a powerful tool to be used for clinical purposes, for example, to indagate abnormalities in cortical pathways that occur in neurological disease, to assess the efficacy of several drugs treatment and to design new neuromodulation protocols. However, a standardization of TMS-EEG data acquisition and analysis is highly required. Further studies should investigate the potential role of TMS-EEG for clinical application using a proper TMS-EEG acquisition process.

Bibliography

Allen G, McColl R, Barnard H, Ringe WK, Fleckenstein J, Cullum CM. Magnetic resonance imaging of cerebellar-prefrontal and cerebellar-parietal functional connectivity. Neuroimage 2005;28:39–48. https://doi.org/10.1016/j.neuroimage.2005.06.013.

Amassian VE, Stewart M, Quirk GJ, Rosenthal JL. Physiological basis of motor effects of a transient stimulus to cerebral cortex. Neurosurgery 1987;20:74–93. https://doi.org/10.1097/00006123-198701000-00022.

Assenza G, Capone F, di Biase L, Ferreri F, Florio L, Guerra A, et al. Corrigendum: Oscillatory activities in neurological disorders of elderly: Biomarkers to target for neuromodulation [Front. Aging Neurosci, (2017),(189),9] DOI: 10.3389/fnagi.2017.00189. Frontiers in Aging Neuroscience 2017;9:252. https://doi.org/10.3389/fnagi.2017.00252.

Barker AT, Jalinous R, Freeston IL. Non-invasive magnetic stimulation of human motor cortex. The Lancet 1985;325:1106–7. https://doi.org/10.1016/S0140-6736(85)92413-4.

Battaglia F, Quartarone A, Ghilardi MF, Dattola R, Bagnato S, Rizzo V, et al. Unilateral cerebellar stroke disrupts movement preparation and motor imagery. Clin Neurophysiol 2006;117:1009–16. https://doi.org/10.1016/j.clinph.2006.01.008.

Bédard P, Sanes JN. Basal ganglia-dependent processes in recalling learned visual-motor adaptations. Exp Brain Res 2011;209:385–93. https://doi.org/10.1007/s00221-011-2561-y.

Belardinelli P, Biabani M, Blumberger DM, Bortoletto M, Casarotto S, David O, et al. Reproducibility in TMS–EEG studies: A call for data sharing, standard procedures and effective experimental control. Brain Stimulation 2019. https://doi.org/10.1016/J.BRS.2019.01.010.

Benagiano V, Rizzi A, Lorusso L, Flace P, Saccia M, Cagiano R, et al. The functional anatomy of the cerebrocerebellar circuit: A review and new concepts. J Comp Neurol 2018;526:769–89. https://doi.org/10.1002/cne.24361.

Benjamini Y, Hochberg Y. Controlling the False Discovery Rate: A Practical and Powerful Approach to Multiple Testing. Journal of the Royal Statistical Society: Series B (Methodological) 1995;57:289–300. https://doi.org/10.1111/j.2517-6161.1995.tb02031.x.

Berger H. On the Electroencephalogram of Man. J Psychol Neurol 1929;40:160–79.

Bernard JA, Seidler RD. Cerebellar contributions to visuomotor adaptation and motor sequence learning: an ALE meta-analysis. Front Hum Neurosci 2013;7:27. https://doi.org/10.3389/fnhum.2013.00027.

Biabani M, Fornito A, Mutanen TP, Morrow J, Rogasch NC. Characterizing and minimizing the contribution of sensory inputs to TMS-evoked potentials. Brain Stimul 2019;12:1537–52. https://doi.org/10.1016/j.brs.2019.07.009.

Bonato C, Miniussi C, Rossini PM. Transcranial magnetic stimulation and cortical evoked potentials: a TMS/EEG co-registration study. Clinical Neurophysiology : Official Journal of the International Federation of Clinical Neurophysiology 2006;117:1699–707. https://doi.org/10.1016/j.clinph.2006.05.006.

Bonita JD, Ambolode LCC 2nd, Rosenberg BM, Cellucci CJ, Watanabe TAA, Rapp PE, et al. Time domain measures of inter-channel EEG correlations: a comparison of linear, nonparametric and nonlinear measures. Cogn

Neurodyn 2014;8:1–15. https://doi.org/10.1007/s11571-013-9267-8.

Boukrina O, Chen P. Neural Mechanisms of Prism Adaptation in Healthy Adults and Individuals with Spatial Neglect after Unilateral Stroke: A Review of fMRI Studies. Brain Sci 2021;11. https://doi.org/10.3390/brainsci11111468.

ter Braack EM, de Vos CC, van Putten MJAM. Masking the Auditory Evoked Potential in TMS–EEG: A Comparison of Various Methods. Brain Topography 2015;28:520–8. https://doi.org/10.1007/s10548-013-0312-z.

Brandt ME. Visual and auditory evoked phase resetting of the alpha EEG. International Journal of Psychophysiology, vol. 26, 1997, p. 285–98. https://doi.org/10.1016/S0167-8760(97)00771-X.

Caligiore D, Arbib MA, Miall RC, Baldassarre G. The super-learning hypothesis: Integrating learning processes across cortex, cerebellum and basal ganglia. Neurosci Biobehav Rev 2019;100:19–34. https://doi.org/10.1016/j.neubiorev.2019.02.008.

Casula Elias P, Bertoldo A, Tarantino V, Maiella M, Koch G, Rothwell JC, et al. TMS-evoked long-lasting artefacts: A new adaptive algorithm for EEG signal correction. Clinical Neurophysiology 2017;128:1563–74. https://doi.org/10.1016/j.clinph.2017.06.003.

Casula Elias P., Bertoldo A, Tarantino V, Maiella M, Koch G, Rothwell JC, et al. TMS-evoked long-lasting artefacts: A new adaptive algorithm for EEG signal correction. Clin Neurophysiol 2017;128:1563–74. https://doi.org/10.1016/j.clinph.2017.06.003.

Casula E P, Rocchi L, Hannah R, Rothwell JC. Effects of pulse width, waveform and current direction in the cortex: A combined cTMS-EEG study. Brain Stimulation 2018;11:1063–70. https://doi.org/10.1016/j.brs.2018.04.015.

Casula E. P., Rocchi L, Hannah R, Rothwell JC. Effects of pulse width, waveform and current direction in the cortex: A combined cTMS-EEG study. Brain Stimul 2018;11:1063–70. https://doi.org/10.1016/j.brs.2018.04.015.

Casula Elias Paolo, Stampanoni Bassi M, Pellicciari MC, Ponzo V, Veniero D, Peppe A, et al. Subthalamic stimulation and levodopa modulate cortical reactivity in Parkinson's patients. Parkinsonism and Related Disorders 2017;34:31–7. https://doi.org/10.1016/j.parkreldis.2016.10.009.

Cipollari S, Veniero D, Razzano C, Caltagirone C, Koch G, Marangolo P. Combining TMS-EEG with transcranial direct current stimulation language treatment in aphasia. Expert Review of Neurotherapeutics 2015;15:833–45. https://doi.org/10.1586/14737175.2015.1049998.

Conde V, Tomasevic L, Akopian I, Stanek K, Saturnino GB, Thielscher A, et al. The non-transcranial TMS-evoked potential is an inherent source of ambiguity in TMS-EEG studies. NeuroImage 2019;185:300–12. https://doi.org/10.1016/J.NEUROIMAGE.2018.10.052.

Cracco RQ, Amassian VE, Maccabee PJ, Cracco JB. Comparison of human transcallosal responses evoked by magnetic coil and electrical stimulation. Electroencephalography and Clinical Neurophysiology/ Evoked Potentials 1989;74:417–24. https://doi.org/10.1016/0168-5597(89)90030-0.

Cruccu G, Aminoff MJ, Curio G, Guerit JM, Kakigi R, Mauguiere F, et al. Recommendations for the clinical use of somatosensory-evoked potentials. Clinical Neurophysiology 2008;119:1705–19. https://doi.org/10.1016/j.clinph.2008.03.016.

Currà A, Modugno N, Inghilleri M, Manfredi M, Hallett M, Berardelli A. Transcranial magnetic stimulation techniques in clinical investigation. Neurology 2002;59:1851–9.

https://doi.org/10.1212/01.WNL.0000038744.30298.D4.

Daskalakis ZJ, Farzan F, Barr MS, Maller JJ, Chen R, Fitzgerald PB. Long-interval cortical inhibition from the dorsolateral prefrontal cortex: A TMS-EEG study. Neuropsychopharmacology 2008;33:2860–9. https://doi.org/10.1038/npp.2008.22.

Daskalakis ZJ, Farzan F, Radhu N, Fitzgerald PB. Combined transcranial magnetic stimulation and electroencephalography: its past, present and future. Brain Research 2012;1463:93–107. https://doi.org/10.1016/j.brainres.2012.04.045.

Day BL, Dressler D, Maertens de Noordhout A, Marsden CD, Nakashima K, Rothwell JC, et al. Electric and magnetic stimulation of human motor cortex: surface EMG and single motor unit responses. The Journal of Physiology 1989;412:449–73. https://doi.org/10.1113/jphysiol.1989.sp017626.

Day BL, Rothwell JC, Thompson PD, Dick JP, Cowan JM, Berardelli A, et al. Motor cortex stimulation in intact man. 2. Multiple descending volleys. Brain : A Journal of Neurology 1987;110 (Pt 5):1191–209. https://doi.org/10.1093/brain/110.5.1191.

Delorme A, Makeig S. EEGLAB: An open source toolbox for analysis of single-trial EEG dynamics including independent component analysis. Journal of Neuroscience Methods 2004;134:9–21. https://doi.org/10.1016/j.jneumeth.2003.10.009.

Di Biasio F, Conte A, Bologna M, Iezzi E, Rocchi L, Modugno N, et al. Does the cerebellum intervene in the abnormal somatosensory temporal discrimination in Parkinson's disease? Parkinsonism Relat Disord 2015;21:789–92. https://doi.org/10.1016/j.parkreldis.2015.04.004.

Douglas RJ, Martin KAC, Whitteridge D. A Canonical Microcircuit for Neocortex. Neural Computation 1989;1:480–8. https://doi.org/10.1162/neco.1989.1.4.480.

Doyon J, Bellec P, Amsel R, Penhune V, Monchi O, Carrier J, et al. Contributions of the basal ganglia and functionally related brain structures to motor learning. Behav Brain Res 2009;199:61–75. https://doi.org/10.1016/j.bbr.2008.11.012.

Du X, Rowland LM, Summerfelt A, Choa F-S, Wittenberg GF, Wisner K, et al. Cerebellar-Stimulation Evoked Prefrontal Electrical Synchrony Is Modulated by GABA. Cerebellum 2018;17:550–63. https://doi.org/10.1007/s12311-018-0945-2.

Farzan F, Vernet M, Shafi MMD, Rotenberg A, Daskalakis ZJ, Pascual-Leone A. Characterizing and modulating brain circuitry through transcranial magnetic stimulation combined with electroencephalography. Frontiers in Neural Circuits 2016;10. https://doi.org/10.3389/fncir.2016.00073.

Fernandez L, Biabani M, Do M, Opie GM, Hill AT, Barham MP, et al. Assessing cerebellar-cortical connectivity using concurrent TMS-EEG: a feasibility study. Journal of Neurophysiology 2021;125:1768–87. https://doi.org/10.1152/jn.00617.2020.

Fernandez L, Major BP, Teo W-P, Byrne LK, Enticott PG. The Impact of Stimulation Intensity and Coil Type on Reliability and Tolerability of Cerebellar Brain Inhibition (CBI) via Dual-Coil TMS. Cerebellum 2018;17:540–9. https://doi.org/10.1007/s12311-018-0942-5.

Ferreri F, Pasqualetti P, Määttä S, Ponzo D, Ferrarelli F, Tononi G, et al. Human brain connectivity during single and paired pulse transcranial magnetic stimulation. NeuroImage 2011;54:90–102.

https://doi.org/10.1016/j.neuroimage.2010.07.056.

Ferreri F, Ponzo D, Hukkanen T, Mervaala E, Könönen M, Pasqualetti P, et al. Human brain cortical correlates of short-latency afferent inhibition: A combined EEG-TMS study. Journal of Neurophysiology 2012;108:314–23. https://doi.org/10.1152/jn.00796.2011.

Galea JM, Jayaram G, Ajagbe L, Celnik P. Modulation of cerebellar excitability by polarity-specific noninvasive direct current stimulation. J Neurosci 2009;29:9115–22. https://doi.org/10.1523/JNEUROSCI.2184-09.2009.

Galea JM, Mallia E, Rothwell J, Diedrichsen J. The dissociable effects of punishment and reward on motor learning. Nat Neurosci 2015;18:597–602. https://doi.org/10.1038/nn.3956.

Galea JM, Vazquez A, Pasricha N, de Xivry J-JO, Celnik P. Dissociating the roles of the cerebellum and motor cortex during adaptive learning: the motor cortex retains what the cerebellum learns. Cereb Cortex 2011;21:1761–70. https://doi.org/10.1093/cercor/bhq246.

Gassmann L, Gordon PC, Ziemann U. Assessing effective connectivity of the cerebellum with cerebral cortex using TMS-EEG. Brain Stimulation 2022;15:1354–69. https://doi.org/10.1016/j.brs.2022.09.013.

Gerloff C, Corwell B, Chen R, Hallett M, Cohen LG. The role of the human motor cortex in the control of complex and simple finger movement sequences. Brain 1998;121 (Pt 9):1695–709. https://doi.org/10.1093/brain/121.9.1695.

Gordon PC, Desideri D, Belardinelli P, Zrenner C, Ziemann U. Comparison of cortical EEG responses to realistic sham versus real TMS of human motor cortex. Brain Stimulation 2018;11:1322–30. https://doi.org/10.1016/J.BRS.2018.08.003.

Gordon PC, Jovellar DB, Song Y, Zrenner C, Belardinelli P, Siebner HR, et al. Recording brain responses to TMS of primary motor cortex by EEG - utility of an optimized sham procedure. Neuroimage 2021;245:118708. https://doi.org/10.1016/j.neuroimage.2021.118708.

Gosseries O, Sarasso S, Casarotto S, Boly M, Schnakers C, Napolitani M, et al. On the Cerebral Origin of EEG Responses to TMS: Insights From Severe Cortical Lesions. Brain Stimulation 2015;8:142–9. https://doi.org/10.1016/J.BRS.2014.10.008.

Groppa S, Oliviero A, Eisen A, Quartarone A, Cohen LG, Mall V, et al. A practical guide to diagnostic transcranial magnetic stimulation: Report of an IFCN committee. Clinical Neurophysiology 2012;123:858–82. https://doi.org/10.1016/j.clinph.2012.01.010.

Haar S, Donchin O, Dinstein I. Dissociating visual and motor directional selectivity using visuomotor adaptation. J Neurosci 2015;35:6813–21. https://doi.org/10.1523/JNEUROSCI.0182-15.2015.

Hallett M. Transcranial Magnetic Stimulation: A Primer. Neuron 2007;55:187–99. https://doi.org/10.1016/j.neuron.2007.06.026.

Hallett M, Di Iorio R, Rossini PM, Park JE, Chen R, Celnik P, et al. Contribution of transcranial magnetic stimulation to assessment of brain connectivity and networks. Clinical Neurophysiology 2017;128:2125–39. https://doi.org/10.1016/j.clinph.2017.08.007.

Halsband U, Lange RK. Motor learning in man: a review of functional and clinical studies. J Physiol Paris 2006;99:414–24. https://doi.org/10.1016/j.jphysparis.2006.03.007.

Hardwick RM, Lesage E, Miall RC. Cerebellar transcranial magnetic stimulation: the role of coil geometry and tissue depth. Brain Stimul 2014;7:643–9. https://doi.org/10.1016/j.brs.2014.04.009.

Hill AT, Rogasch NC, Fitzgerald PB, Hoy KE. TMS-EEG: A window into the neurophysiological effects of transcranial electrical stimulation in non-motor brain regions. Neuroscience and Biobehavioral Reviews 2016;64:175–84. https://doi.org/10.1016/j.neubiorev.2016.03.006.

Huber R, Määttä S, Esser SK, Sarasso S, Ferrarelli F, Watson A, et al. Measures of cortical plasticity after transcranial paired associative stimulation predict changes in electroencephalogram slow-wave activity during subsequent sleep. The Journal of Neuroscience : The Official Journal of the Society for Neuroscience 2008;28:7911–8. https://doi.org/10.1523/JNEUROSCI.1636-08.2008.

Ilmoniemi RJ, Virtanen J, Ruohonen J, Karhu J, Aronen HJ, Näätänen R, et al. Neuronal responses to magnetic stimulation reveal cortical reactivity and connectivity. NeuroReport 1997;8:3537–40. https://doi.org/10.1097/00001756-199711100-00024.

Ingber L, Nunez PL. Neocortical dynamics at multiple scales: EEG standing waves, statistical mechanics, and physical analogs. Mathematical Biosciences 2011;229:160–73. https://doi.org/10.1016/j.mbs.2010.12.003.

Inghilleri M, Berardelli A, Cruccu G, Manfredi M. Silent period evoked by transcranial stimulation of the human cortex and cervicomedullary junction. The Journal of Physiology 1993;466:521–34. https://doi.org/10.1113/jphysiol.1993.sp019732.

Ives JR, Rotenberg A, Poma R, Thut G, Pascual-Leone A. Electroencephalographic recording during transcranial magnetic stimulation in humans and animals. Clinical Neurophysiology 2006;117:1870–5. https://doi.org/10.1016/j.clinph.2006.04.010.

Iwata NK, Ugawa Y. The effects of cerebellar stimulation on the motor cortical excitability in neurological disorders: a review. Cerebellum 2005;4:218–23. https://doi.org/10.1080/14734220500277007.

Jiang X, Wang G, Lee AJ, Stornetta RL, Zhu JJ. The organization of two new cortical interneuronal circuits. Nature Neuroscience 2013;16:210–8. https://doi.org/10.1038/nn.3305.

Julkunen P, Pääkkönen A, Hukkanen T, Könönen M, Tiihonen P, Vanhatalo S, et al. Efficient reduction of stimulus artefact in TMS-EEG by epithelial short-circuiting by mini-punctures. Clinical Neurophysiology : Official Journal of the International Federation of Clinical Neurophysiology 2008;119:475–81. https://doi.org/10.1016/j.clinph.2007.09.139.

Kerwin Lewis J, Keller CJ, Wu W, Narayan M, Etkin A. Test-retest reliability of transcranial magnetic stimulation EEG evoked potentials. Brain Stimulation 2018;11:536–44. https://doi.org/10.1016/j.brs.2017.12.010.

Kerwin Lewis J., Keller CJ, Wu W, Narayan M, Etkin A. Test-retest reliability of transcranial magnetic stimulation EEG evoked potentials. Brain Stimul 2018;11:536–44. https://doi.org/10.1016/j.brs.2017.12.010.

Kicić D, Lioumis P, Ilmoniemi RJ, Nikulin V V. Bilateral changes in excitability of sensorimotor cortices during unilateral movement: combined electroencephalographic and transcranial magnetic stimulation study. Neuroscience 2008;152:1119–29. https://doi.org/10.1016/j.neuroscience.2008.01.043.

King TS, Chinchilli VM, Carrasco JL. A repeated measures concordance correlation coefficient. Stat Med 2007;26:3095–113. https://doi.org/10.1002/sim.2778.

Kirschstein T, Köhling R. What is the source of the EEG? Clinical EEG and Neuroscience 2009;40:146–9.

https://doi.org/10.1177/155005940904000305.

Klein J, Roach N, Burdet E. 3DOM: A 3 Degree of Freedom Manipulandum to Investigate Redundant Motor Control. IEEE Transactions on Haptics 2014;7:229–39.

Koch G, Esposito R, Motta C, Casula EP, Di Lorenzo F, Bonnì S, et al. Improving visuo-motor learning with cerebellar theta burst stimulation: Behavioral and neurophysiological evidence. Neuroimage 2020;208:116424. https://doi.org/10.1016/j.neuroimage.2019.116424.

Komssi S, Kähkönen S. The novelty value of the combined use of electroencephalography and transcranial magnetic stimulation for neuroscience research. Brain Research Reviews 2006;52:183–92. https://doi.org/10.1016/j.brainresrev.2006.01.008.

Koponen LM, Goetz SM, Peterchev AV. Double-Containment Coil With Enhanced Winding Mounting for Transcranial Magnetic Stimulation With Reduced Acoustic Noise. IEEE Trans Biomed Eng 2021;68:2233–40. https://doi.org/10.1109/TBME.2020.3048321.

Koponen LM, Goetz SM, Tucci DL, Peterchev AV. Sound comparison of seven TMS coils at matched stimulation strength. Brain Stimulation 2020;13:873–80. https://doi.org/10.1016/j.brs.2020.03.004.

Krakauer JW, Ghez C, Ghilardi MF. Adaptation to visuomotor transformations: consolidation, interference, and forgetting. J Neurosci 2005;25:473–8. https://doi.org/10.1523/JNEUROSCI.4218-04.2005.

Krienen FM, Buckner RL. Segregated fronto-cerebellar circuits revealed by intrinsic functional connectivity. Cereb Cortex 2009;19:2485–97. https://doi.org/10.1093/cercor/bhp135.

Di Lazzaro V. Biological effects of non-invasive brain stimulation. Handbook of Clinical Neurology, 2013, p. 367–74. https://doi.org/10.1016/B978-0-444-53497-2.00030-9.

Di Lazzaro V, Oliviero A, Mazzone P, Pilato F, Saturno E, Insola A, et al. Direct demonstration of long latency cortico-cortical inhibition in normal subjects and in a patient with vascular parkinsonism. Clinical Neurophysiology 2002;113:1673–9. https://doi.org/10.1016/S1388-2457(02)00264-X.

Di Lazzaro V., Oliviero A, Meglio M, Cioni B, Tamburrini G, Tonali P, et al. Direct demonstration of the effect of lorazepam on the excitability of the human motor cortex. Clinical Neurophysiology 2000;111:794–9. https://doi.org/10.1016/S1388-2457(99)00314-4.

Di Lazzaro V, Oliviero A, Profice P, Pennisi MA, Di Giovanni S, Zito G, et al. Muscarinic receptor blockade has differential effects on the excitability of intracortical circuits in the human motor cortex. Experimental Brain Research 2000;135:455–61.

Di Lazzaro V, Restuccia D, Oliviero A, Profice P, Ferrara L, Insola A, et al. Magnetic transcranial stimulation at intensities below active motor threshold activates intracortical inhibitory circuits. Experimental Brain Research 1998;119:265–8. https://doi.org/10.1007/s002210050341.

Di Lazzaro V, Rothwell JC. Corticospinal activity evoked and modulated by non-invasive stimulation of the intact human motor cortex. Journal of Physiology 2014;592:4115–28. https://doi.org/10.1113/jphysiol.2014.274316.

Di Lazzaro V, Ziemann U. The contribution of transcranial magnetic stimulation in the functional evaluation of microcircuits in human motor cortex. Frontiers in Neural Circuits 2013;7. https://doi.org/10.3389/fncir.2013.00018.

Di Lazzaro V, Ziemann U, Lemon RN. State of the art: Physiology of transcranial motor cortex stimulation. Brain Stimulation 2008;1:345–62. https://doi.org/10.1016/j.brs.2008.07.004.

Leandri M, Parodi CI, Favale E. Early evoked potentials detected from the scalp of man following infraorbital nerve stimulation. Electroencephalography and Clinical Neurophysiology/ Evoked Potentials 1985;62:99–107. https://doi.org/10.1016/0168-5597(85)90021-8.

Lehmann D, Skrandies W. Reference-free identification of components of checkerboard-evoked multichannel potential fields. Electroencephalography and Clinical Neurophysiology 1980a;48:609–21. https://doi.org/10.1016/0013-4694(80)90419-8.

Lehmann D, Skrandies W. Reference-free identification of components of checkerboard-evoked multichannel potential fields. Electroencephalogr Clin Neurophysiol 1980b;48:609–21. https://doi.org/10.1016/0013-4694(80)90419-8.

Lin LI. A concordance correlation coefficient to evaluate reproducibility. Biometrics 1989;45:255–68.

Lioumis P, Kičić D, Savolainen P, Mäkelä JP, Kähkönen S. Reproducibility of TMS-Evoked EEG responses. Human Brain Mapping 2009;30:1387–96. https://doi.org/10.1002/hbm.20608.

Litvak V, Komssi S, Scherg M, Hoechstetter K, Classen J, Zaaroor M, et al. Artifact correction and source analysis of early electroencephalographic responses evoked by transcranial magnetic stimulation over primary motor cortex. NeuroImage 2007;37:56–70. https://doi.org/10.1016/j.neuroimage.2007.05.015.

Mäki H, Ilmoniemi RJ. Projecting out muscle artifacts from TMS-evoked EEG. NeuroImage 2011;54:2706–10. https://doi.org/10.1016/j.neuroimage.2010.11.041.

Mancuso M, Sveva V, Cruciani A, Brown K, Ibáñez J, Rawji V, et al. Transcranial Evoked Potentials Can Be Reliably Recorded with Active Electrodes. Brain Sciences 2021;11:145. https://doi.org/10.3390/brainsci11020145.

Maris E, Oostenveld R. Nonparametric statistical testing of EEG- and MEG-data. J Neurosci Methods 2007a;164:177–90. https://doi.org/10.1016/j.jneumeth.2007.03.024.

Maris E, Oostenveld R. Nonparametric statistical testing of EEG- and MEG-data. Journal of Neuroscience Methods 2007b;164:177–90. https://doi.org/10.1016/j.jneumeth.2007.03.024.

Massimini M, Ferrarelli F, Huber R, Esser SK, Singh H, Tononi G. Breakdown of cortical effective connectivity during sleep. Science 2005;309:2228–32. https://doi.org/10.1126/science.1117256.

Mehrabyan A, Guest S, Essick G, McGlone F. Tactile and thermal detection thresholds of the scalp skin. Somatosens Mot Res 2011;28:31–47. https://doi.org/10.3109/08990220.2011.602764.

Middleton FA, Strick PL. Cerebellar projections to the prefrontal cortex of the primate. J Neurosci 2001;21:700–12. https://doi.org/10.1523/JNEUROSCI.21-02-00700.2001.

Monaco J, Rocchi L, Ginatempo F, D'Angelo E, Rothwell JC. Cerebellar Theta-Burst Stimulation Impairs Memory Consolidation in Eyeblink Classical Conditioning. Neural Plast 2018;2018:6856475. https://doi.org/10.1155/2018/6856475.

Mouraux A, Iannetti GD. Nociceptive laser-evoked brain potentials do not reflect nociceptive-specific neural activity. Journal of Neurophysiology 2009;101:3258–69. https://doi.org/10.1152/jn.91181.2008.

Mutanen T, Mäki H, Ilmoniemi RJ. The effect of stimulus parameters on TMS-EEG muscle artifacts. Brain

Stimulation 2013;6:371–6. https://doi.org/10.1016/j.brs.2012.07.005.

Nezafat R, Shadmehr R, Holcomb HH. Long-term adaptation to dynamics of reaching movements: a PET study. Exp Brain Res 2001;140:66–76. https://doi.org/10.1007/s002210100787.

Ni Z, Gunraj C, Wagle-Shukla A, Udupa K, Mazzella F, Lozano AM, et al. Direct demonstration of inhibitory interactions between long interval intracortical inhibition and short interval intracortical inhibition. The Journal of Physiology 2011;589:2955–62. https://doi.org/10.1113/jphysiol.2011.207928.

Nikouline V, Ruohonen J, Ilmoniemi RJ. The role of the coil click in TMS assessed with simultaneous EEG. Clinical Neurophysiology 1999;110:1325–8. https://doi.org/10.1016/S1388-2457(99)00070-X.

Noda Y, Cash RFH, Zomorrodi R, Dominguez LG, Farzan F, Rajji TK, et al. A combined TMS-EEG study of short-latency afferent inhibition in the motor and dorsolateral prefrontal cortex. Journal of Neurophysiology 2016;116:938–48. https://doi.org/10.1152/jn.00260.2016.

Noda Y, Zomorrodi R, Cash RFH, Barr MS, Farzan F, Rajji TK, et al. Characterization of the influence of age on GABAA and glutamatergic mediated functions in the dorsolateral prefrontal cortex using paired-pulse TMS-EEG. Aging 2017;9:556–72. https://doi.org/10.18632/aging.101178.

Oldfield RC. The assessment and analysis of handedness: The Edinburgh inventory. Neuropsychologia 1971;9:97–113. https://doi.org/10.1016/0028-3932(71)90067-4.

Onton J, Westerfield M, Townsend J, Makeig S. Imaging human EEG dynamics using independent component analysis. Neuroscience and Biobehavioral Reviews 2006;30:808–22. https://doi.org/10.1016/j.neubiorev.2006.06.007.

Oostenveld R, Fries P, Maris E, Schoffelen JM. FieldTrip: Open source software for advanced analysis of MEG, EEG, and invasive electrophysiological data. Computational Intelligence and Neuroscience 2011;2011. https://doi.org/10.1155/2011/156869.

Opie GM, Rogasch NC, Goldsworthy MR, Ridding MC, Semmler JG. Investigating TMS-EEG Indices of Long-Interval Intracortical Inhibition at Different Interstimulus Intervals. Brain Stimul 2017;10:65–74. https://doi.org/10.1016/j.brs.2016.08.004.

Pascual-Leone A, Dhuna A, Roth BJ, Cohen L, Hallett M. Risk of burns during rapid-rate magnetic stimulation in presence of electrodes. Lancet (London, England) 1990;336:1195–6. https://doi.org/10.1016/0140-6736(90)92815-y.

Patton HD, Amassian VE. Single and multiple-unit analysis of cortical stage of pyramidal tract activation. Journal of Neurophysiology 1954;17:345–63. https://doi.org/10.1152/jn.1954.17.4.345.

Paus T, Sipila PK, Strafella AP. Synchronization of neuronal activity in the human primary motor cortex by transcranial magnetic stimulation: An EEG study. Journal of Neurophysiology 2001;86:1983–90. https://doi.org/10.1152/jn.2001.86.4.1983.

Pernet CR, Latinus M, Nichols TE, Rousselet GA. Cluster-based computational methods for mass univariate analyses of event-related brain potentials/fields: A simulation study. J Neurosci Methods 2015;250:85–93. https://doi.org/10.1016/j.jneumeth.2014.08.003.

Picton TW, Hillyard SA, Krausz HI, Galambos R. Human auditory evoked potentials. I: Evaluation of components. Electroencephalography and Clinical Neurophysiology 1974;36:179–90. https://doi.org/10.1016/0013-

4694(74)90155-2.

Premoli I, Rivolta D, Espenhahn S, Castellanos N, Belardinelli P, Ziemann U, et al. Characterization of GABAB-receptor mediated neurotransmission in the human cortex by paired-pulse TMS–EEG. NeuroImage 2014;103:152–62. https://doi.org/10.1016/j.neuroimage.2014.09.028.

Rawji V, Kaczmarczyk I, Rocchi L, Fong P-Y, Rothwell JC, Sharma N. Preconditioning Stimulus Intensity Alters Paired-Pulse TMS Evoked Potentials. Brain Sci 2021;11. https://doi.org/10.3390/brainsci11030326.

Reichenbach A, Whittingstall K, Thielscher A. Effects of transcranial magnetic stimulation on visual evoked potentials in a visual suppression task. NeuroImage 2011;54:1375–84. https://doi.org/10.1016/j.neuroimage.2010.08.047.

Reis J, Swayne OB, Vandermeeren Y, Camus M, Dimyan MA, Harris-Love M, et al. Contribution of transcranial magnetic stimulation to the understanding of cortical mechanisms involved in motor control. J Physiol 2008;586:325–51. https://doi.org/10.1113/jphysiol.2007.144824.

Rocchi L, Erro R, Antelmi E, Berardelli A, Tinazzi M, Liguori R, et al. High frequency somatosensory stimulation increases sensori-motor inhibition and leads to perceptual improvement in healthy subjects. Clinical Neurophysiology 2017;128:1015–25. https://doi.org/10.1016/j.clinph.2017.03.046.

Rocchi L, Ibáñez J, Benussi A, Hannah R, Rawji V, Casula E, et al. Variability and predictors of response to continuous theta burst stimulation: A TMS-EEG study. Frontiers in Neuroscience 2018a;12. https://doi.org/10.3389/fnins.2018.00400.

Rocchi L, Ibáñez J, Benussi A, Hannah R, Rawji V, Casula E, et al. Variability and Predictors of Response to Continuous Theta Burst Stimulation: A TMS-EEG Study. Front Neurosci 2018b;12:400. https://doi.org/10.3389/fnins.2018.00400.

Rocchi L, Latorre A, Ibanez Pereda J, Spampinato D, Brown KE, Rothwell J, et al. A case of congenital hypoplasia of the left cerebellar hemisphere and ipsilateral cortical myoclonus. Mov Disord 2019;34:1745–7. https://doi.org/10.1002/mds.27881.

Rogasch NC, Daskalakis ZJ, Fitzgerald PB. Cortical inhibition of distinct mechanisms in the dorsolateral prefrontal cortex is related to working memory performance: A TMS-EEG study. Cortex 2015;64:68–77. https://doi.org/10.1016/j.cortex.2014.10.003.

Rogasch NC, Sullivan C, Thomson RH, Rose NS, Bailey NW, Fitzgerald PB, et al. Analysing concurrent transcranial magnetic stimulation and electroencephalographic data: A review and introduction to the open-source TESA software. NeuroImage 2017;147:934–51. https://doi.org/10.1016/j.neuroimage.2016.10.031.

Rogasch NC, Thomson RH, Daskalakis ZJ, Fitzgerald PB. Short-latency artifacts associated with concurrent TMS-EEG. Brain Stimulation 2013;6:868–76. https://doi.org/10.1016/j.brs.2013.04.004.

Rogasch NC, Thomson RH, Farzan F, Fitzgibbon BM, Bailey NW, Hernandez-Pavon JC, et al. Removing artefacts from TMS-EEG recordings using independent component analysis: Importance for assessing prefrontal and motor cortex network properties. NeuroImage 2014. https://doi.org/10.1016/j.neuroimage.2014.07.037.

Romero Lauro LJ, Rosanova M, Mattavelli G, Convento S, Pisoni A, Opitz A, et al. TDCS increases cortical excitability: direct evidence from TMS-EEG. Cortex; a Journal Devoted to the Study of the Nervous System and Behavior 2014;58:99–111. https://doi.org/10.1016/j.cortex.2014.05.003.

Rose NS, LaRocque JJ, Riggall AC, Gosseries O, Starrett MJ, Meyering EE, et al. Reactivation of latent working memories with transcranial magnetic stimulation. Science 2016;354:1136–9. https://doi.org/10.1126/science.aah7011.

Rosler KM, Hess CW, Schmid UD. Investigation of facial motor pathways by electrical and magnetic stimulation: Sites and mechanisms of excitation. Journal of Neurology Neurosurgery and Psychiatry 1989;52:1149–56. https://doi.org/10.1136/jnnp.52.10.1149.

Ross JM, Ozdemir RA, Lian SJ, Fried PJ, Schmitt EM, Inouye SK, et al. A structured ICA-based process for removing auditory evoked potentials. Sci Rep 2022;12:1391. https://doi.org/10.1038/s41598-022-05397-3.

Rossini PM, Barker AT, Berardelli A, Caramia MD, Caruso G, Cracco RQ, et al. Non-invasive electrical and magnetic stimulation of the brain, spinal cord and roots: basic principles and procedures for routine clinical application. Report of an IFCN committee. Electroencephalography and Clinical Neurophysiology 1994;91:79–92. https://doi.org/10.1016/0013-4694(94)90029-9.

Rossini PM, Burke D, Chen R, Cohen LG, Daskalakis Z, Di Iorio R, et al. Non-invasive electrical and magnetic stimulation of the brain, spinal cord, roots and peripheral nerves: Basic principles and procedures for routine clinical and research application: An updated report from an I.F.C.N. Committee. Clinical Neurophysiology 2015;126:1071–107. https://doi.org/10.1016/j.clinph.2015.02.001.

Rotenberg A, Horvath JC, Pascual-Leone A. The Transcranial Magnetic Stimulation (TMS) device and foundational techniques. Neuromethods 2014;89:3–13. https://doi.org/10.1007/978-1-4939-0879-0_1.

Roth BJ, Pascual-Leone A, Cohen LG, Hallett M. The heating of metal electrodes during rapid-rate magnetic stimulation: a possible safety hazard. Electroencephalography and Clinical Neurophysiology/ Evoked Potentials 1992;85:116–23. https://doi.org/10.1016/0168-5597(92)90077-O.

Rothwell JC. Transcranial electrical and magnetic stimulation of the brain: basic physiological mechanisms. In: M. Hallett and S. Chokroverty eds., editor. Magnetic Stimulation in Clinical Neurophysiology. Magnetic S, Philadelphia: Elsevier, Butterworth Heinemann; 2004, p. 43–60.

Rothwell JC. Techniques and mechanisms of action of transcranial stimulation of the human motor cortex. Journal of Neuroscience Methods 1997;74:113–22. https://doi.org/10.1016/S0165-0270(97)02242-5.

Ruohonen Jarmo; Ilmoniemi Risto. Basic Physics and Design of Transcranial Magnetic Stimulation Devices and Coils. In: Hallett MCS, editor. Magnetic Stimulation in Clinical Neurophysiology. Second edi, Philadelphia, Pennsylvania 19106: Elsevier; 2005, p. 17–30.

Sasaki R, Hand BJ, Liao WY, Rogasch NC, Fernandez L, Semmler JG, et al. Utilising TMS-EEG to Assess the Response to Cerebellar-Brain Inhibition. Cerebellum 2022. https://doi.org/10.1007/s12311-022-01419-y.

Schlerf JE, Galea JM, Spampinato D, Celnik PA. Laterality Differences in Cerebellar-Motor Cortex Connectivity. Cereb Cortex 2015;25:1827–34. https://doi.org/10.1093/cercor/bht422.

Sekiguchi H, Takeuchi S, Kadota H, Kohno Y, Nakajima Y. TMS-induced artifacts on EEG can be reduced by rearrangement of the electrode's lead wire before recording. Clinical Neurophysiology : Official Journal of the International Federation of Clinical Neurophysiology 2011;122:984–90. https://doi.org/10.1016/j.clinph.2010.09.004.

Shadmehr R, Holcomb HH. Neural correlates of motor memory consolidation. Science 1997;277:821–5.

https://doi.org/10.1126/science.277.5327.821.

Spampinato D, Avci E, Rothwell J, Rocchi L. Frequency-dependent modulation of cerebellar excitability during the application of non-invasive alternating current stimulation. Brain Stimulation 2021;14:277–83. https://doi.org/10.1016/j.brs.2021.01.007.

Spampinato D, Celnik P. Multiple Motor Learning Processes in Humans: Defining Their Neurophysiological Bases. Neuroscientist 2021;27:246–67. https://doi.org/10.1177/1073858420939552.

Spampinato D, Ibáñez J, Spanoudakis M, Hammond P, Rothwell JC. Cerebellar transcranial magnetic stimulation: The role of coil type from distinct manufacturers. Brain Stimul 2020;13:153–6. https://doi.org/10.1016/j.brs.2019.09.005.

Starck J, Rimpiläinen I, Pyykkö I, Esko T. The noise level in magnetic stimulation. Scandinavian Audiology 1996;25:223–6. https://doi.org/10.3109/01050399609074958.

Strata P. The emotional cerebellum. Cerebellum 2015;14:570–7. https://doi.org/10.1007/s12311-015-0649-9.

Strick PL, Dum RP, Fiez JA. Cerebellum and nonmotor function. Annu Rev Neurosci 2009;32:413–34. https://doi.org/10.1146/annurev.neuro.31.060407.125606.

Striemer CL, Enns JT, Whitwell RL. Visuomotor adaptation in the absence of input from early visual cortex. Cortex 2019;115:201–15. https://doi.org/10.1016/j.cortex.2019.01.022.

Taylor JA, Ivry RB. Cerebellar and prefrontal cortex contributions to adaptation, strategies, and reinforcement learning. Prog Brain Res 2014;210:217–53. https://doi.org/10.1016/B978-0-444-63356-9.00009-1.

Tokimura H, Di Lazzaro V, Tokimura Y, Oliviero A, Profice P, Insola A, et al. Short latency inhibition of human hand motor cortex by somatosensory input from the hand. Journal of Physiology 2000;523:503–13. https://doi.org/10.1111/j.1469-7793.2000.t01-1-00503.x.

Tremblay S, Rogasch NC, Premoli I, Blumberger DM, Casarotto S, Chen R, et al. Clinical utility and prospective of TMS–EEG. Clinical Neurophysiology 2019. https://doi.org/10.1016/j.clinph.2019.01.001.

Tzvi E, Koeth F, Karabanov AN, Siebner HR, Krämer UM. Cerebellar - Premotor cortex interactions underlying visuomotor adaptation. Neuroimage 2020;220:117142. https://doi.org/10.1016/j.neuroimage.2020.117142.

Tzvi E, Loens S, Donchin O. Mini-review: The Role of the Cerebellum in Visuomotor Adaptation. Cerebellum 2022;21:306–13. https://doi.org/10.1007/s12311-021-01281-4.

Ugawa Y, Uesaka Y, Terao Y, Hanajima R, Kanazawa I. Magnetic stimulation over the cerebellum in humans. Ann Neurol 1995;37:703–13. https://doi.org/10.1002/ana.410370603.

Veniero D, Bortoletto M, Miniussi C. TMS-EEG co-registration: on TMS-induced artifact. Clinical Neurophysiology : Official Journal of the International Federation of Clinical Neurophysiology 2009;120:1392–9. https://doi.org/10.1016/j.clinph.2009.04.023.

Wagner T, Valero-Cabre A, Pascual-Leone A. Noninvasive Human Brain Stimulation. Annual Review of Biomedical Engineering 2007;9:527–65. https://doi.org/10.1146/annurev.bioeng.9.061206.133100.

Watson TC, Becker N, Apps R, Jones MW. Back to front: cerebellar connections and interactions with the prefrontal cortex. Front Syst Neurosci 2014;8:4. https://doi.org/10.3389/fnsys.2014.00004.

Weise D, Mann J, Ridding M, Eskandar K, Huss M, Rumpf J-J, et al. Microcircuit mechanisms involved in paired

associative stimulation-induced depression of corticospinal excitability. The Journal of Physiology 2013;591:4903–20. https://doi.org/10.1113/jphysiol.2013.253989.

Werhahn KJ, Taylor J, Ridding M, Meyer BU, Rothwell JC. Effect of transcranial magnetic stimulation over the cerebellum on the excitability of human motor cortex. Electroencephalogr Clin Neurophysiol 1996;101:58–66. https://doi.org/10.1016/0013-4694(95)00213-8.

de Winter JCF, Gosling SD, Potter J. Comparing the Pearson and Spearman correlation coefficients across distributions and sample sizes: A tutorial using simulations and empirical data. Psychol Methods 2016;21:273–90. https://doi.org/10.1037/met0000079.

Zhu J, Zhang X, Zhao H, Tang Y Da, Ying TT, Li ST. Utility of Brainstem Trigeminal Evoked Potentials in Patients with Primary Trigeminal Neuralgia Treated by Microvascular Decompression. Journal of Craniofacial Surgery 2017;28:e571–7. https://doi.org/10.1097/SCS.0000000000003882.

Ziemann U, Rothwell JC. I-waves in motor cortex. Journal of Clinical Neurophysiology : Official Publication of the American Electroencephalographic Society 2000;17:397–405.

Ziemann U, Rothwell JC, Ridding MC. Interaction between intracortical inhibition and facilitation in human motor cortex. Journal of Physiology 1996;496:873–81. https://doi.org/10.1113/jphysiol.1996.sp021734.